UNIVERSITÀ DI PARMA

UNIVERSITA' DEGLI STUDI DI PARMA

DOTTORATO DI RICERCA IN FISICA

CICLO XXXII

Biophysical studies on photoreceptors from plant-associated bacteria

Coordinatore:

Chiar.mo Prof. Stefano Carretta

Tutore:

Prof.ssa Aba Losi

Dottoranda:

Eleonora Consiglieri

Anni 2016/2019

Abstract

The project here presented aims at understanding the photophysical and photochemical properties of: a. biliverding-binding phytochromes, *i.e.* photoreceptors for red light, from the plant-associated bacterial species *Pseudomonas syringae* pv *tomato* (*Pst*), *Pseudomonas aeruginosa* (*Pa*), *Xanthomonas campestris* pv. *campestris* (*Xcc*) and the fungus *Aspergillus nidulans*: b. photoreceptors for red and blue light from *Methylobacterium radiotolerans* (*Mr*), belonging to the plant microbiota. The former are important and well-studied pathogens of agronomic plants, while *Mr* is a methylotrophic phytosymbiont of great industrial and agronomical interest.

This work starts with biliverdin-bindig photoreceptors, [1] as recent works have shown that the photoreceptors from *Pst* and *Xcc* play a role in controlling infectivity, virulence and invasiveness towards the model plant *Arabidopsis thaliana* and citrus plants. In the case of *Mr*, instead, the functional role of these photoactive proteins still awaits investigation, despite the finding that a genomic survey indicates that these organisms may possess quite a large number of potential and diverse photoreceptors for visible light.

The proteins were studied at the molecular level with an array of biophysical techniques: primarily steady-state and time-resolved optical spectroscopy, then time-resolved photoacoustics. Beside the molecular and spectroscopic characterisation of these photoreceptors and their interest as photosensors in prokaryots, the blue-light photoreceptor *Mr*4511 showed a particular feature: in contrast to the majority of LOV domains, this protein lacks the, in other LOV photoreceptors highly conserved, tryptophan residue, which was previously identified as the major quencher for the FMN triplet-state in LOV-based singlet oxygen (SO) photosensitisers. This

experimental work demonstrates that "for *Mr*4511 it is sufficient to only mutate the reactive cysteine responsible for the photocycle (Cys71) in the native protein to generate an efficient SO photosensitiser: both C71S and C71G variants exhibit SO quantum yields of formation Φ_Δ around 0.2 in air-saturated solutions. Under oxygen saturated conditions, Φ_Δ reaches ~ 0.5 in deuterated buffer. Also, this protein showed to be exceedingly robust against denaturation with urea and it is more photostable than free FMN." [2]

As a whole, future continuation on this work could reveal the novel potential of photoreceptors from bacteria that are part of plant microbiota, i.e. for environmental, agronomical and biotechnological applications.

1. **Consiglieri, E.** *et al.* Dynamics and efficiency of photoswitching in biliverdin-binding phytochromes. *Photochem. Photobiol. Sci.* **18**, 2484–2496 (2019).
2. **Consiglieri, E**. *et al.* Single mutation in a novel bacterial LOV protein yields a singlet oxygen generator. *Photochem. Photobiol. Sci.* (2019). doi:10.1039/C9PP00328B

Abbreviations

The following list contains all abbreviations repeatedly used in this thesis excluding common SI units. For DNA bases and amino acids the standard one or three letter codes were used, respectively.

aa: amino acid
BL: blue-light
BLUF: blue-light sensor Using Flavins
BphP: Bacterial phytochrome
BV: biliverdin
ET: energy transfer
FAD: flavin adenine dinucleotide
FbFPs: FMN-binding fluorescent proteins
Fl-Blues: flavin-binding blue/UVA light sensors
FMN: Flavin MonoNucleotide
FP: fluorescent protein
FRL: Far-Red Light
GAF: cGMP phosphodiesterase, adenylyl cyclase and FhlA protein
HB: hydrogen bond/-ing
HK: Histidine Kinase (domain)
HTH: helix- turn- helix DNA-binding domain
LADS: Lifetime-Associated Difference Spectra
LFP: Laser Flash Photolysis
LOV: Light, Oxygen, Voltage (domain)
miniSOG: mini Singlet Oxygen Generator
PA: photoacoustic

PAS: Per Arnt Sim domain

PCB: phycocyanobilin

PΦB: phytochromobilin

Phot: phototropin

PHY: phytochrome

PPFM: pink-pigmented facultative methylotroph

PYP: photoactive yellow protein

RL: Red Light

RF: riboflavin

ROS: reactive oxygen species

RR: response regulator

SO: singlet oxygen

SOSG: singlet oxygen sensor green

SOPP: singlet oxygen photosensitising protein

UV: ultraviolet

VIS: visible light

WT: wild type

Table of contents

Introduction

Light is a ubiquitous environmental stimulus for biological organisms, which have evolved dedicated proteins sensing light quality and quantity: the photoreceptors. Photoreceptors are integrated protein-chromophore complexes that evoke a physiological response upon photon absorption. Absorption of a photon within a short time-period of *ca.* 1 fs is a physical process intimately coupled to subsequent chemical reactions. Whereas the primary events are tightly linked to the chromophore of photoreceptors, the following steps can be considered as a translation process between two languages: information generated from absorption of photonic energy are thus trasferred into the language of biology and into protein functions. Thanks to their photoswitching properties, these activated photoreceptors are able to transmit biological signals into a living cell or organism (bacteria. fungi, plants, animals), in order to allow appropriate response to the environmental illumination conditions. A large number of sensory photoreceptors have recently been discovered in bacteria, opening up novel research fields and stimulating new biophysical applications. The most spread bacterial photoreceptors belong to BL (blue light)-sensing LOV (Light, Oxygen, Voltage) and BLUF (Blue Light sensing Using Flavins) proteins, and to the photochromic RL/FRL (red/far red light)-sensing BphPs (Bacteriophytochromes): they bind respectively riboflavins (vitamin B2) derivatives and biliverdin IXα (BV) as chromophores. Plant-associated bacteria are particularly rich in BL and RL/FRL photoreceptors, whose characterisation is still in its infancy.[1] These bacteria thus mimic the light-sensing ability of the host plants, which possess well known LOV and phytochrome (phy) photoreceptors, even though they are in many cases non-phototrophs. The occurrence of similar photoreceptors in the plant microbiota prompted the question whether this shared light-sensing ability is important during colonisation, infectivity and virulence. The

few cases studied until now point to a positive, albeit mostly surprising, answer: photoreceptors in important plant pathogens such as *Pseudomonas syringae* and *Xanthomonas* seem to down-regulate and control virulence and necrotic effects in host plants. [1–3] Recently, researchers have also been exploiting photoreceptors as genetically-encoded tools to trigger and study cellular events, an approach named optogenetics (actual definition including actuators and sensors). [4,5] In-silico analysis has evidenced that bacteria from the genus *Methylobacterium* are fully rich in photoreceptors (Appendix A1), and up to now none of them has been characterised. Alpha-proteobacteria of the genus *Methylobacterium* are pink-pigmented facultative methylotrophs (PPFMs), colored due to the presence of carotenoids and able to feed on carbon compounds, e.g. methanol and methylamine; [6] several species are also resistant to γ-radiation [7,8]. Some species previously included in *Methylobacteria* have been recently separated in the new genus *Methylorubrum*. [9] The majority of *Methylobacteria* and *Methylorubra* have genes for the synthesis of bacteriochlorophylls (Appendix A1), carotenoids [10] and reaction center proteins [11], although the physiological relevance of photosynthesis in these microbes remains poorly explored. *Methylobacteria* mainly reside in the phyllopshere, where thay can utilise methanol produced in the demethylation of macromolecules, principally during pectin metabolism [12]. In exchange, *Methylobacteria* can promote plant growth and fitness by the synthesis of phytohormones (auxins and cytokinins), nitrogen fixation, phosphorus uptake, production of iron-chelating compunds, defence against plant-pathogenic microorganims [13–15] , as such they are held as biofertilisers and plant probiotics, representing a resource in the frame of sustainable agriculture [16]. Furthermore, they have been proposed as tools to detoxify polluted grounds and air [17]. *Methylobacteria* are also becoming important for human health: they are configuring as resistant pathogens in certain diseases [6] and in immune-compromised hosts, especially due to their ability to form robust biofilms [18]. All species belonging to the genera possess many genes encoding for LOV, BLUF and BphP, until now fully unexplored, both in their molecular properties and as for their roles *in vivo*. Genes encoding for BphP and hybrid PYP (photoactive yellow protein)-BphP proteins have

been reported from *in silico* analysis [19,20], as well as for BLUF and LOV photoreceptors [21–23] and, more rarely, rhodopsins (possibly proton pumps) [24]. Moreover, *Methylobacterium spp.* isolated from the phyllosphere contain UVA-absorbing compounds, absorbing maximally at ca. 380 nm [25]. A blue-light effect on UV and temperature resistance has been reported for *Methylobacterium extorquens* AM1, by affecting the activity of the circadian-clock protein-kinase KaiC, but the photoreceptor responsible for this effect remains unknown [26]. As part of the plant microbiota, *Methylobacterium radiotolerans*, formerly *Pseudomonas radiora* [27] is PPFM (pink-pigmented facultative methylotroph), epiphytic plant symbiont that can promote plant growth [13]. It expresses a photosynthesis apparatus [28,29] and has recently been assessed as an opportunistic human pathogen. [30]

This thesis is focused on two main topics: a. the study of BV-binding BphPs from plant-related microbes with spectroscopy techniques; b. the molecular and spectroscopic characterisation of new bacterial photoreceptors from *Methylobacterium radiotolerans.*

Sensing red and far-red light: bacteriophytochromes BphPs

Phytochromes (phy) comprise a large superfamily of photosensory proteins that are present in plants, fungi, algae and bacteria. [31–33] They sense light through their covalently-bound bilin chromophore and generate a biological signal that regulates temperature response and reactions to vital light. [34,35] Chromophores of phy proteins are bilins, derived from the heme-degradation pathway: PΦB (phytochromobilin) is the chromophore of plant phys, PCB (phycyanobilin) is bound in cyanobacterial phys, while BV (biliverdin IXα) is the chromophore of BphPs (Figure 1). The

photosensory module of canonical phy proteins is composed of the three domains PAS-GAF-PHY (PGP, PAS = Per Arnt Sim; GAF = cGMP-specific phosphodiesterases, cyanobacterial adenylate cyclases, and formate hydrogen lyase transcription activator FhlA; PHY = Phytochrome domain, see also Appendix A1). [36] Phys are photochromic proteins, which means that they can switch between two forms that maximally absorb in the red and in the far-red/near-infrared regions of the light spectrum (for canonical phy proteins), named respectively Pr and Pfr. Illumination triggers photoisomerisation of the C15=C16 double bond between rings C and D of the bilin chromophore within few ps, [37,38] followed by conformational rearrangements of chromophore and protein. [39,40]

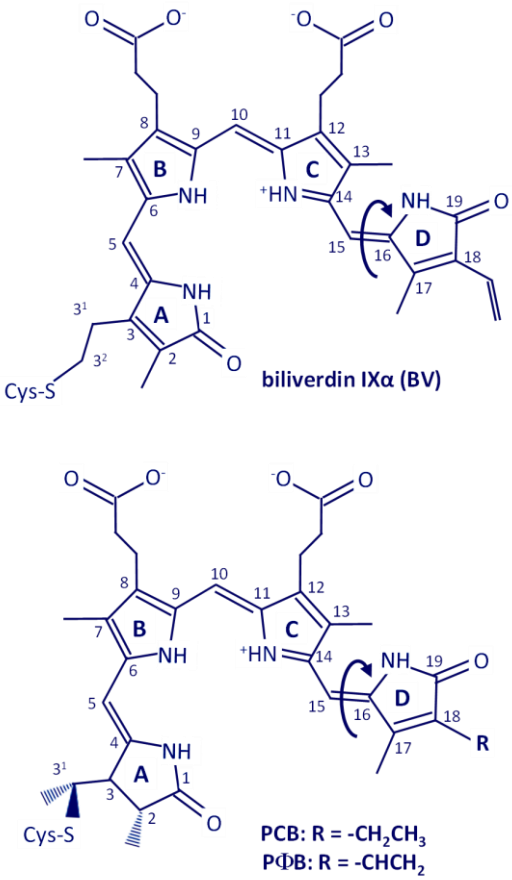

Figure 1: Open-chain tetrapyrroles (bilins) in phytochromes. Top: biliverdin IXα (BV). Bottom: phytochromobilin (PΦB) and phycocyanobilin (PCB). The chromophores are presented in protein-bound form. Photoisomerisation around the double bond 15=16 is indicated by an arrow.

However, structural changes associated with transient intermediates are poorly understood: for both Pfr-to-Pr and Pr-to-Pfr routes it is up to now unclear how chromophore isomerisation leads to signal transfer in the protein. [41] In the photoconversion, photoisomerisation results in the formation of at least two intermediates, named Lumi and Meta (-R or –F depending on the Pr-to-Pfr or Pfr-to-Pr conversion) (Figure 2). [42] Even though a PAS-GAF fragment of a BphP was the first phy to be crystallised, [43] the BphP family is much less characterised than plant and cyanobacterial phys, especially with regard to kinetics of light-triggered reactions and the nature of optical intermediates.

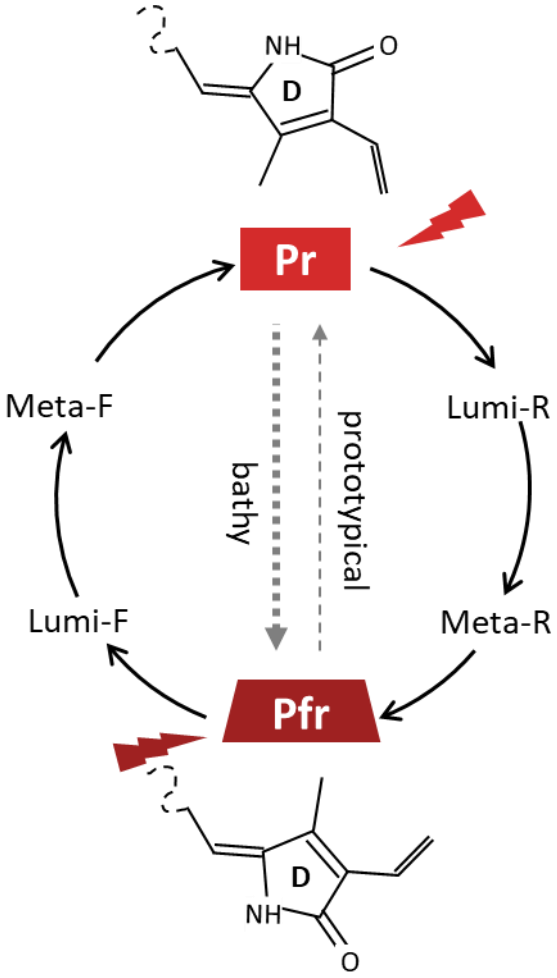

Figure 2: Simplified photocycle of BphPs. Upon RL irradiation, the BphP undergoes a photocycle that can be reverted by FR light, involving the formation of at least two intermediates for each route. Adapted from [44].

In the BV-binding phys, named BphPs, [45,46] the chromophore is embedded within the GAF domain as in the other phys, but in the case of BphPs it is anchored to a cysteine of the N-terminal PAS domain through its 3" position. [34] As plant phys, prototypical BphPs are photochromic systems: Pr is the parental state and can be photoswitched to the Pfr state, with thermal recovery in the dark within minutes to days. Instead, the so called "bathy" phys have their dark-adapted state in the Pfr form and Pr can be only partially photoswitched to Pfr; the thermal Pr-to-Pfr recovery represents here an efficient pathway. Given the photochromism, interconversion between Pr and Pfr states in these proteins can be followed by time-resolved spectroscopy techniques, such as laser flash photolysis.[47–49]

This thesis work presents a full scale analysis of the kinetic processes in the μs-to-ms time scale for the conversion between the parental state and the photoproduct and *vice versa* for some BphPs, representative of the BphP superfamily (Figure 3):

- *Pst*BphP1 from *Pseudomonas siringae* pv. *tomato*. This bacterium is an agronomically important pathogen of tomato plants, for which photoreceptors have been demonstrated to downregulate virulence and infectiveness during infection in *Arabidopsis thaliana.* [2]
- *Pa*BphP from the important human [50] and plant pathogen *Pseudomonas aeruginosa*. Plant pathogenicity of *P.aeruginosa* has long been known, [51] typical symptoms include promotion of fruit rotting [52] and inhibition of seed germination [53], although this microorganism does not produce normally large damages unless high temperature and humidity are present.
- *Xc*BphP-PGP from *Xanthomonas campestris* pv. *campestris*. This is a plant pathogen for which the phytochrome *Xc*BphP downregulates light-mediated activities that contribute to virulence, upregulating traits that trigger plant defense. [1]
- FphAN753 from the fungus *Aspergillus nidulans*. This fungus is a not plant-associated, but closely related to plant pathogens and produces aflatoxins [1]. The fungal BphP-like FphA is a RL/FRL sensor that represses sexual

development and mycotoxin synthesis, [54] and recently has been identified as a temperature sensor [55]. Furthermore, FphA binds BV as a chromophore, and exhibits the same photochromism of BphPs. [56]

- *Mr*BphP1 from *Methylobacterium radiotolerans*. Alpha-proteobacteria of the genus *Methylobacterium* are pink-pigmented facultative methylotrophs (PPFMs), colored due to the presence of carotenoids and able to feed on carbon compounds, e.g. methanol and methylamine; [6] several species are also resistant to γ-radiation [7,8]. *Methylobacteria* mainly reside in the phyllopshere, where thay can utilise methanol produced in the demethylation of macromolecules, principally during pectin metabolism. [12]

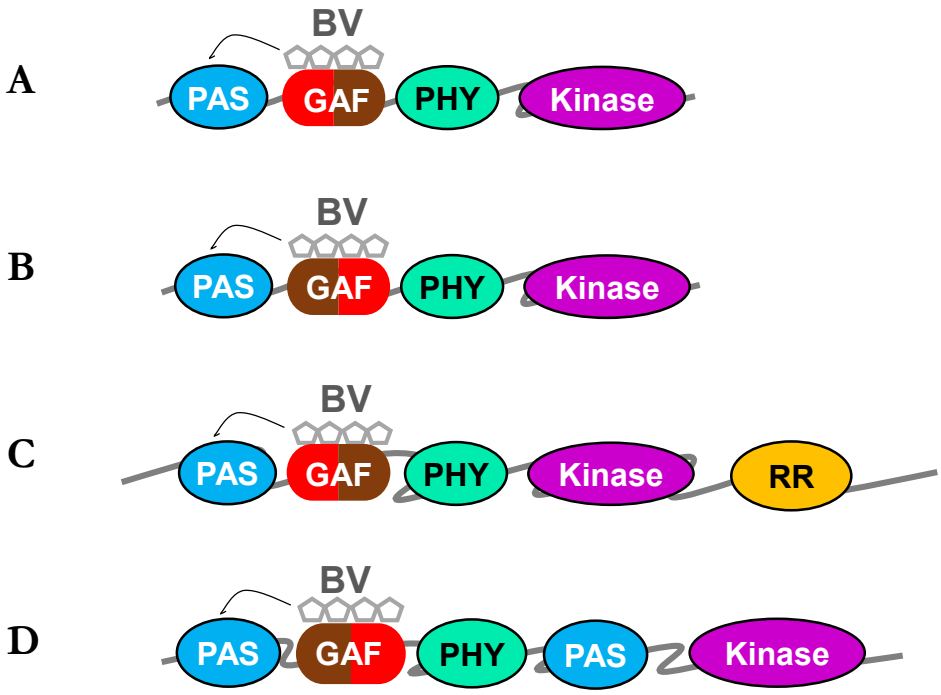

Figure 3: Domain architecture of the here studied BphPs. A: *Pst*BphP1, *Mr*BphP; B: *Pa*BphP; C: FphAN753; D: *Xca*BphP. The BV chromophore is embedded in the GAF domain and a black line indicates that, different to canonical plant phys, it is bound to the N-terminal PAS-domain. The colours of the GAF domains indicate the correct photochromism. Kinase = His-kinase of the two-component signal transduction system; see Appendix A1 for a full legenda.

Sensing blue light: a new LOV protein from *Methylobacterium radiotolerans*

LOV domains are small photosensing units for BL of *ca.* 100-110 aa, with a quite compact α/β structure, first discovered as part of plant phototropin photoreceptors (phot). [57] They belong to the PAS superfamily and preserve the typical, globular α/β fold (LOV core), flanked by variable and often helical N- and C-terminal extensions, denominated A'α and Jα respectively, involved in signal transduction (Figure 4). The chromophore is most often FMN (flavin mononucleotide), albeit fungal LOV domains preferentially bind FAD (flavin adenine dinucleotide) thanks to an insertion between Eα and Fα. The cysteine responsible for the photocycle is located at the very end of the Dα-Eα loop. [58] The pleated β-sheet builds a quite hydrophobic pavement for the face of the isoalloxazine ring, just opposite to the reactive cysteine. At the same time, it bears polar residues, which form a well-defined HB network with C2=O, N3 and C4=O, comprising conserved asparagine and glutamine residues. [58,59]

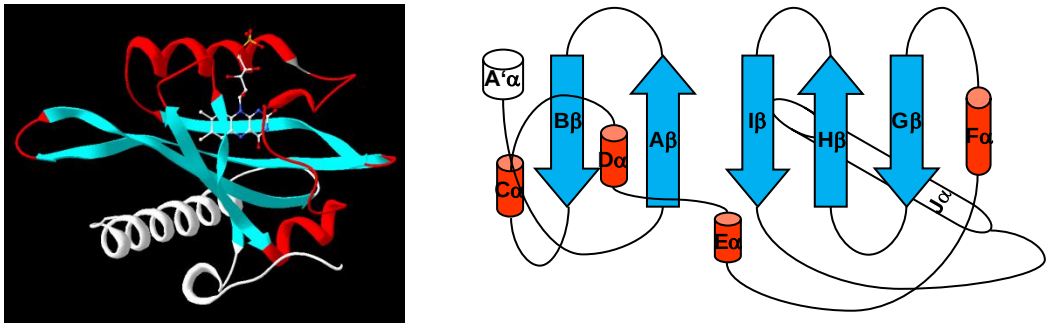

Figure 4: Left, structure of a typical LOV-domain (As-phot1-LOV2 from *Avena sativa*, Protein Databank cooordinates 2VOU), showing the location of the LOV α/β core, enclosing the FMN chromophore, the effector A'α and Jα helices on adjacent faces of the β-sheet; right, topology of LOV domains with usual nomenclature of secondary structure elements. Arrows: strands; cylinders: helices. The caps at the N- or C-terminal of the LOV core are whited out. Relative size of loops, strands and helices are not respected.

As full-length proteins, LOV photosensors have a highly modular structure: the light-sensing domain is linked to a variety of effector and regulator modules, which ultimately determine the functionality of the protein itself as a light-regulated device. Standalone LOV domains without linked effectors are also well represented [59](referred to as "short-LOV"). As with BphPs, LOV-proteins photochemistry is better understood than their biological functions, especially for bacteria. [1] The photocycle is well described in [58] and summarised in

Figure 5. The dark-adapted state of LOV domains absorbs maximally at *ca.* 450 nm and shows the typical green fluorescence of flavins, with Φ_F = 0.15-0.2. As a consequence of BL excitation, the chromophore triplet-state is formed with a quantum yield of *ca.* Φ_P up to 0.7 within few nanoseconds. The triplet state absorbs in the red spectral region (maximum ca. 660-720 nm) and decays within few μs into the so-called photo-adduct, LOV_{390}. According to this generally accepted model, radical recombination is coupled to protonation of N5 and subsequent formation of a FMN-C4a-Cys covalent bond in LOV_{390}. [58] Quantum yield for LOV_{390} formation (Φ_{390}) is 0.3-0.6 with BL excitation, but is lower upon UVA activation. In LOV_{390} fluorescence is completely lost, as well as the sharp vibrational structure in the absorption spectrum. Protonation of N5 in LOV_{390} triggers a flipping of the lateral chain of a conserved hydrogen-bonding glutamine located on strand Iβ, the first step in signal propagation to the LOV domain surface. [60–69] In turn, water-assisted deprotonation of N5 is considered as the rate limiting step during thermal recovery of LOV_{390} to the dark-adapted state and completion of the photocycle. For this process, time constants (τ_{rec}) on the second-to-hour or even days' time-scale at room temperature have been reported. [70–72] Besides recovering thermally, LOV domains can be driven into a photoequilibrium with violet (ca. 400 nm) or UVA light (ca. 360 nm), whereby LOV_{390} can be photoswitched back to LOV_{450} in a fast reaction (< 10 ns) and with low efficiency (ca. 5-10%), meaning that LOV domains are intrinsically photochromic.

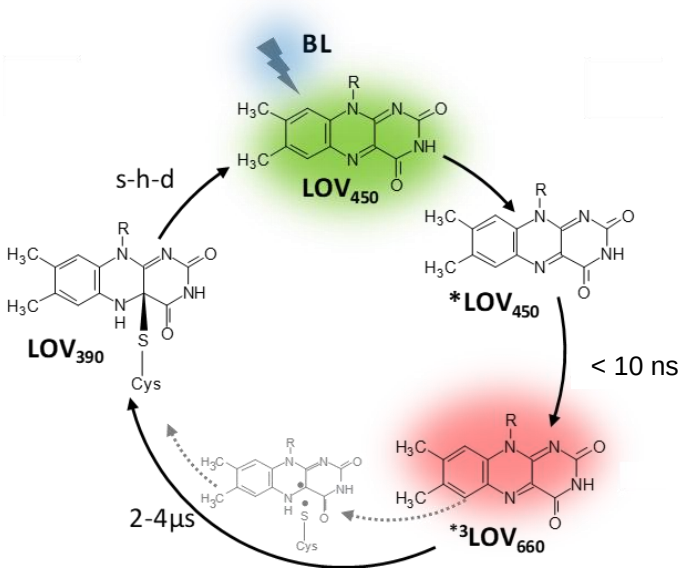

Figure 5: Typical photocycle of LOV-domains, with the indication of the FMN binding scheme. The green colour in LOV_{450} indicates its fluorescence in the green spectral region, while the red colour in $^{*3}LOV_{660}$ shows its absorption in the red spectral region. The alternative route from LOV_{390} to LOV_{450} by violet or UVA excitation light is not shown, for a complete scheme see [73].

LOV proteins are currently known to include diverse families, which vary on the basis of their effector domain: LOV proteins in plant-associated bacteria usually have the structure LOV-Kinase-RR (RR = response regulator). [1]

An interesting feature comes from the possibility to use modified versions of BL-sensing LOV domains as generators for singlet oxygen (SO), a reactive species which is a primary agent of photooxidative stress in microorganisms and can be applied in the so called photodynamic therapy: the triplet state of the FMN (here photosensitiser PS) performs ET to oxygen via the collisional Dexter mechanism, [i] leading to transition of oxygen from the triplet ground state to the strong-oxidant excited state SO. [74] This is a diffusion-limited mechanism, thus long-lived excited states of the PS chromophore are relevant. The triplet state of LOV-bound FMN

[i] It is important to mention that this is known as type-II mechanism of ROS (Reactive Oxygen Species) formation. A type-I mechanism is also possible for a photosensitiser, through electron transfer from a donor to produce a radical anion, which can react with the molecular oxygen to produce the superoxide radical anion and then other ROS, such as hydrogen peroxide and hydroxyl radicals. [76]

has an energy level of 200 kJ/mol and can perform energy transfer to oxygen to generate SO, which lies at 94 kJ/mol above the ground state of oxygen (Figure 6, adapted from [58]).

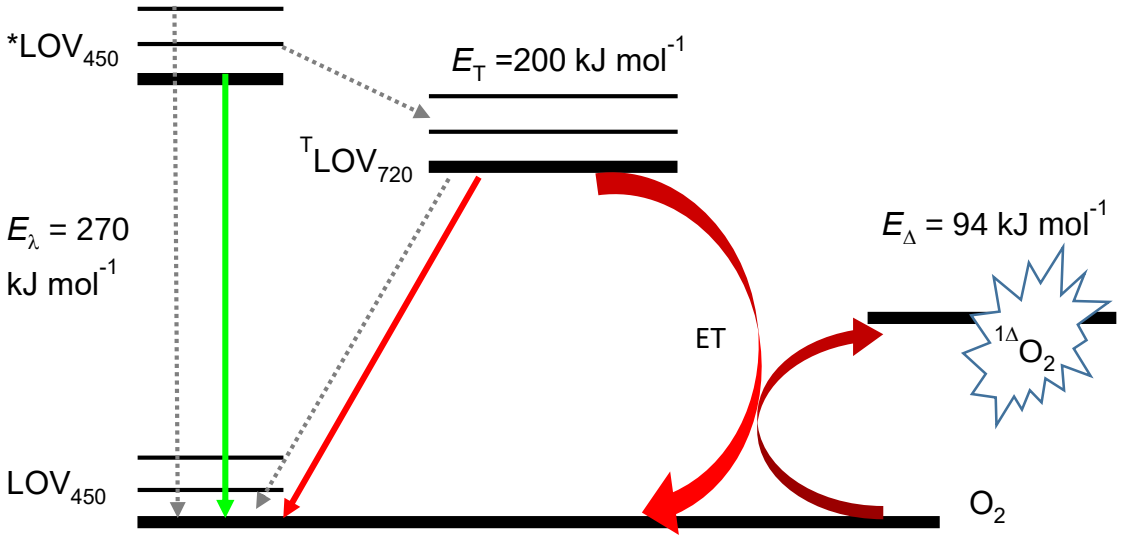

Figure 6: Scheme of processes involved in SO generation by a LOV-based photosensitiser. $^{T}LOV_{720}$ contains ^{T}FMN and is able to perform energy tranfer to the oxygen triplet state via a diffusion-limited process to form the singlet oxygen reactive species $^{1\Delta}O_2$.

In the WT (wild type) LOV-domains, formation of the photoadduct occurs in 2-4 µs, so that the formation of SO is negligible. Thus, a prerequisite of a LOV-based SO photosensitiser is the reactive-cysteine mutation to prevent adduct formation and extend the lifetime of the FMN triplet state, plus other mutations aiming at minimising FMN-triplet quenching by sorrounding aa and increasing oxygen accessibility to the chromophore cavity. [75–77] During the last years, starting from the miniSOG (mini Singlet Oxygen Generator) scientists designed an evergrowing pool of enhaced variants of these protein to increase Φ_Δ, which for miniSOG is very low around 0.03 [78]: the latest derivative is called SOPP3 and presently is the best photosensitising protein with $\Phi_\Delta = 0.6$ [79]. This enhancement was primarily due to the mutation of W81 (localised on strand Hb and conserved in ca. 75% of LOV domains[80]), which was identified as the most efficient electron donor for the triplet-

state quenching, resulting in a reduced value of Φ_Δ. However, to obtain these values from these variants, more than one mutation have been necessary, often resulting in low stability towards prolonged illumination: [77] as a goal, it could be interesting to identify robust LOV-based photosensitisers that can efficiently produce SO with only one mutation.

Besides the study of *Mr*BphP1 (*vide supra*), in this project a new BL photoreceptor from *Methylobacterium radiotolerans* has been investigated, *Mr*4511. This is a full-length protein composed of a LOV core with N- and C- terminal extensions. Besides the WT form, several variants have been studied, i-e- I37V, Q112W, C71X (X=G or X=S), C71X/Q112W. All these proteins were studied with steady-state and time-resolved biophysical techniques; in particular, for the C71X variants, their potential as SO generators has been explored.

Bibliography

1. Beattie, G. A., Hatfield, B. M., Dong, H. & McGrane, R. S. Seeing the Light: The Roles of Red- and Blue-Light Sensing in Plant Microbes. *Annu. Rev. Phytopathol.* **56**, 41–66 (2018).

2. Ricci, A., Dramis, L., Shah, R., Gärtner, W. & Losi, A. Visualizing the relevance of bacterial blue- and red-light receptors during plant-pathogen interaction. *Environ. Microbiol. Rep.* **7**, 795–802 (2015).

3. Bonomi, H. R. *et al.* Xanthomonas campestris attenuates virulence by sensing light through a bacteriophytochrome photoreceptor . *EMBO Rep.* **17**, 1565–1577 (2016).

4. Chernov, K. G., Redchuk, T. A., Omelina, E. S. & Verkhusha, V. V. Near-Infrared Fluorescent Proteins, Biosensors, and Optogenetic Tools Engineered from Phytochromes. *Chem. Rev.* **117**, 6423–6446 (2017).

5. Ziegler, T. & Möglich, A. Photoreceptor engineering. *Front. Mol. Biosci.* **2**, 30 (2015).

6. Boden, R. Methanotrophy, Methylotrophy, the Human Body, and Disease. in *Health Consequences of Microbial Interactions with Hydrocarbons, Oils, and Lipids* 1–20 (Springer International Publishing, 2019). doi:10.1007/978-3-319-72473-7_19-1

7. Nogueira, F., Luisa Botelho, M. & Tenreiro, R. Radioresistance studies in Methylobacterium spp. *Radiat. Phys. Chem.* **52**, 15–19 (1998).

8. Shuryak, I. Review of microbial resistance to chronic ionizing radiation exposure under environmental conditions. *Journal of Environmental Radioactivity* **196**, 50–63 (2019).

9. Green, P. N. & Ardley, J. K. Review of the genus Methylobacterium and closely related organisms: a proposal that some Methylobacterium species be reclassified into a new genus, Methylorubrum gen. nov. *Int. J. Syst. Evol. Microbiol.* **68**, 2727–2748 (2018).

10. Van Dien, S. J., Marx, C. J., O'Brien, B. N. & Lidstrom, M. E. Genetic Characterization of the Carotenoid Biosynthetic Pathway in Methylobacterium extorquens AM1 and Isolation of a Colorless Mutant. *Appl. Environ. Microbiol.* **69**, 7563–7566 (2003).

11. Imhoff, J. F., Rahn, T., Künzel, S. & Neulinger, S. C. Photosynthesis is widely distributed among Proteobacteria as demonstrated by the phylogeny of PufLM reaction center proteins. *Front. Microbiol.* **8**, (2018).

12. Dorokhov, Y. L., Sheshukova, E. V. & Komarova, T. V. Methanol in Plant Life. *Front. Plant Sci.* **9**, 1623 (2018).

13. Sy, A. *et al.* Methylotrophic Methylobacterium bacteria nodulate and fix nitrogen in symbiosis with legumes. *J. Bacteriol.* **183**, 214–220 (2001).

14. Kumar, M., Tomar, R. S., Lade, H. & Paul, D. Methylotrophic bacteria in sustainable agriculture. *World J. Microbiol. Biotechnol.* **32**, 120 (2016).

15. Carvalho, S. D. & Castillo, J. A. Influence of Light on Plant–Phyllosphere Interaction. *Frontiers in Plant Science* **9**, (2018).

16. Kumar, M. *et al.* Biodiversity of methylotrophic microbial communities and their potential role in mitigation of abiotic stresses in plants. *Biologia* **74**, 287–308 (2019).

17. Dourado, M. N., Camargo Neves, A. A., Santos, D. S. & Araújo, W. L. Biotechnological and agronomic potential of endophytic pink-pigmented methylotrophic methylobacterium spp. *BioMed Research International* **2015**, (2015).

18. Kovaleva, J., Degener, J. E. & Van Der Mei, H. C. Methylobacterium and its role in health care-associated infection. *Journal of Clinical Microbiology* **52**, 1317–1321 (2014).

19. Meyer, T. E. *et al.* The growing family of photoactive yellow proteins and their presumed functional roles. *Photochem. Photobiol. Sci.* **11**, 1495 (2012).

20. Raffelberg, S. *et al.* The amino acids surrounding the flavin 7a-methyl group determine the UVA spectral features of a LOV protein. *Biol. Chem.* **394**, 1517–28 (2013).

21. Losi, A., Mandalari, C. & Gärtner, W. The Evolution and Functional Role of Flavin-based Prokaryotic Photoreceptors. *Photochem. Photobiol.* **91**, 1021–1031 (2015).

22. Kaushik, M., Sharma, R., Veetil, S., Srivastava, S. & Kateriya, S. Modular Diversity of the BLUF Proteins and Their Potential for the Development of Diverse Optogenetic Tools. *Appl. Sci.* **9**, 3924 (2019).

23. Kwak, M. J. *et al.* Genome information of Methylobacterium oryzae, a plant-probiotic methylotroph in the phyllosphere. *PLoS One* **9**, (2014).

24. Harris, A. *et al.* A new group of eubacterial light-driven retinal-binding proton pumps with an unusual cytoplasmic proton donor. *Biochim. Biophys. Acta - Bioenerg.* **1847**, 1518–1529 (2015).

25. Yoshida, S., Hiradate, S., Koitabashi, M., Kamo, T. & Tsushima, S. Phyllosphere Methylobacterium bacteria contain UVA-absorbing compounds. *J. Photochem. Photobiol. B Biol.* **167**, 168–175 (2017).

26. Iguchi, H. *et al.* KaiC family proteins integratively control temperature-dependent UV resistance in Methylobacterium extorquens AM1. *Environ. Microbiol. Rep.* **10**, 634–643 (2018).

27. Geen, P. N. & Bousfield, I. J. Emendation of Methylobacterium Patt, Cole, and Hanson 1976; Methylobacterium rhodinum (Heumann 1962) comb. nov. corrig.; Methylobacterium radiotolerans (Ito and Iizuka 1971) comb. nov. corrig.; and Methylobacterium mesophilicum (Austin and Goodfellow 1979. *Int. J. Syst. Bacteriol.* **33**, 875–877 (1983).

28. Nishimura, Y., Mukasa, S., Iizuka, H. & Shimada, K. Isolation and characterization of bacteriochlorophyll-protein complexes from an aerobic bacterium, Pseudomonas radiora. *Arch. Microbiol.* **152**, 1–5 (1989).

29. Hanada, S. Anoxygenic photosynthesis —A photochemical reaction that does not contribute to oxygen reproduction—. *Microbes Environ.* **31**, 1–3 (2016).

30. Cordovana, M., Deni, A., Kostrzewa, M., Abdalla, M. & Ambretti, S. First report of Methylobacterium radiotolerans bacteraemia identified by MALDI-TOF mass spectrometry. *New Microbes and New Infections* **30**, (2019).

31. Fankhauser, C. The Phytochromes, a Family of Red/Far-red Absorbing Photoreceptors. *Journal of Biological Chemistry* **276**, 11453–11456 (2001).

32. Rockwell, N. C. *et al.* Eukaryotic algal phytochromes span the visible spectrum. *Proc. Natl. Acad. Sci. U. S. A.* **111**, 3871–3876 (2014).

33. Hughes, J. *et al.* A prokaryotic phytochrome [6]. *Nature* **386**, 663 (1997).

34. Anders, K. & Essen, L.-O. The family of phytochrome-like photoreceptors: diverse, complex and multi-colored, but very useful. *Curr. Opin. Struct. Biol.* **35**, 7–16 (2015).

35. Legris, M. *et al.* Phytochrome B integrates light and temperature signals in Arabidopsis. *Science* **354**, 897–900 (2016).

36. Nagano, S. From photon to signal in phytochromes: similarities and differences between prokaryotic and plant phytochromes. *J. Plant Res.* **129**, 123–135 (2016).

37. Müller, M. G., Lindner, I., Martin, I., Gärtner, W. & Holzwarth, A. R. Femtosecond Kinetics of Photoconversion of the Higher Plant Photoreceptor Phytochrome Carrying Native and Modified Chromophores. *Biophys. J.* **94**, 4370–4382 (2008).

38. Ihalainen, J. A., Takala, H. & Lehtivuori, H. Fast Photochemistry of Prototypical Phytochromes-A Species vs. Subunit Specific Comparison. *Front. Mol. Biosci.* **2**, 75 (2015).

39. Björling, A. *et al.* Structural photoactivation of a full-length bacterial phytochrome. *Sci. Adv.* **2**, e1600920 (2016).

40. Heyes, D. J. *et al.* Light-induced structural changes in a full-length cyanobacterial phytochrome probed by time-resolved X-ray scattering. *Commun. Biol.* **2**, 1 (2019).

41. Ihalainen, J. A. *et al.* Chromophore–Protein Interplay during the Phytochrome Photocycle Revealed by Step-Scan FTIR Spectroscopy. *J. Am. Chem. Soc.* **140**, 12396–12404 (2018).

42. Buhrke, D., Kuhlmann, U., Michael, N. & Hildebrandt, P. The Photoconversion of Phytochrome Includes an Unproductive Shunt Reaction Pathway. *ChemPhysChem* **19**, 566–570 (2018).

43. Wagner, J. R., Brunzelle, J. S., Forest, K. T. & Vierstra, R. D. A light-sensing knot revealed by the structure of the chromophore-binding domain of phytochrome. *Nature* **438**, 325–331 (2005).

44. Consiglieri, E. *et al.* Dynamics and efficiency of photoswitching in biliverdin-binding phytochromes. *Photochem. Photobiol. Sci.* **18**, 2484–2496 (2019).

45. Gourinchas, G., Etzl, S. & Winkler, A. Bacteriophytochromes – from informative model systems of phytochrome function to powerful tools in cell biology. *Curr. Opin. Struct. Biol.* **57**, 72–83 (2019).

46. Auldridge, M. E. & Forest, K. T. Bacterial phytochromes: More than meets the light. *Crit. Rev. Biochem. Mol. Biol.* **46**, 67–88 (2011).

47. Braslavsky, S. E., Gärtner, W. & Schaffner, K. Phytochrome photoconversion. *Plant, Cell Environ.* **20**, 700–706 (1997).

48. Foerstendorf, H., Lamparter, T., Hughes, J., Gärtner, W. & Siebert, F. The Photoreactions of Recombinant Phytochrome from the Cyanobacterium Synechocystis: A Low-Temperature UV-Vis and FT-IR Spectroscopic Study. *Photochem. Photobiol.* **71**, 655–661 (2000).

49. Chizhov, I., Zorn, B., Manstein, D. J. & Gärtner, W. Kinetic and Thermodynamic Analysis of the Light-induced Processes in Plant and Cyanobacterial Phytochromes. *Biophys. J.* **105**, 2210–2220 (2013).

50. De Bentzmann, S. & Plésiat, P. The Pseudomonas aeruginosa opportunistic pathogen and human infections. *Environ. Microbiol.* **13**, 1655–1665 (2011).

51. Elrod, R. P. & Braun, A. C. Pseudomonas aeruginosa: Its Rôle as a Plant Pathogen. *J. Bacteriol.* **44**, 633–45 (1942).

52. Schroth, M. N., Cho, J. J., Green, S. K. & Kominos, S. D. Epidemiology of Pseudomonas aeruginosa in agricultural areas. *J. Med. Microbiol.* **67**, 1191–1201 (2018).

53. Chahtane, H. *et al.* The plant pathogen Pseudomonas aeruginosa triggers a DELLA-

dependent seed germination arrest in Arabidopsis. doi:10.7554/eLife.37082.001

54. Purschwitz, J. *et al.* Functional and physical interaction of blue- and red-light sensors in Aspergillus nidulans. *Curr. Biol.* **18**, 255–9 (2008).

55. Yu, Z. *et al.* Two hybrid histidine kinases, TcsB and the phytochrome FphA, are involved in temperature sensing in Aspergillus nidulans . *Mol. Microbiol.* (2019). doi:10.1111/mmi.14395

56. Brandt, S., von Stetten, D., Günther, M., Hildebrandt, P. & Frankenberg-Dinkel, N. The fungal phytochrome FphA from Aspergillus nidulans. *J. Biol. Chem.* **283**, 34605–14 (2008).

57. Losi, A. Flavin-based Blue-light Photosensors: A Photobiophysics Update. *Photochem. Photobiol.* **83**, 1283–1300 (2007).

58. Losi, A. & Gärtner, W. Solving Blue Light Riddles: New Lessons from Flavin-binding LOV Photoreceptors. *Photochem. Photobiol.* **93**, 141–158 (2017).

59. Glantz, S. T. *et al.* Functional and topological diversity of LOV domain photoreceptors. *Proc. Natl. Acad. Sci. U. S. A.* **113**, E1442-1451 (2016).

60. Crosson, S. & Moffat, K. Photoexcited structure of a plant photoreceptor domain reveals a light-driven molecular switch. *Plant Cell* **14**, 1067–1075 (2002).

61. Nozaki, D. *et al.* Role of Gln1029 in the Photoactivation Processes of the LOV2 Domain in *Adiantum* Phytochrome3 †. *Biochemistry* **43**, 8373–8379 (2004).

62. Zoltowski, B. D. *et al.* Conformational switching in the fungal light sensor vivid. *Science (80-.).* **316**, 1054–1057 (2007).

63. Möglich, A. & Moffat, K. Structural Basis for Light-dependent Signaling in the Dimeric LOV Domain of the Photosensor YtvA. *J. Mol. Biol.* **373**, 112–126 (2007).

64. Matsuoka, D., Iwata, T., Zikihara, K., Kandori, H. & Tokutomi, S. Primary Processes During the Light-signal Transduction of Phototropin. *Photochem. Photobiol.* (2006). doi:10.1562/2006-03-29-ra-861

65. Nash, A. I., Ko, W. H., Harper, S. M. & Gardner, K. H. A conserved glutamine plays a central role in LOV domain signal transmission and Its duration. *Biochemistry* **47**, 13842–13849 (2008).

66. Avila-Pérez, M. *et al.* In vivo mutational analysis of YtvA from bacillus subtilis. Mechanism of light activation of the general stress response. *J. Biol. Chem.* **284**, 24958–24964 (2009).

67. Herrou, J. & Crosson, S. Function, structure and mechanism of bacterial photosensory LOV proteins. *Nature Reviews Microbiology* **9**, 713–723 (2011).

68. Peter, E., Dick, B. & Baeurle, S. A. Illuminating the early signaling pathway of a fungal light-oxygen-voltage photoreceptor. *Proteins Struct. Funct. Bioinforma.* **80**, 471–481 (2012).

69. Freddolino, P. L., Gardner, K. H. & Schulten, K. Signaling mechanisms of LOV domains: New insights from molecular dynamics studies. *Photochem. Photobiol. Sci.* **12**, 1158–1170 (2013).

70. Pennacchietti, F. *et al.* The Dark Recovery Rate in the Photocycle of the Bacterial Photoreceptor YtvA Is Affected by the Cellular Environment and by Hydration. *PLoS One* **9**, e107489 (2014).

71. Endres, S. *et al.* Structure and function of a short LOV protein from the marine phototrophic bacterium Dinoroseobacter shibae. *BMC Microbiol.* **15**, (2015).

72. Kasahara, M., Torii, M., Fujita, A. & Tainaka, K. FMN binding and photochemical properties of plant putative photoreceptors containing two LOV domains, LOV/LOV proteins. *J. Biol. Chem.* **285**, 34765–34772 (2010).

73. Losi, A. *et al.* A photochromic bacterial photoreceptor with potential for super-resolution microscopy. *Photochem. Photobiol. Sci.* **12**, 231–235 (2013).

74. Baptista, M. S. *et al.* Type I and Type II Photosensitized Oxidation Reactions: Guidelines and Mechanistic Pathways. *Photochemistry and Photobiology* **93**, 912–919 (2017).

75. Torra, J. *et al.* Tailing miniSOG: structural bases of the complex photophysics of a flavin-binding singlet oxygen photosensitizing protein. *Sci. Rep.* **9**, 2428 (2019).

76. Endres, S. *et al.* An optogenetic toolbox of LOV-based photosensitizers for light-driven killing of bacteria. *Sci. Rep.* **8**, 15021 (2018).

77. Westberg, M., Etzerodt, M. & Ogilby, P. R. Rational design of genetically encoded singlet oxygen photosensitizing proteins. *Curr. Opin. Struct. Biol.* **57**, 56–62 (2019).

78. Ruiz-González, R. *et al.* Singlet oxygen generation by the genetically encoded tag minisog. *J. Am. Chem. Soc.* **135**, 9564–9567 (2013).

79. Westberg, M., Bregnhøj, M., Etzerodt, M. & Ogilby, P. R. No Photon Wasted: An Efficient and Selective Singlet Oxygen Photosensitizing Protein. *J. Phys. Chem. B* **121**, 9366–9371 (2017).

80. Losi, A., Mandalari, C. & Gärtner, W. From plant infectivity to growth patterns: The role of blue-light sensing in the prokaryotic world. *Plants* **3**, 70–94 (2014).

Materials and Methods

Introduction

The purified proteins were investigated by a set of spectroscopic methods. Measurements were performed in the dark or, when possible, under safety light conditions, in order to prevent unintended photochemistry of the sample. For optical measurements, fluorescence quartz cuvettes with (10×4) mm path length were used. Solutions were always filtered using 0.22 μm PES syringe filters before experiments in order to remove scattering particles that could deteriorate the quality of the recorded data. During spectroscopic measurements, samples were continuously mantained at the desired temperature with water from thermostated baths. For measurements in D_2O, samples were buffer-exchanged on gel filtration columns (CentriPure P25, EMP Biotech) or by centrifugation with Amicon® centrifugal filters using D_2O-based NaPi buffer as the eluent.

Materials

*Xc*BphP-PGP was provided by Hernán R. Bonomi, Fundación Istituto Leloir, Buenos Aires, Argentina, and Norbert Michael, Technische Universität Berlin, Germany. [1] Proteins used as references in fluorescence and photoconversion quantum yields (*Syn*Cph1, *Slr*1393g3) and all the other proteins investigated in this work were kindly provided by prof. Wofgang Gärtner, University of Leipzig, Germany. The samples were produced and purified according to standard protocols by Alexander Gutt, Max-Planck-Institute for Chemical Energy Conversion, Mülheim an der Ruhr, Germany (*Pst*BphP1, *Pa*BphP, FphAN753) [2] and Qianzhao Xu,

University of Leipzig, Germany (*Mr*4511 WT and mutants, *Mr*BphP1), as briefly described below.

The gene encoding full-length *Pst*BphP1 (UNIPROT code Q885D3, 772 aa) from *Pseudomonas syringae* pv. *tomato* strain DC3000 (strain ATCC BAA-871 / DC3000) was expressed from the pET52 3C/LIC vector. [3] *Pa*BphP from *Pseudomonas aeruginosa* strain JCM 14847 (also known as ATCC 15692 / DSM 22644 / CIP 104116 / JCM 14847 / LMG 12228 / 1C / PRS 101 / PAO1, UNIPROT code Q9HWR3, 728 aa) was cloned into pET24a vector as the complete photosensory module (aa positions 1-497) for expression. [4] FphAN753 from *Aspergillus nidulans* (also known as *Emericella nidulans*, UNIPROT code Q5K039, 1280 aa) was also expressed as the complete photosensory module (aa position 1-753) pASK-IBA3 vector. [4] The truncated *Xcc*BphP-ΔPAS9 = *Xcc*BphP-PGP (residues 1-511) from *Xanthomonas campestris* pv. *campestris* DSM 3586 (strain ATCC 33913 / DSM 3586, NCPPB 528 / LMG 568 / P 25, UNIPROT code Q8P3C2, 634 aa) was produced using a pET24A expression vector. [1,4] The gene encoding full-length *Mr*4511 (UNIPROT code B1M516, 164 aa) from *Methylobacterium radiotolerans* (strain JCM 2831, also known as strain ATCC 27329 / DSM 1819 / JCM 2831 / NBRC 15690 / NCIMB 10815 / 0-1) was cloned into pET30 vector for expression. *Syn*Cph1 from *Synechocistis sp.* (strain PCC 6803 / Kazusa, UNIPROT code Q55168, 748 aa) and the GAF3 (g3) PCB-binding domain (residues 441-597) *Slr*1393g3 from *Synechocystis* CBCR sp. PCC 6803, (UNIPROT code P73184, 974 aa), were produced as N-terminal 6xHis-tag using a pET30 expression vector. [1] For all the protein expressed, the ligation products were transformed into *E. Coli* BL21 cells. The BphPs and *Mr*4511 were furnished with C- (*Pst*BphP1, *Mr*BphP1, *Mr*4511) or N-terminal (*Pa*BphP) 6xHis-tags, the fungal protein carried an N-terminal Strep-tag.

For spectroscopic measurements, proteins were dissolved in buffers as described in Table 1.

Table 1: Composition of buffer solutions used for spectroscopic measurements.

	Buffer composition	pH
*Pst*BphP1	50 mM Tris, 200 mM NaCl	7.5
*Pa*BphP	50 mM Tris, 200 mM NaCl	7.5
FphAN753	100 mM Tris, 15 mM NaCl, 1 mM EDTA	8
*Xc*BphP-PGP	50 mM Tris, 200 mM NaCl	7.7
*Mr*4511	10 mM NaPi, 100 mM NaCl	8
*Mr*BphP1	50 mM Tris, 200 mM NaCl	8
*Syn*Cph1	10 mM NaPi, 10 mM NaCl	7.5
*Slr*1393g3	10 mM NaPi, 10 mM NaCl	7.5

Methods

Absorbance and emission spectroscopy

"Steady state absorption spectra and dark recovery kinetics were recorded at (20 ± 1) °C with a Jasco 7850 UV/Vis spectrophotometer (Jasco Europe, Cremella, LC, Italy), while steady-state fluorescence measurements were performed with a Perkin-Elmer LS50 luminescence spectrometer (PerkinElmer, Waltham, MA, USA). Photoconversions between the parental state and the photoproduct were performed by exhaustive irradiation from LEDs of the appropriate wavelengths (Roithner LaserTechnik, Wien, Austria)." [4] For *circular dichroism* (CD) measurements a Jasco J715 spectropolarimeter was used; measurements were performed in the far ultraviolet region (190-250 nm) at (20 ± 1) °C, with a 0.1 cm of optical path, subtracting the buffer spectrum as a baseline.

The fluorescence quantum yields (Φ_F) were measured through a comparative way, [4] using as references: *Syn*Cph1-R (Φ_F = 0.024 [5]), *Xc*BphP-PGP-R (Φ_F = 0.022 [1]), FMN (Φ_F = 0.26 [6]).

Photoconversion quantum yields (Φ_P) between parental state and photoproduct and viceversa were determined at (20 ± 1) °C as previously described, [7,1] by monitoring the formation dynamics of the two photoactive forms during illumination with LEDs of the proper wavelength; kinetics were recorded as the rise of absorbance of the photoproduct; *Xc*BphP-PGP (Φ_P = 0.12 for both directions [1]), *Slr*1393g3 (Φ_P = 0.09 for the Red to Green route [7]), YtvA (Φ_P = 0.49 for the adduct formation) *Mr*BphP1 (Φ_P = 0.2 here measured for the Red to Far red route) served as references. [4]

Absorption coefficients (ε) of *Mr*-proteins were determined by diluting stock buffer solutions of *Mr*4511 proteins in Guanidine hydrochloride (GuCl) 8 M (50 µl of protein stock solution/950 µl of GuCl) and by dilution of a *Mr*BphP1 in Urea 8 M adjusted to pH 2 with 37% of HCl (50 µl of protein stock solution/950 µl of Urea). Absorption and fluorescence spectra were measured at t = 0 and after 20 h; at t = 0 the proteins appeared intact, with spectra resembling those in buffer. At t = 20 h the chromophore was completely dissociated and his concentration was the same as in the intact protein. Knowing the absorption coefficient of FMN and Biliverdin (BV) at 445 nm (12500 M^{-1} cm^{-1} [8]) and at 696 nm (30800 M^{-1} cm^{-1} [9]) respectively, the values for protein-bound chromophores were calculated.

Time-resolved spectroscopy

Time-resolved flash photolysis was used to measure transient absorption changes of light-induced reactions in the micro-to-second time range. This methodology is described in detail in ref. [10]. Samples were excited by a laser pulse (duration about 10 ns, energy always kept less than 1.5 mJ per pulse), obtained from an OPO (GWU Lasertechnik-Erftstadt, Germany, built into the InnoLas cage), which was driven by the third harmonic (355 nm) of a Q-switched Nd:YAG laser (InnoLas, Krailling, Germany). [4]

Triplet-triplet absorption decays in *Mr*4511 mutants were determined using directly the 355 nm third harmonic of the laser. "Kinetics were monitored by means of a further optical line: two monochromators selected the probe wavelength from a continuous-wave 75 W Xenon lamp (AMKO, Utting, Germany). In order to avoid accumulation of photoproduct, after each laser pulse a continuous light from LEDs of appropriate wavelength was used to switch back the sample to its initial absorbance. The transmitted light was collected by a photomultiplier coupled to a digital oscilloscope (LeCroy LT374, 500 MHz, 4GS/s, Lcroy corp., Ramapo, NY, USA). For these experiments, the sample absorbance at the detection wavelength did not exceed 0.6 to avoid filter effects. The right-angle arrangement of the irradiation lines allowed a uniform illumination of the sample and minimised the laser scattered light at the photomultiplier. Traces were monitored at (20±1) °C for different wavelengths of the detection light. When required, in order to improve signal-to-noise ratio, for each probe wavelength a minimum of 9 laser pulses were averaged and 2 bit enhanced-resolution processed. Three automatic software-controlled shutters were used to select the correct irradiation line impinging on the sample for excitation, detection and backconversion. The time-resolved differential absorbances $\Delta A(\lambda,t)$ were calculated and analysed by a multi-exponential global-fit procedure [11] using Origin Professional (Microcal Software, Inc., Northampton, MA, USA). As an outcome, lifetimes for formation and decay of intermediates were obtained, and the lifetimes-associated amplitudes (with the meaning of ΔA) were plotted as Lifetimes-Associated Difference Spectra (LADS) as described earlier [12] ". [4]

Triplet-triplet absorption decays in *Mr*4511 mutants were used to determine triplet formation quantum yields (Φ_T), measuring the value of the parent-state maximum bleaching, exciting the proteins at 475 nm. Calculations were corrected for the determined absorption coefficient values and FMN was taken as a reference with a $\Phi_T = 0.6$ [13].

Time-Correlated Single-Photon Counting (TCSPC) measurements of fluorescence lifetimes were performed using FLS920 (Edinburgh Instruments, Livingston, UK).

This tecnique is well described in ref. [14]. The sample excitation was achieved through a pulsed LED with maximum emission at 600 or 450 nm, depending on the protein absorbance range, with 20 or 6 MHz repetition rate (PicoQuant, Berlin, Germany). "The sample absorbance at the excitation wavelength did not exceed 0.1. The Instrument Response Function (IRF) was determined at the excitation wavelength using a very diluted solution of colloidal silica (LUDOX). In order to ensure that only one photon per light pulse was detected, the photon rate did not exceed 5% of the exciting-light rate." [4] Data were analysed with F900 Software (Edinburgh instruments, Livingston, UK), by using a single- or multi-exponential decay fitting function: the average fluorescence lifetimes $\langle \tau_F \rangle$ were calculated according to Eq. 1.[4]

Eq. 1

$$\langle \tau_F \rangle = \sum \tau_i f_i$$

where τ_i is the lifetime of the *i*-th-component and f_i the associated fraction of the total amplitude.

Triplet transient-absorption spectra were measured in a way described before [15]. The filtered output of a Xenon lamp (Oriel) was passed through the sample and into a spectrograph (Andor Shamrock 303). To record transient absorption spectra was used a time-gated CCD camera (Andor iStar) from one port of the spectrograph. Samples were excited at 420 nm using the frequency doubled output of a femtosecond pulsed laser (Spectra-Physics Spitfire) operated at a repetition rate of 100 Hz.

[These measurements were performed at the University of Århus, Denmark]

Singlet oxygen (SO) quantum yields (Φ_Δ) were determined by detecting *transient phosphorescence* of SO at 1275 nm with the procedure described in [16,17]. Samples were excited at 420 nm using the frequency-doubled output of a femtosecond pulsed laser

(Spectra-Physics Spitfire) with a repetition rate between 100 Hz - 1 kHz, able to ensure a full decay of the phosphorescence signal before the next excitation pulse. The characteristic phosphorescence from SO at 1275 nm was isolated with a 1064 nm long-pass and a 1270/20 nm band-pass filters in front of a NIR sensitive PMT (Hamamatsu R5509). For the analysis of the kinetics was used a fitting function that incorporates the possibility to have two independent populations of triplet FMN, because some of the signal might come from free unbound FMN in solution. [18] Therefore, the signal was approximated with a single mono-exponential decay superimposed on the rise-and-decay behavior from protein-bound FMN. The resulting expression is shown below in Eq. 2:

Eq. 2

$$I(t) = \frac{A}{\tau_T - \tau_\Delta}\left(exp\left(-\frac{t}{\tau_T}\right) - exp\left(-\frac{t}{\tau_\Delta}\right)\right) + B \cdot exp\left(-\frac{t}{\tau_\Delta}\right) + C$$

Here, amplitudes have the meaning of the total integrated signal intensity, which is proportional to Φ_Δ, the first two exponential terms represent SO phosphorescence due to protein-bound FMN, the third exponential term represents SO phosphorescence due to free FMN, and the last term is a background. From Eq. 2 is evident that the lifetime of the triplet-state, τ_T, and the lifetime of SO, τ_Δ, determine the temporal evolution of the SO phosphorescence signal: in particular, the value of τ_T reflects the accessibility of oxygen to the triplet state of the photosensitiser, since the photosensitiser triplet state is the direct singlet-oxygen precursor through an energy-transfer step. [19,20] For our systems $\tau_T > \tau_\Delta$, so the initial rise of the signal can be assigned to τ_Δ while the signal decay is directly associated with τ_T, as deduced from the sign of the pre-exponential factor of Eq. 2. [21]. The triplet lifetimes were determined also by independent experiments of laser flash photolysis (*vide supra*), in order to reduce the number of variables and therefore guide the fitting procedure. Quantification of Φ_Δ was obtained in a relative way, [22] comparing the recorded signal against the signal generated by Sulphonated

Phenalenone (PNS) in H_2O or D_2O-based NaPi buffer (Φ_Δ = 0.97 ± 0.06) [17], here used as a reference sensitiser.
[These measurements were performed at the University of Århus, Denmark]

"For *determination of Φ_Δ with with a fluorescence probe*, Singlet Oxygen Sensor Green (SOSG) was purchased from Thermo Fisher Scientific (Waltham, MA-USA). The content of one vial of SOSG was dissolved in 33 µl of methanol to make a stock solution of ≈ 5 mM. Then a working solution of ≈ 10 µM was prepared in buffer immediately before use. Concentrations used for measurements were ≈ 2 µM of SOSG and ≈ 8 µM of protein/FMN in Napi buffer 10 mM, 100 mM NaCl, pH=8 or pD=8. Increasing in SOSG fluorescence was monitored at 530 nm with a Perkin Elmer LS50 luminescence spectrometer (Perkin Elmer, Waltham, MA-USA) operating in the kinetic mode, exciting the sample at 500 nm (to minimize FMN absorbance) and keeping the cuvette illuminated from above with LED 462 nm. FMN was used as a reference, with Φ_Δ = 0.56 ± 0.05 and 0.64 ± 0.05 in H_2O and D_2O solutions respectively. [18] Control measurements were performed with: a. SOSG alone having the same concentration as in the sample containing SOSG and the photosensitiser (protein or FMN); b. protein or FMN alone having the same concentration as in the sample containing SOSG and the photosensitiser; c. adding 20-40 mM of the SO quencher azide (NaN_3) to the sample containing SOSG and the photosensitiser." [4]

For the *time-resolved photoacoustic* (PA) measurements of *Mr*4511 proteins, excitation at 450 nm was achieved with the same ns laser employed for transient UV-Vis spectroscopy, as previously described [23]. The samples (ca. 2.8 ml) were temperature controlled to ± 0.02 °C into the cuvette holder FLASH 100 (Quantum Northwest, Spokane, WA, USA). PA signals were detected by a V103-RM ultrasonic transducer and fed into a 5662 preamplifier (Panametrics Inc., Waltham, MA, USA). The laser beam was shaped by a 1 × 12 mm slit, ensuring a time resolution of ca. 60 ns with a

deconvolution software (Sound Analysis 3000, Quantum Northwest Inc., Spokane, WA) [24]. The pulse energy was measured with a pyroelectric energy meter (RJP735 head connected to a meter RJ7620 from Laser Precision Corp). The experiments were performed in the linear regime of amplitude versus laser fluence, varied with a neutral density filter. The incident energy used was ≤ 40 μJ/pulse (corresponding to 15×10^{-11} Einstein for 450 nm excitation, photonic energy $E\lambda$ =265.84 kJ/mol). The sample concentration was ca. 15 μM, yielding ca. 1.8×10^{-9} mol in the excitation volume V_0 = 0.12 mL, corresponding to ca. 0.08 photons per protein molecule. The dye new coccine (FLUKA, Neu-Ulm, Germany) was used as calorimetric reference [25]. For the reference, 100 shots were acquired for each of the two waveforms. At each temperature 4 deconvolution results were summed up.

For the deconvolution of PA signals, the time evolution of the pressure is assumed to be a sum of monoexponential functions. Deconvolution analysis yields the fractional amplitudes (φ_i) and the lifetimes (τ_i) of the transients, with a time window between 20 ns and 5 μs and a time resolution of ca. 60 ns. At a given temperature and for each resolved *i*-th step the fractional amplitude φ_i is the sum of the fraction of absorbed energy released as heat (α_i) and the structural volume change *per* absorbed einstein (ΔV_i), according to Eq. 3 [26]:

Eq. 3

$$\varphi_i = \alpha_i + \frac{\Delta V_i}{E_\lambda}\frac{c_P \rho}{\beta}$$

where $E\lambda$ is the molar excitation energy, $\beta = (\partial V/\partial T)_p \Delta V$ is the volume expansion coefficient, c_p is the heat capacity at constant pressure, and ρ is the mass density of the solvent. The "two temperature" (TT) method was used in order to separate α_i from ΔV_i [23]. The sample waveform was acquired at a temperature for which heat transport is zero, $T_{\beta=0}$ = 2.5 °C for the buffer employed here (Na-phosphate 10 mM, NaCl 100 mM, pH = 8) and at a slightly higher temperature, here $T_{\beta>0}$ = 10 °C. At

$T_{\beta=0}$ the PA signal is only due to ΔV_i, while at 10 °C both heat release and ΔV_i contribute to the sample signal. The reference for deconvolution was recorded at $T_{\beta>0}$, Eq. 4 and Eq. 5 were then used to derive α_i and ΔV_i; note that for the reference compound the PA signal is zero at $T_{\beta=0}$.

Eq. 4

$$\Phi_i \Delta V_i = \varphi_i|_{T_{\beta=0}} \times E_\lambda \frac{\beta}{c_P \rho}\Big|_{T_{\beta>0}}$$

Eq. 5

$$\alpha_i = \varphi_i|_{T_{\beta>0}} - \varphi_i|_{T_{\beta=0}}$$

The thermoelastic parameters of the working buffer at the various temperatures were evaluated by comparing the PA signals of the reference compound against the same reference in water, for which tabulated chemico-physical parameters give $\beta/(c_p\rho)$ = 0.0495 mL/(kJ/mol) at 20 °C.

For the samples at each temperature two waveforms were acquired, each of 10 shots with stirring in between the shots: given that only a small percentage of the total volume was illuminated (4%), this ensures that only a tiny fraction of the total molecules were photolysed.

Bibliography

1. Losi, A., Bonomi, H. R., Michael, N., Tang, K. & Zhao, K.-H. Time-Resolved Energetics of Photoprocesses in Prokaryotic Phytochrome-Related Photoreceptors. *Photochem. Photobiol.* **93**, 733–740 (2017).

2. Gutt, A. Photochemische und strukturelle Untersuchungen neuartiger Bilin-bindender Photorezeptoren. PhD Dissertation, Mathematisch-Naturwissenschaftlichen Fakultät der Heinrich-Heine-Universität Düsseldorf (2016).

3. Shah, R., Schwach, J., Frankenberg-Dinkel, N. & Gärtner, W. Complex formation between heme oxygenase and phytochrome during biosynthesis in Pseudomonas syringae pv. tomato. *Photochem. Photobiol. Sci.* **11**, 1026 (2012).

4. Consiglieri, E. *et al.* Dynamics and efficiency of photoswitching in biliverdin-binding phytochromes. *Photochem. Photobiol. Sci.* **18**, 2484–2496 (2019).

5. Mailliet, J. *et al.* Spectroscopy and a High-Resolution Crystal Structure of Tyr263 Mutants of Cyanobacterial Phytochrome Cph1. *J. Mol. Biol.* **413**, 115–127 (2011).

6. van den Berg, P. A. ., Widengren, J., Hink, M. A., Rigler, R. & Visser, A. J. W. . Fluorescence correlation spectroscopy of flavins and flavoenzymes: photochemical and photophysical aspects. *Spectrochim. Acta Part A Mol. Biomol. Spectrosc.* **57**, 2135–2144 (2001).

7. Pennacchietti, F. *et al.* Photochromic conversion in a red/green cyanobacteriochrome from Synechocystis PCC6803: Quantum yields in solution and photoswitching dynamics in living E. coli cells. *Photochem. Photobiol. Sci.* **14**, 229–237 (2015).

8. Whitby, L. G. A new method for preparing flavin-adenine dinucleotide. *Biochem. J.* **54**, 437–42 (1953).

9. McDonagh, A. F. & Palma, L. A. Preparation and properties of crystalline biliverdin IX alpha. Simple methods for preparing isomerically homogeneous biliverdin and [14C]biliverdin by using 2,3-dichloro-5,6-dicyanobenzoquinone. *Biochem. J.* **189**, 193–208 (1980).

10. Abbruzzetti, S. *et al.* Time-resolved methods in Biophysics. 2. Monitoring haem proteins at work with nanosecond laser flash photolysis. *Photochem. Photobiol. Sci.* **5**, 1109 (2006).

11. Beechem, J. M. Global analysis of biochemical and biophysical data. *Methods Enzymol.* **210**, 37–54 (1992).

12. Braslavsky, S. E., Gärtner, W. & Schaffner, K. Phytochrome photoconversion. *Plant, Cell Environ.* **20**, 700–706 (1997).

13. Losi, A., Polverini, E., Quest, B. & Gärtner, W. First evidence for phototropin-related blue-light receptors in prokaryotes. *Biophys J* **82**, 2627–2634 (2002).

14. Lakowicz, J. R. *Principles of Fluorescence Spectroscopy Joseph R . Lakowicz*. (2006). doi:10.1007/978-0-387-46312-4

15. Westberg, M., Holmegaard, L., Pimenta, F. M., Etzerodt, M. & Ogilby, P. R. Rational design of an efficient, genetically encodable, protein-encased singlet oxygen photosensitizer. *J. Am. Chem. Soc.* **137**, 1632–42 (2015).

16. Arnbjerg, J., Johnsen, M., Frederiksen, P. K., Braslavsky S. E. & Ogilby, P. R.. Two-Photon Photosensitized Production of Singlet Oxygen: Optical and Optoacoustic Characterization

of Absolute Two-Photon Absorption Cross Sections for Standard Sensitizers in Different Solvents. (2006). doi:10.1021/JP0609986

17. Martí, C., Jürgens, O., Cuenca, O., Casals, M. & Nonell, S. Aromatic ketones as standards for singlet molecular oxygen O2(1Δg) photosensitization. Time-resolved photoacoustic and near-IR emission studies. *J. Photochem. Photobiol. A Chem.* **97**, 11–18 (1996).

18. Westberg, M., Bregnhøj, M., Etzerodt, M. & Ogilby, P. R. Temperature Sensitive Singlet Oxygen Photosensitization by LOV-Derived Fluorescent Flavoproteins. *J. Phys. Chem. B* **121**, 2561–2574 (2017).

19. Nonell, S. & Braslavsky, S. Methods Enzymol. 2000 319 37-49. *Methods Enzymol.* **319**, 37–49 (2000).

20. Comas-Barceló, J. *et al.* A self-assembled nanostructured material with photosensitising properties. *RSC Adv.* **3**, 17874 (2013).

21. Jiménez-Banzo, A., Ragàs, X., Kapusta, P. & Nonell, S. Time-resolved methods in biophysics. 7. Photon counting vs. analog time-resolved singlet oxygen phosphorescence detection. *Photochem. Photobiol. Sci.* **7**, 1003 (2008).

22. Scurlock, R. D., Martire, D. O., Ogilby, P. R., Taylor, V. L. & Clough, R. L. Quantum Yield of Photosensitized Singlet Oxygen (a1.DELTA.g) Production in Solid Polystyrene. *Macromolecules* **27**, 4787–4794 (1994).

23. Raffelberg, S., Mansurova, M., Gärtner, W. & Losi, A. Modulation of the photocycle of a LOV domain photoreceptor by the hydrogen-bonding network. *J. Am. Chem. Soc.* **133**, 5346–5356 (2011).

24. Rudzki, J. E., Goodman, J. L. & Peters, K. S. Simultaneous determination of photoreaction dynamics and energetics using pulsed, time-resolved photoacoustic calorimetry. *J. Am. Chem. Soc.* **107**, 7849–7854 (1985).

25. Abbruzzetti, S., Viappiani, C., Murgida, D. H., Erra-Balsells, R. & Bilmes, G. M. Non-toxic, water-soluble photocalorimetric reference compounds for UV and visible excitation. *Chem. Phys. Lett.* **304**, 167–172 (1999).

26. Braslavsky, S. E. & Heibel, G. E. Time-resolved photothermal and photoacoustic methods applied to photoinduced processes in solution. *Chem. Rev.* **92**, 1381–1410 (1992).

Results and discussion

Introduction

In this section the results of the studies on biliverdin-binding phytochromes are presented, at first showing spectral characteristics and steady-state spectroscopy measurements; then, the attention will be focused on the results of time-resolved laser-induced flash photolysis experiments, able to detect transient species during the photoconversion. The proteins here presented are four bacteriophytochromes (*Pst*BphP1 from *Pseudomonas syringae* pv. *tomato*, *Pa*BphP from *Pseudomonas aeruginosa,* *Xcc*BphP-PGP (PGP = PAS-GAF-PHY) from *Xanthomonas campestris* pv. *campestris* and *Mr*BphP1 from *Methylobacterium radiotolerans*) and a phytochrome from a fungus (FphAN753 from *Aspergillus nidulans*).[ii] These proteins have a canonical PGP photosensory module found in plant phytochromes, but in contrast to these, they bind biliverdin IXa (BV) as a chromophore. It should be noticed that these proteins were investigated in their truncated forms, i.e. the complete PGP photosensory module, with the exception of *Pst*BphP1 for which the full-length protein was available, with the architecture PAS-GAF-PHY-Kinase. [1]

A second results section deals with a novel blue-light photoreceptor of the LOV superfamily from *Methylobacterium radiotolerans* (*Mr*4511): this new protein has been spectroscopically investigated in comparison with some mutated variants, and in particular it has been discovered that this blue-light photoreceptor can be converted into an efficient photosensitiser for singlet oxygen upon mutating a single residue, the cysteine responsible for the photocycle in native LOV domains.

[ii] See the section "Materials and methods" for details.

Biliverdin-binding phytochromes

Spectral characteristics and photoconversion efficiency

The BV-binding photoreceptors studied in this research work show the steady-state spectral characteristics reported in the literature [2,3,4,5] and similar to other BphPs (bacterial phytochromes). These proteins present a photochromism between a red (Pr) and a far red/near infrared (Pfr) form (see Table 2 for absorption maxima). Photoswitching between the parental state and the photoproduct was obtained by irradiation with LEDs emitting red-light (RL, 650 or 670 nm) or far-red light (FRL, 760 nm). The light source was put on the top of the sample to ensure that the cuvette was entirely illuminated.

Table 2: Absorption maxima of the Pr and Pfr forms of the investigated BV-binding phytochromes.

	Pr form abs peak / nm	Pfr form abs peak / nm
*Pst*BphP1	703	751
*Pa*BphP	701	752
FphAN753	689	751
*Xc*BphP-PGP	684	757
*Mr*BphP1	707	764

Absorption and fluorescence spectra are shown in Figure 7 for *Pst*BphP1 and FphAN753, in Figure 8 for *Pa*BphP *Xc*BphP-PGP and in Figure 9 for *Mr*BphP1.

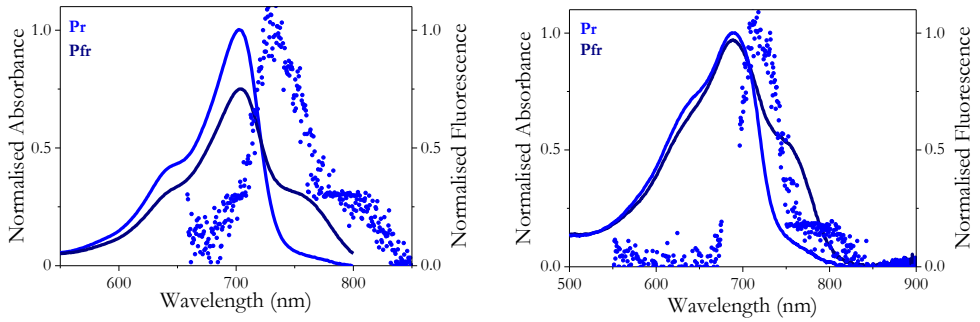

Figure 7: Normalised absorption (continuous line) and fluorescence spectra (dotted line) of *Pst*BphP1 (left) and FphAN753 (right) in the Pr (blue) and Pfr (dark blue) forms. Fluorescence emission was obtained exciting the sample at 610 nm (*Pst*BphP1) and 680nm (FphAN753). Pfr is non fluorescent, Pr represents the dark-adapted form. Adapted from [1].

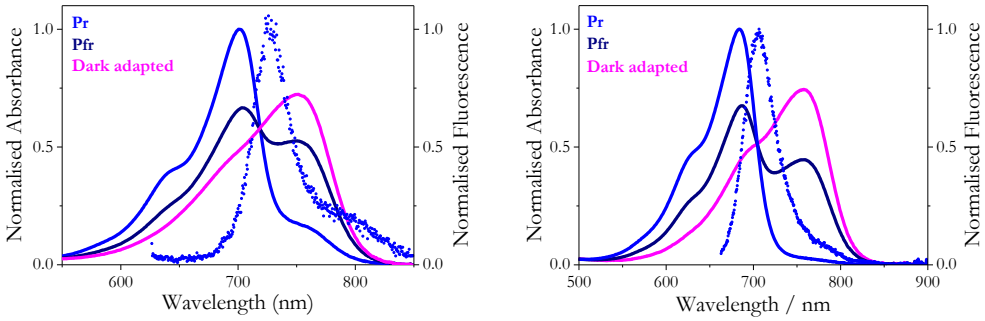

Figure 8: Normalised absorption (continuous line) and fluorescence spectra (dotted line) of *Pa*BphP (left) and *Xc*BphP-PGP (right) in the Pr (blue) and Pfr (dark blue) forms. The pink line is the dark-adapted state = 100% Pfr. Fluorescence emission was obtained exciting the sample at 610 nm (*Pa*BphP) and 650 nm (*Xc*BphP-PGP). Pfr is non fluorescent. The graph of *Pa*BphP is adapted from [1].

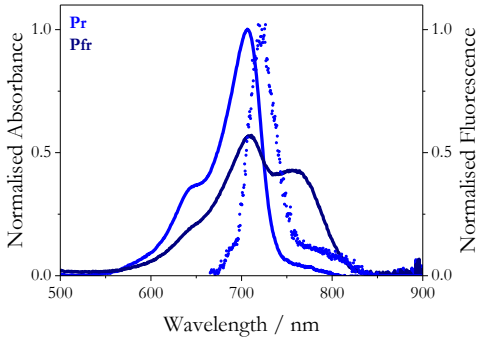

Figure 9: Normalised absorption (continous line) and fluorescence spectra (dotted line) of *Mr*BphP1 in the Pr (blue) and Pfr (dark blue) forms: the absorption coefficient on the maximum of the Pr form is 98200 $M^{-1}cm^{-1}$. Fluorescence emission was obtained exciting the sample at 650 nm. Pfr is non fluorescent. Pr represents the dark-adapted form.

The five BphPs here investigated emit a very weak fluorescence, only from the Pr state. This indicates that the fluorescence quantum yield Φ_F are extremely low, in the order of 10^{-3} for the Pr form (with a maximum value of 0.022 for *Xc*BphP-PGP) and virtually zero for Pfr. Accordingly, the average fluorescence lifetimes $\langle\tau_F\rangle$, here measured exciting the Pr form at 600 nm, are very short, less than 600 ps. A summary of these values is presented in Table 3.

Table 3: Fluorescence quantum yields and lifetimes.

	Fluor. Max / nm	Stokes shift / nm	Φ_F	$\langle\tau_F\rangle$ / ns
*Pst*BphP1	730	27	0.007	0.22 ± 0.02
*Pa*BphP	726	25	0.006	0.45 ± 0.03
FphAN753	719	30	0.002	0.31 ± 0.01
*Xc*BphP-PGP	706	22	0.022	0.53 ± 0.02
*Mr*BphP1	722	16	0.006	< 200 ps *

*not properly measurable because of instrumentation sensitivity

For *Pst*BphP1 and *Mr*BphP1 the Pr parental state can be photo-converted into the Pfr photoproduct and *viceversa*. On the other hand, the complete re-conversion of the Pr to the pure Pfr state in the bathys *Pa*BphP and *Xc*BphP-PGP was only thermally possible after prolonged incubation in the dark: illumination of Pr by RL produced a photoequilibrium between the Pr and the pure Pfr forms. The pure Pfr fraction in the photoequilibrium could be back-converted to the complete Pr form by illumination with FRL. On the contrary, the Pfr photoproduct of FphAN753 was fully stable in the dark and could be re-converted only by illumination with FRL.

The stability of photoproducts was determined by recording thermal recovery kinetics at 20 °C, measuring the absorbance at a specific wavelength as a function of time. *Pst*BphP1 and *Pa*BphP showed only moderate thermal stability: kinetics were

fitted by mono-exponential equations yielding the recovery lifetimes (τ_{rec}) as shown in Table 4.

Table 4: Thermal recovery lifetimes of *Pst*BphP1[1,6], *Pa*BphP [1,6] and *Xc*BphP-PGP.

	τ_{rec} / min
*Pst*BphP1	4.5
*Pa*BphP	12
*Xc*BphP-PGP	150

On the contrary, *Xc*BphP-PGP and *Mr*BphP1 appeared more stable: recover kinetics, measured at 20 °C as an increasing in absorbance at 757 nm (*Xc*BphP-PGP) and as a decreasing in absorbance at 760 nm (*Mr*BphP1), showed respectively a monoexponential decay with a lifetime τ = 2.5 h (Aba Losi, unpublished results) and a bi-exponential decay, giving the lifetimes τ_1 = 23 min and τ_2 = 6.4 h (with normalised amplitudes of A_1 = 0.05 and A_2 = 0.95). The recovery kinetics for *Mr*BphP1 is shown in Figure 10.

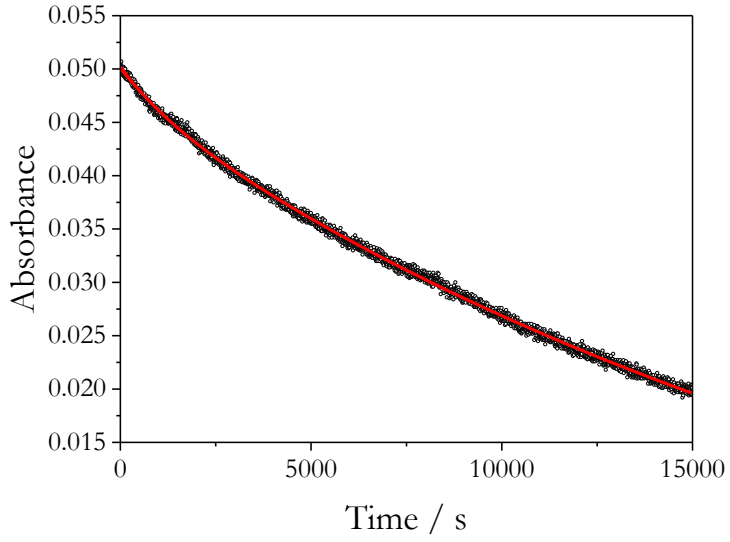

Figure 10: Thermal-recovery kinetic for MrBphP1, followed as decreasing in absorbance at 760 nm. The fitting line (red) is superimposed.

In order to determine the Φ_P, it was necessary to calculate the photoconverted fraction: therefore, spectrally pure form of Pfr state must be known. For the bathy phytochromes, pure Pfr spectra were experimentally available, while for the other proteins the pure Pfr forms were obtained by assuming a linear combination of Pr and Pfr fractions summing up to 1, according to Eq. 6. [7]

Eq. 6

$$A_{pure\ Pfr} = \frac{A_{Pfr} - f \times A_{Pr}}{1 - f}$$

where $f = \frac{Pr}{Pfr}$ is the photoconverted fraction. The calculated pure Pfr spectra for *Mr*BphP1 and *Pst*BphP1 are presented in Figure 11.

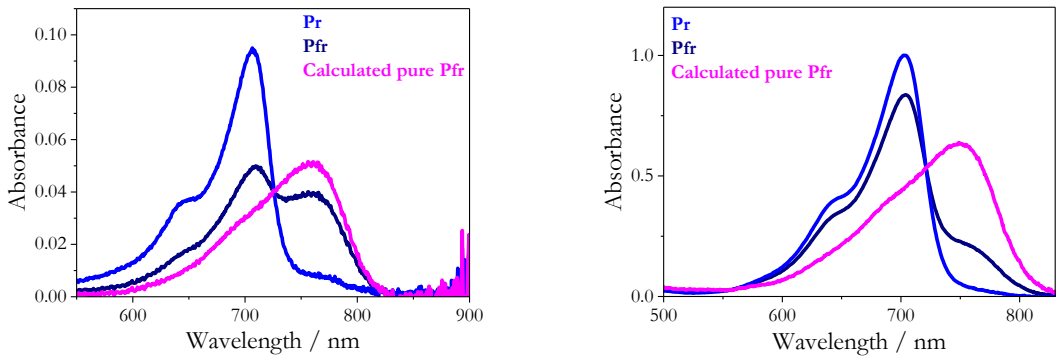

Figure 11: Absorption spectra of calculated pure Pfr form (pink line) for *Mr*BphP1 (left) and *Pst*BphP1 (right).

The photoconversion quantum yields (Φ_P) between both Pr and Pfr states of *Pst*BphP1, *Pa*BphP and FphAN753 were found to be less efficient than those for plant and cyanobacterial phys: [1,8] for example, *Syn*Cph1 $\Phi_{P,\ R\rightarrow FR}$ = 0.16 [9] and 0.17 for PhyA [10]. Interestingly, the photoconversion quantum yield for *Mr*BphP1 turned out to be larger than Φ_P of the other BphPs here investigated, performing Φ_P = 0.2

in both directions: plots for *Mr*BphP1 are presented in Figure 12. The values are resumed in Table 5.

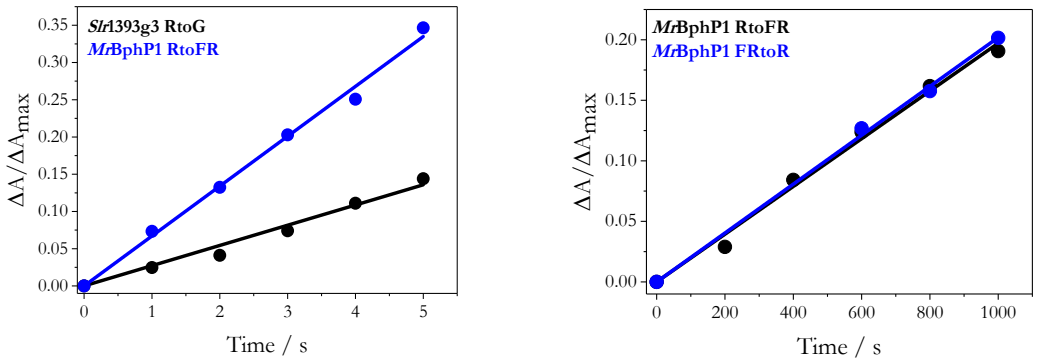

Figure 12: Kinetics of photoconversion of *Mr*BphP1 for the red-to-far red route (left) and the far red-to-red route (right). The Φ_P was calculated in comparison with the *Slr*1393g3 [11] (the GAF3 domain of the cynobacteriochrome *Slr*1393 from *Synechocystis*) for the red-to-far red route and this value was used as a reference for the far red-to-red route. For the red-to-far red route, absorbance was recorded using the spectrophotometer in the kinetic mode and recording absorbances for 5 s under illumination with a 670 nm laser light. Photoconversion for determination of $\Phi_{P,FRtoR}$ was achieved through irradiation of the sample at 660 nm or 760 nm using the fluorimeter light excitation source. In order to be compared, the sample and the reference were always prepaired with the same absorbance at the excitation wavelength.

Table 5: Photoconversion quantum yields between both Pr and Pfr states of *Pst*BphP1, *Pa*BphP, FphAN753. [1]

	Φ_P
*Pst*BphP1	$\Phi_{P,\,R\rightarrow FR} = 0.02$
	$\Phi_{P,\,FR\rightarrow R} = 0.08$
*Pa*BphP	$\Phi_{P,\,R\rightarrow FR} = 0.12$
	$\Phi_{P,\,FR\rightarrow R} = 0.06$
FphAN753	$\Phi_{P,\,R\rightarrow FR} = 0.04$
	$\Phi_{P,\,FR\rightarrow R} = 0.04$
*Mr*BphP1	$\Phi_{P,\,R\rightarrow FR} = 0.2$
	$\Phi_{P,\,FR\rightarrow R} = 0.2$

It is important to note that these Φ_P values do not necessarily reflect the isomerisation quantum yield and the LUMI formation, since shunt reactions could be present during phy photoconversion. [12]

Time-resolved laser-induced absorption changes

The proteins were investigated for the light-driven conversion between the parental state and the photoproduct and *viceversa*. Absorption changes were measured at different wavelengths of the probe light, from 600 nm to 780 nm. Since these signals were extended in time and the acquisition memory was limited, data acquisition was repeated on several time scales, up to 500 ms after the laser pulse. Before and after the flash-photolysis experiments, samples were controlled for absorption spectral integrity. In Table 6 are reported the calculated lifetimes of transient intermediates for all the BV-binding phytochromes. [1]

Table 6: Lifetimes of reaction intermediates in BV-binding phytochromes.

Pr-to-Pfr route					
	τ_1	τ_2	τ_3	τ_4	τ_5
*Pst*BphP1	3.1 μs ± 0.2	77 μs ± 8	1.51 ms ± 0.04	13.2 ms ± 0.3	62 ms ± 1
*Pa*BphP	1.01 μs ± 0.09	96 μs ± 2	0.78 ms ± 0.01		
*Xc*BphP-PGP	0.9 μs ± 0.1	184 μs ± 3	1.64 ms ± 0.02		
FphAN753	6.3 μs ± 0.5	520 μs ± 70	8.4 ms ± 0.7		
*Mr*BphP1			1.28 ms ± 0.08	67 ms ± 1	
Pfr-to-Pr route					
	τ_1	τ_2	τ_3	τ_4	
*Pst*BphP1	4.4 μs ± 0.1	270 μs ± 10	2.95 ms ± 0.5		
*Pa*BphP	6 μs ± 1	230 μs ± 40	15.9 ms ± 0.9		
*Xc*BphP-PGP	1.0 μs ± 0.1	160 μs ± 20	1.4 ms ± 0.1	15.8 ms ± 0.4	
FphAN753	30 μs ± 3	860 μs ± 60			
*Mr*BphP1		290 μs ± 30	2.4 ms ± 0.2		

*Pst*BphP1 – bacterial phytochrome 1 from *Pseudomonas syringae* pv. *tomato*

To have information about the quality of the transient measurements, the time-resolved equilibrium ΔAbsorbances, *i.e.* measured at the end of the kinetics, were compared to the difference spectra obtained by exhaustive irradiation in a steady-state experiment: data in Figure 13 show that they are consistent between each other and in this way it is possible to calculate the percentage of photoconverted protein, here giving the value of *ca.* 6% for the Pr-to-Pfr conversion and 5% for the Pfr-to-Pr.

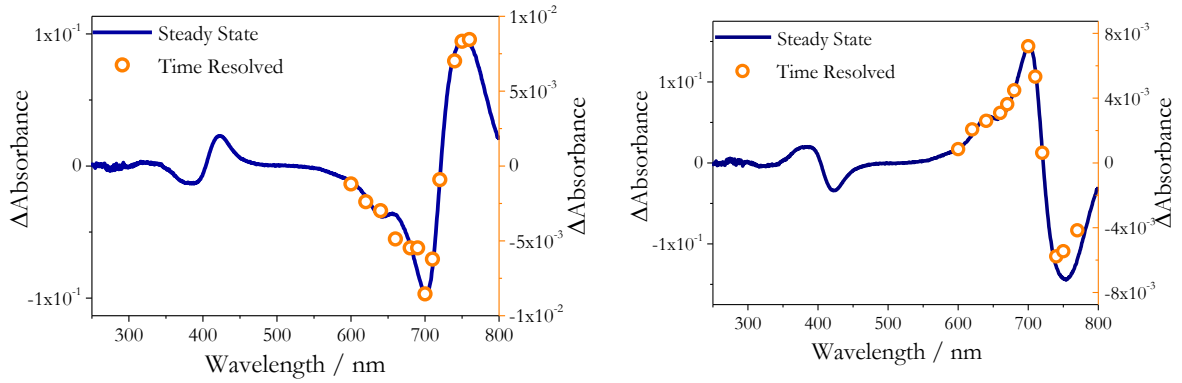

Figure 13: Comparison of matched ΔAbsorbance values for *Pst*BphP1 from time-resolved measurements (orange circles) with the steady-state difference spectrum (blue line) for the Pr-to-Pfr route (left) and for the Pfr-to Pr route (right). Adapted from [1].

Kinetic traces for the Pr-to-Pfr route subjected to global-fit analysis are presented in Figure 14. They show five lifetimes for formation and decay of intermediates taking place during the Pr-to-Pfr conversion: 3.1 and 77 μs, 1.5, 13.2 and 62 ms (correspondent to components A1-A5 in Figure 15). The red-shifted [13] intermediate LUMI-R (see the Introduction chapter) is assumed to be formed after the chromophore photoisomerisation on a time scale too short for being detectable with our setup: the fitting was started from 1 μs to avoid the disturbed signal produced by the recovery of the photomultiplier due to laser scattering light or sample fluorescence . The decay of LUMI-R (red shifted with respect to Pr) into a putative META-R appears more complex for this protein than for other BphPs,

encompassing three transitions on the µs-ms time scale (as shown by the LADS spectra in figure Figure 15, right). This last step on the ms time scale could correspond to the so-called Meta-Ra to Meta-Rc conversion in *Dr*BphP from *Deinococcus radiodurans*, for which major structural changes were reported at a lifetime of 1 ms [14]. The final transition for the Pr-to-Pfr conversion of *Pst*BphP1 occurs on the long-ms time scale, yielding a species that has already strong features of Pfr. The difference spectra taken at the calculated lifetimes (Figure 15, left) demonstrate: a) the bleaching of the Pr form; b) the formation of a species spectrally similar to Pfr; c) the negative ΔAbsorbance around 660 nm, leading to the formation of the Pfr form. The kinetically complex Pr-to-Pfr conversion of *Pst*BphP1 could comprise shunt reations leading back to the Pr state, as found for Agp2 [7] from *Agrobacterium tumefaciens* and for other BV-bindig phys [12]. [1] However, it must be noted that *Pst*BphP1 is also the sole BphP investigated here as full-length protein, possibly accounting for the complex dynamics of light-induced reactions.

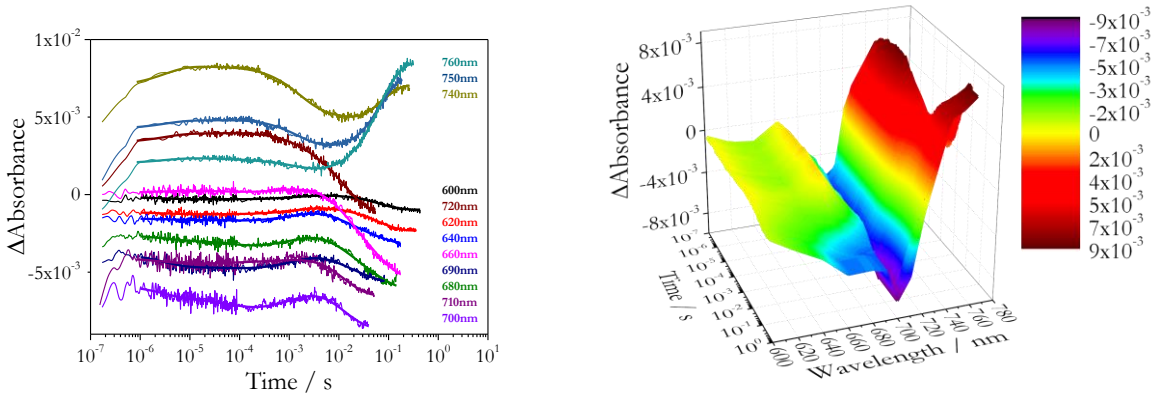

Figure 14: Kinetic traces for the Pr-to-Pfr conversion (left) for *Pst*BphP1, the fitting lines are superimposed. 3D transient representation of ΔAbsorbances (right) is presented as a function of time and the probe wavelengths, the false colours map the time-resolved formation and decay of transient species. Adapted from [1].

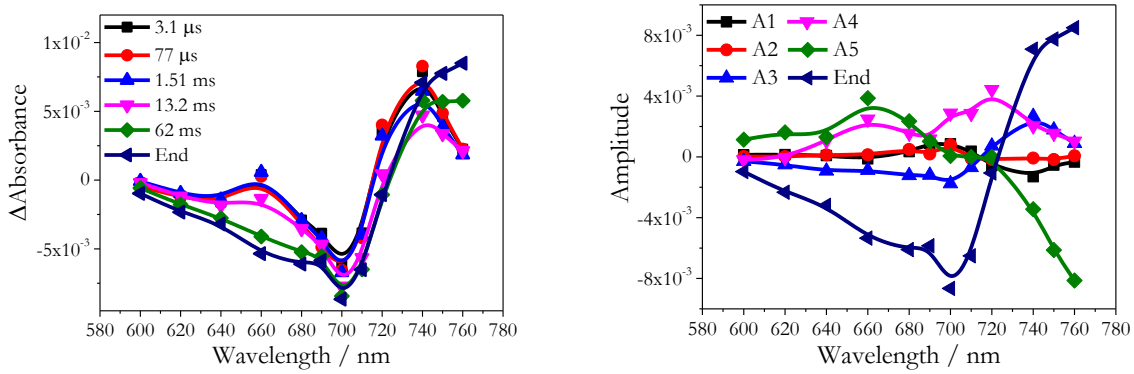

Figure 15: Left, ΔAbsorbances at calculated lifetimes for the Pr-to-Pfr conversion for *Pst*BphP1, the values at the end correspond to equilibrium ΔAbsorbances. Right: Lifetime-Associated Difference Spectra (LADS): note that in LADS a negative amplitude corresponds to a formation of an intermediate, while a positive amplitude refers to a decay of an intermediate, the values at the end correspond to equilibrium ΔAbsorbances. Adapted from [1].

Kinetic traces for Pfr-to-Pr route subjected to global-fit analysis are shown in Figure 16. The photoconversion between the photoproduct and the parental state follows a pathway optically simpler than the reverse route and also the photoconversion quantum yield is four-fold higher than that of the forward reaction (Table 5). The difference spectra in Figure 17 taken at the calculated lifetimes directly show the rise in absorbance around 700 nm concomitant with the loss of absorbance around 750 nm; the LADS confirm that absorption in the far-red region begins to vanish at both lifetimes 4.4 µs and 270 µs forming directly a Pr-like state, and the last lifetime of 2.95 ms completes this process. The progressive Pfr-to-Pr conversion is certified by a clear isosbestic point at *ca.* 720 nm.

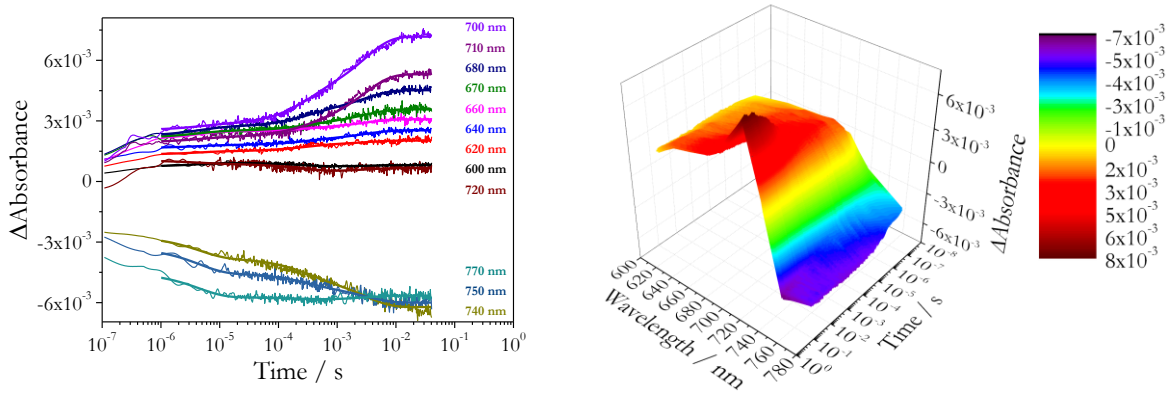

Figure 16: Kinetic traces for the Pfr-to-Pr conversion (left) for *Pst*BphP1, the fitting lines are superimposed. 3D transient representation of ΔAbsorbances (right) is presented as a function of time and the probe wavelengths. The false colours map the time-resolved formation and decay of transient species. Adapted from [1].

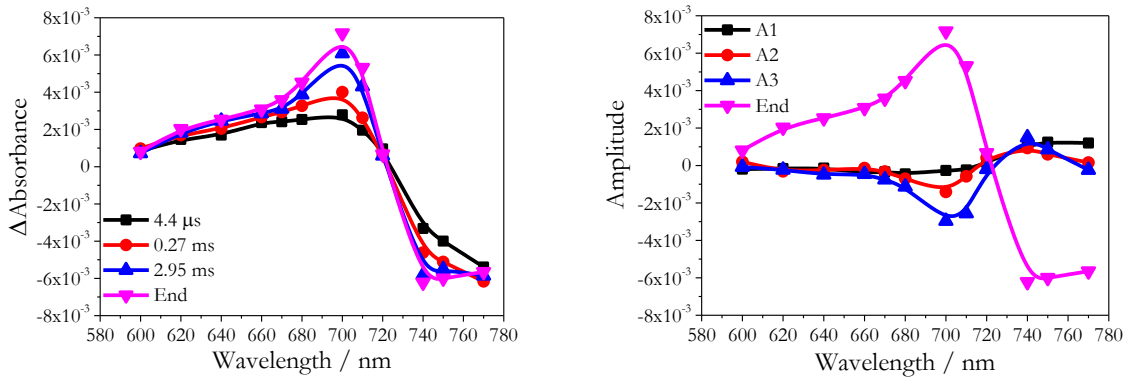

Figure 17: Left, ΔAbsorbances at calculated lifetimes for the Pfr-to-Pr conversion for *Pst*BphP1, the values at the end correspond to equilibrium ΔAbsorbances. Right: Lifetime-Associated Difference Spectra (LADS): note that in LADS a negative amplitude corresponds to a formation of an intermediate, while a positive amplitude refers to a decay of an intermediate, the values at the end correspond to equilibrium ΔAbsorbances.

*Pa*BphP – bacterial phytochrome from *Pseudomonas aeruginosa*

Data in Figure 18 show that, for the "bathy" *Pa*BphP, equilibrium time-resolved ΔAbsorbances are globally consistent with the steady-state spectra and the percentage of photoconverted protein was *ca.* 3% for the Pr-to-Pfr conversion and 2% for the Pfr-to-Pr.

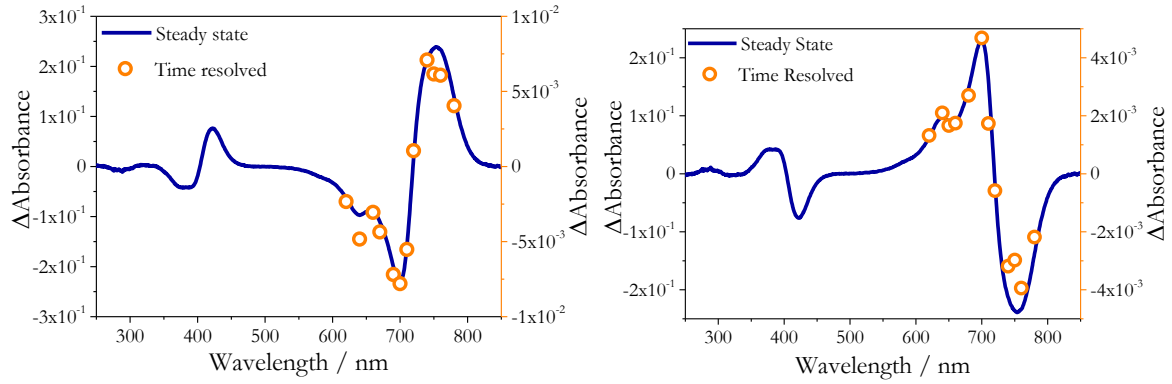

Figure 18: Comparison of matched ΔAbsorbance values for *Pa*BphP from time-resolved measurements (orange circles) with the steady-state difference spectrum (blue line) for the Pr-to-Pfr route (left) and for the Pfr-to Pr route (right). Adapted from [1].

In contrast to the prototypical *Pst*BphP1, in *Pa*BphP the parental state is Pfr. Kinetic traces for Pr-to-Pfr route subjected to global-fit analysis are presented in Figure 19, while for the Pfr-to-Pr route in Figure 20. The difference spectra taken at the calculated lifetimes indicate that the forward Pfr-to-Pr route is spectroscopically more simple than the backward Pr-to-Pfr process (Figure 21 and Figure 22): the LADS in Figure 22 clearly identify the final process as the dominating Pr forming conversion with a lifetime of 15.9 ms. For the Pr-to-Pfr conversion, Figure 21 reveals that the bleaching of the Pr form is concomitant with the formation of a red-shifted intermediate absorbing maximally around 720-730 nm together with a very shallow absorption in the region at 660 nm, then the final formation of the Pfr form takes place with a lifetime of 780 μs: this final process in evident in the LADS, showing loss of absorbance (positive amplitude between 640 and 710 nm) and rise in absorbance around 740-780 nm. The greater velocity of the Pr-to-Pfr route with respect to the Pfr-to-Pr could reflect the higher photoconversion quantum yield (

Table 5). As for other proteins [5,15], it is not possible to fully photoconvert this protein to a pure Pfr form, which can only thermally recover: nevertheless, contribution of residual Pr state to the kinetic traces is negligible, due to selective excitation of the Pfr form at 760 nm and the fact that the photoequilibrium was mantained by back illumination between each shot.

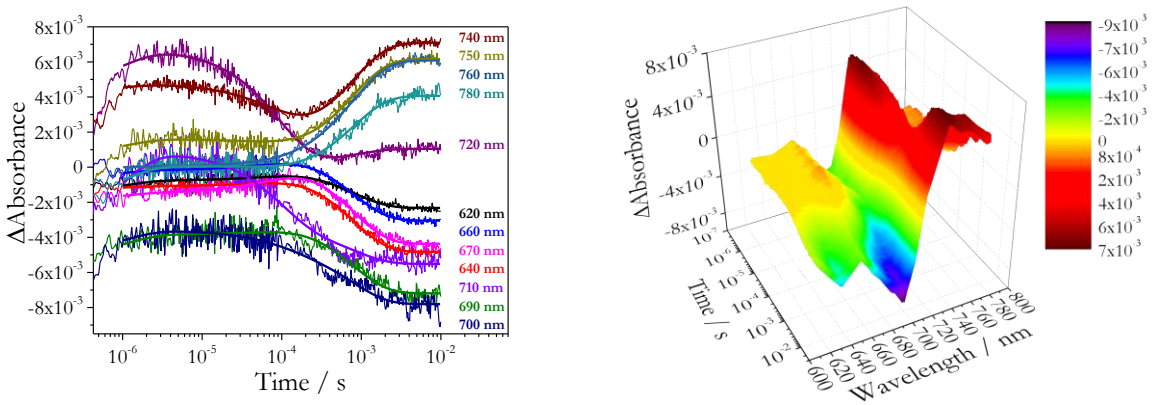

Figure 19: Kinetic traces for the Pr-to-Pfr conversion (left) for *Pa*BphP, the fitting lines are superimposed. 3D transient representation of ΔAbsorbances (right) is presented as a function of time and the probe wavelengths, the false colours map the time-resolved formation and decay of transient species. Adapted from [1].

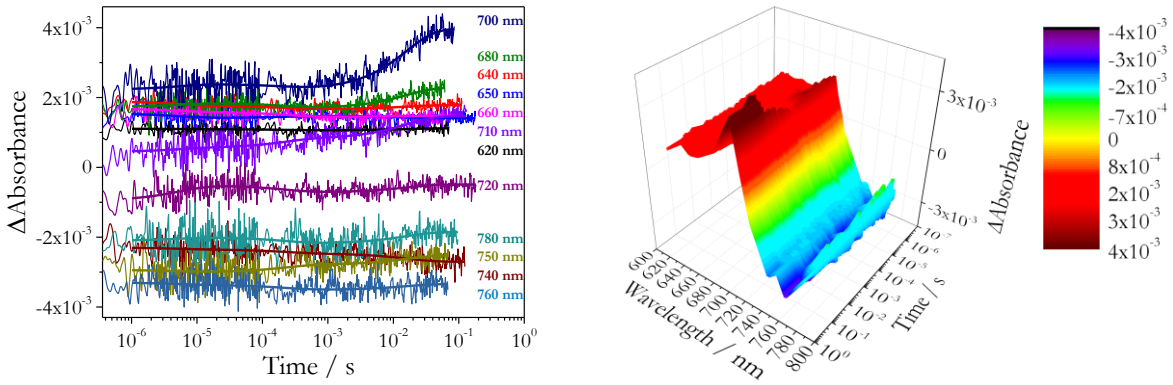

Figure 20: Kinetic traces for the Pfr-to-Pr conversion (left) for *Pa*BphP, the fitting lines are superimposed. 3D transient representation of ΔAbsorbances (right) is presented as a function of time and the probe wavelengths, the false colours map the time-resolved formation and decay of transient species. Adapted from [1].

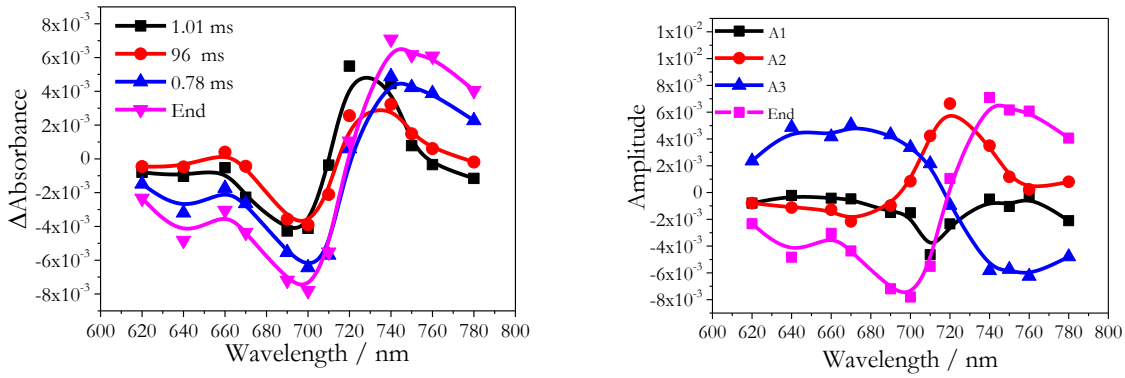

Figure 21: Left: ΔAbsorbances at calculated lifetimes for the Pr-to-Pfr conversion for *Pa*BphP, the values at the end correspond to equilibrium ΔAbsorbances. Right: Lifetime-Associated Difference Spectra (LADS): note that in LADS a negative amplitude corresponds to a formation of an intermediate, while a positive amplitude refers to a decay of an intermediate, the values at the end correspond to equilibrium ΔAbsorbances. Adapted from [1].

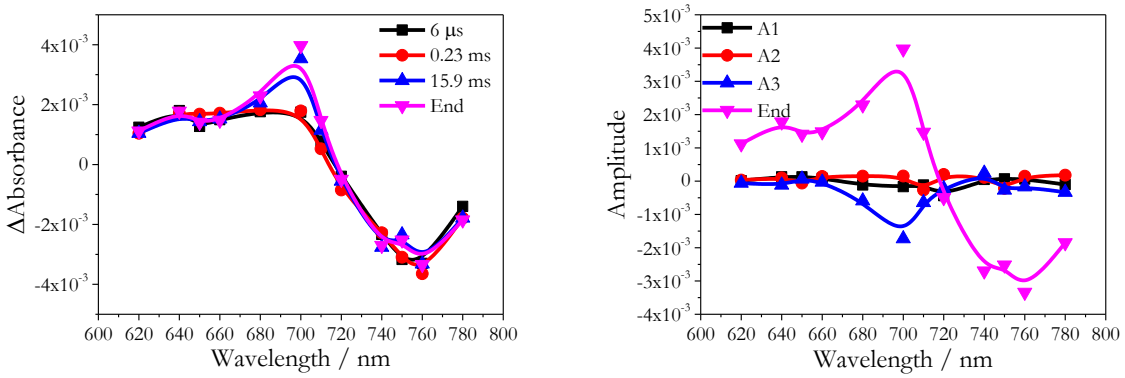

Figure 22: Left: ΔAbsorbances at calculated lifetimes for the Pfr-to-Pr conversion for *Pa*BphP, the values at the end correspond to equilibrium ΔAbsorbances. Right: Lifetime-Associated Difference Spectra (LADS): note that in LADS a negative amplitude corresponds to a formation of an intermediate, while a positive amplitude refers to a decay of an intermediate, the values at the end correspond to equilibrium ΔAbsorbances. Adapted from [1].

In order to have a comparison with another "bathy" phy, we performed time-resolved measurements on the *Xc*BphP-PGP from *Xanthomonas campestris* pv. *campestris*. Like in *Pa*BphP, the Pfr form of this protein can only recover thermally, with a full conversion to Pfr [15]. [iii] In Figure 23 are reported the kinetic traces for both

[iii] On the contrary, the full-length protein with the structure PAS-GAF-PHY-PAS has a Pfr thermally-conversion fraction of ca. 85% at room temperature. [15]

the conversions: the calculated lifetimes and the ΔAbsorbances show that the conversion mechanism is similar to that of *Pa*BphP. Considering the Pr-to-Pfr route, it is evident that the bleaching of Pr is concomitant with the formation of a red-shifted intermediate absorbing maximally around 710-720 nm, the decay of which takes place with the second lifetime of 184 μs; the final formation of Pfr is yielded with a lifetime of 1.64 ms. As in *Pa*BphP, the Pr-to-Pfr conversion has a larger velocity than for the Pfr-to-Pr conversion, which takes place with a tenfold-longer lifetime. Additionally, another common feature between the two proteins is that the forward Pfr-to-Pr route is spectroscopically more simple than the backward process: however, a rise in absorbace at 710 nm, which starts to decay with a lifetime of 160 μs, points to an intermediate species in that spectral region.

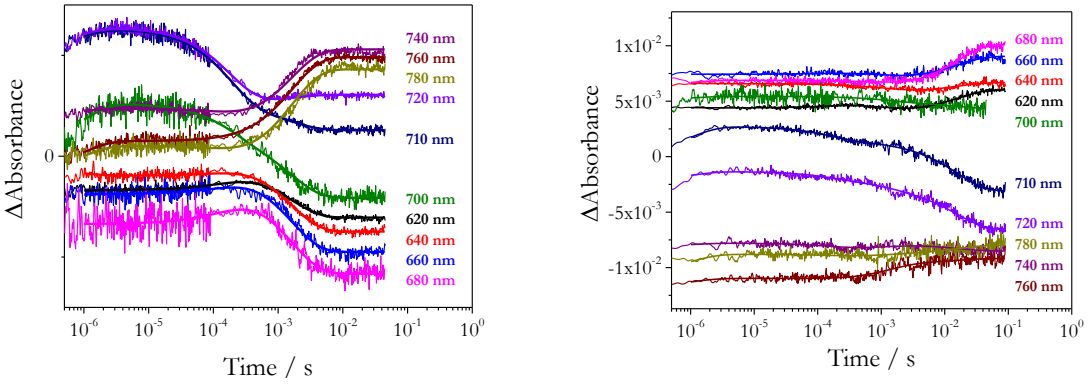

Figure 23: Kinetic traces for the Pr-to-Pfr conversion (left) and for the Pft-to-Pr conversion (right) of *Xc*BphP-PGP, the fitting lines are superimposed.

FphAN753 – fungal BphP-like from *Aspergillus nidulans*

This fungal protein showed a peculiar spectral behaviour: irradiation with RL at 650 nm yielded an absorption spectrum with the characteristic maximum in the far red region around 750 nm, while in the red region there is nearly no decrease of the absorption maximum intensity (Figure 7). This is in contrast with other reported absorption changes upon irradiation for this protein [4]. Careful analysis of steady-state absorption and difference spectra evidenced that our sample contains a considerable

fraction of possibly non-photoconvertible chromophore, absorbing maximally at *ca.* 675 nm: however, the time-resolved experiments, recording only the photoconverting fraction, correctly identify for the Pr-to-Pfr conversion a small final negative peak at 700 nm, as shown in Figure 24.

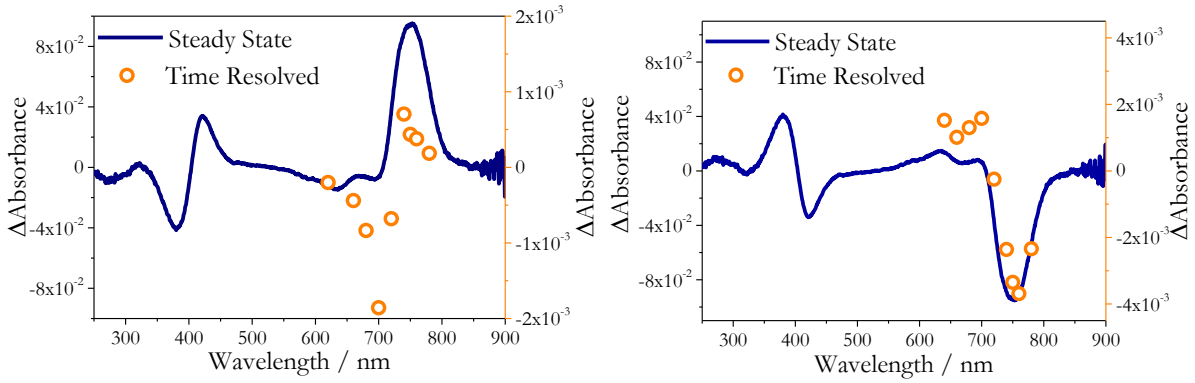

Figure 24: Comparison of matched ΔAbsorbance values for FphAN753 from time-resolved measurements (orange circles) with the steady-state difference spectrum (blue line) for the Pr-to-Pfr route (left) and for the Pfr-to Pr route (right). Adapted from [1].

As for the other BphPs, time-resolved traces of Figure 25 did not follow the formation of the LUMI-R intermediate, thus the first lifetime of 6.3 μs reflects its decay: this component shows in the LADS a loss of absorption around 720-730 nm (red shifted to the Pr form), together with a bleaching at 700 nm visible in the difference spectrum (Figure 26). A positive ΔAbsorbance in the region 620-680 nm decays with a lifetime of 8.4 ms and forming Pfr. The conversion for the Pfr-to-Pr is described in Figure 27 and Figure 28: the transient difference spectra identify the nearly identical shape of the final ΔAbsorbance and both the difference spectra at transient lifetimes. The very small changes in ΔAbsorbance during the conversion give information that the Pr form is already formed during the very early steps of photoconversion, without any formation of further intermediates. [1] This fungal phy is the first phytochrome showing this behaviour. The simpler Pfr-to-Pr route could be related to the fact that the Pr state in this protein shows larger heterogeneity, while

there is a lack of hetherogeneity in the Pfr form associated with the N-H in-plane bending of B and C rings of the chromophore, as evidence by Raman spectroscopy [4]. FphAN753 bears a long extension of about 170 aa, which stabilises the Pfr form: [4] its removal releases the thermal recovery to the parental state, inhibited in FphAN753. This long N-terminal extension is not present in known BphPs. Another sharp difference of this protein from other BphPs is a long insertion of *ca.* 50 aa between the PAS and the GAF domains, which is characteristic of phytochromes from *Ascomycota*. However, the relevance of this region in the functional and structural features of this protein still has to be elucidated.

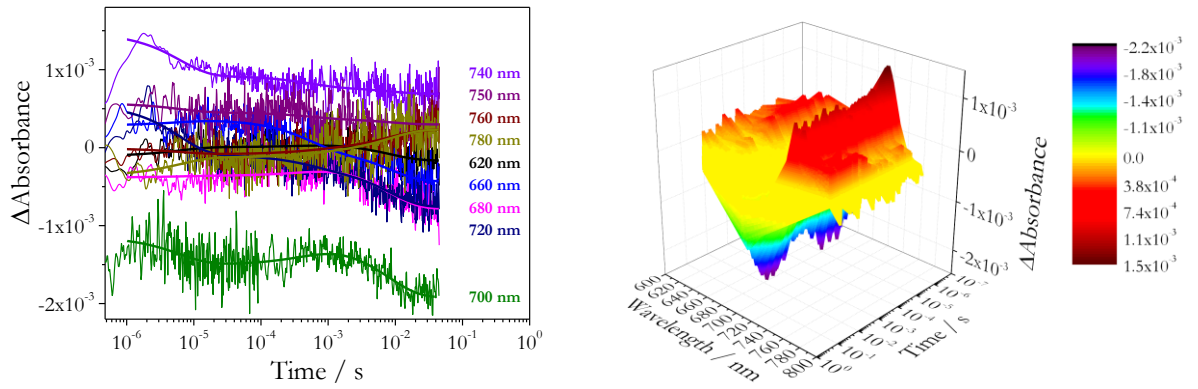

Figure 25: Kinetic traces for the Pr-to-Pfr conversion (left) for FphAN753, the fitting lines are superimposed. 3D transient representation of ΔAbsorbances (right) is presented as a function of time and the probe wavelengths, the false colours map the time-resolved formation and decay of transient species. Adapted from [1].

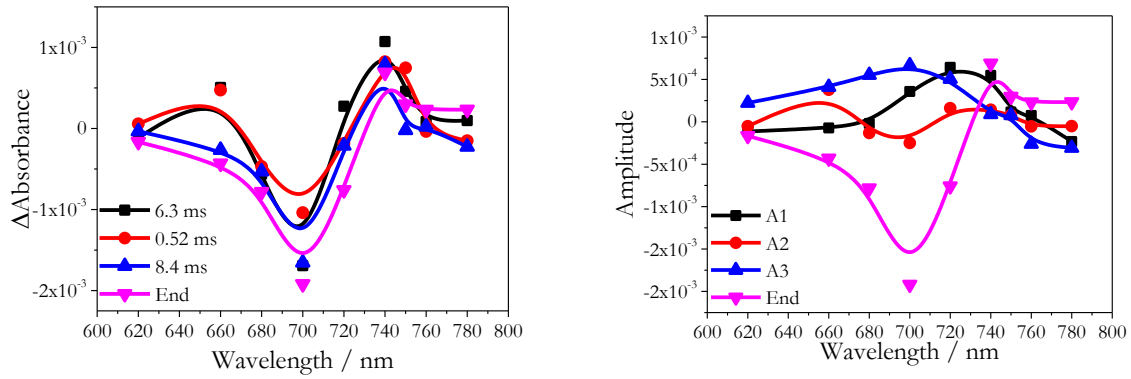

Figure 26: Left, ΔAbsorbances at calculated lifetimes for the Pr-to-Pfr conversion for FphAN753, the values at the end correspond to equilibrium ΔAbsorbances. Right: Lifetime-Associated Difference Spectra (LADS): note that in LADS a negative amplitude corresponds to a formation of an intermediate, while a positive amplitude refers to a decay of an intermediate, the values at the end correspond to equilibrium ΔAbsorbances. Adapted from [1].

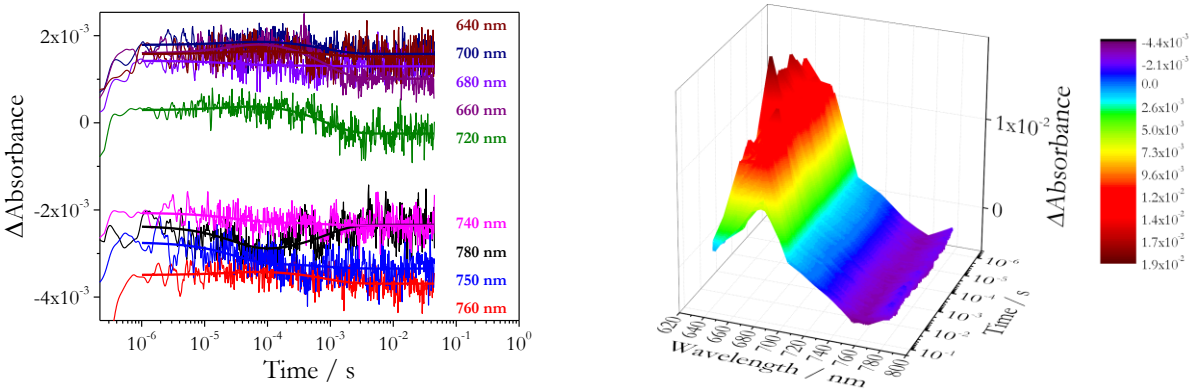

Figure 27: Kinetic traces for the Pfr-to-Pr conversion (left) for FphAN753, the fitting lines are superimposed. 3D transient representation of ΔAbsorbances (right) is presented as a function of time and the probe wavelengths, the false colours map the time-resolved formation and decay of transient species. Adapted from [1].

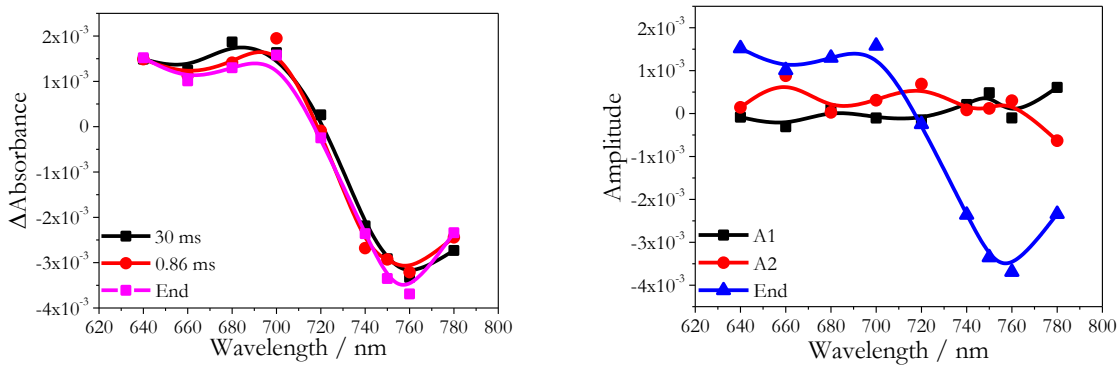

Figure 28: Left, ΔAbsorbances at calculated lifetimes for the Pfr-to-Pr conversion for FphAN753, the values at the end correspond to equilibrium ΔAbsorbances. Right: Lifetime-Associated Difference Spectra (LADS): note that in LADS a negative amplitude corresponds to a formation of an intermediate, while a positive amplitude refers to a decay of an intermediate, the values at the end correspond to equilibrium ΔAbsorbances. Adapted from [1].

*Mr*BphP1 – bacterial phytochrome 1 from *Methylobacterium radiotolerans*

*Mr*BphP1 is the first bacterial phytochrome characterised from the bacterium *Methylobacterium radiotolerans* JCM 2831 and from the genus *Methylobacteria* as a whole. Steady-state measurements revealed peculiar features of this photoreceptor, as already mentioned; also in time-resolved flash photolysis results, *Mr*BphP1 exhibits a different behaviour from the other BphPs here examinated.

The Pr-to-Pfr conversion presented in Figure 29 shows that the transient LUMI-R (detectable as a bleaching in the far-red region and a rise in absorbance at 720-740 nm, red-shifted to the Pr maximum) is stable over the μs time range, while its decay starts at the first calculated lifetime of 1.28 ms. The formation of the Pfr form is reached on the long-ms time scale with a lifetime of 67 ms. The lack of transient lifetimes untill the ms time scale is a typical feature of this first phytochrome from *M. radiotolerans* and it could be releated to the larger photoconversion quantum yield (Table 5), suggesting that there are not shunt reactions or side processes during the Pr-to-Pfr photoconversion.

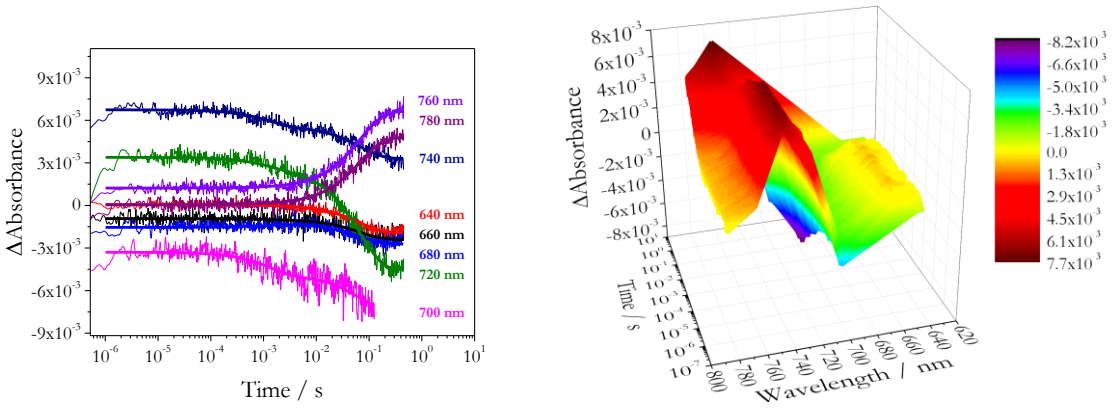

Figure 29: Kinetic traces for the Pr-to-Pfr conversion (left)for *Mr*BphP1, the fitting lines are superimposed. 3D transient representation of ΔAbsorbances (right) is presented as a function of time and the probe wavelengths, the false colours map the time-resolved formation and decay of transient species.

In Figure 30 we can follow the Pfr-to-Pr conversion: from the kinetic traces it is evident a fast bleaching in the Pfr region and the formation of a positive ΔAbsorbance in the red region around 700 nm. This latter Pr-like intermediate is stable on the long-µs time scale (shortest detectable lifetime is 290 µs), in contrast with the other BphPs here examinated, which showed a transient lifetime on the short-µs time scale. With the second lifetime of 2.4 ms the formation of Pr is completed.

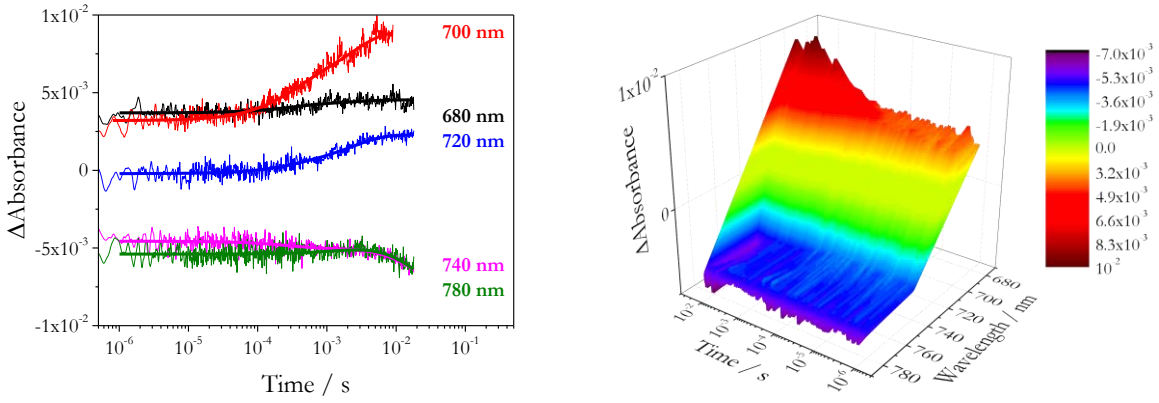

Figure 30: Kinetic traces for the Pfr-to-Pr conversion (left) for *Mr*BphP1, the fitting lines are superimposed. 3D transient representation of ΔAbsorbances (right) is presented as a function of time and the probe wavelengths, the false colours map the time-resolved formation and decay of transient species.

A blue-light photoreceptor from *Methylobacterium radiotolerans*

*Mr*4511 from *Methylobacterium radiotolerans* is a 164-aminoacid photoreceptor composed of a blue-light (BL) responsive LOV (Light, Oxygen, Voltage) core domain plus flanking regions; it binds a riboflavin derivative, most probably flavin mononucleotide (FMN[iv]), as the chromophore and it is fluorescent in the dark state. As in the other LOV domains, BL absorption triggers the photocycle and produces a reversible formation of an FMN-cysteine covelent adduct (light state) through a μs-decay of the FMN triplet state, [16] with a complete loss of fluorescence and a simultaneous activation in the *in-vivo* biological response. In this work the wild type (WT) and different variants of this protein has been investigated with steady-state and time-resolved biophysical techniques: I37V (strand Aβ), Q112W (strand Hβ)„ C71S, C71G, C71S/Q112W, C71G/Q112W, where C71 corresponds to the reactive cysteine of LOV domains (loop Dα-Eα). Figure 31 and Figure 32 show the positions of modified amino acids and the LOV-core topology in comparison with *Bs*YtvA.

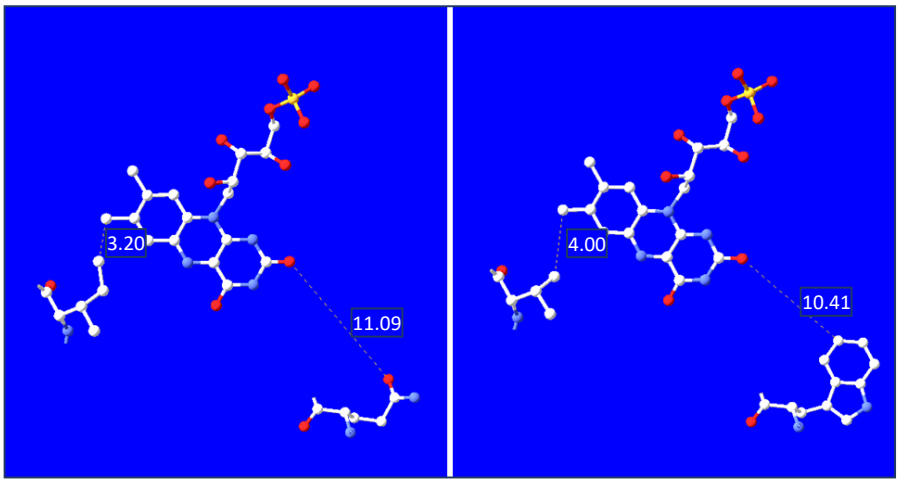

Figure 31: Left: I37 and Q112 in the structural model of *Mr*4511, with closest distance from the chromophore (in Å). Right: the corresponding V28 and W103 in *B. subtilis* YtvA-LOV; for the latter the closest distance to FMN is 10.41 Å, ring center to ring center is ca. 15 Å.

[iv] Chromophore extraction was not performed, but FMN is generally assumed as the chromophore of non-fungal LOV domains.

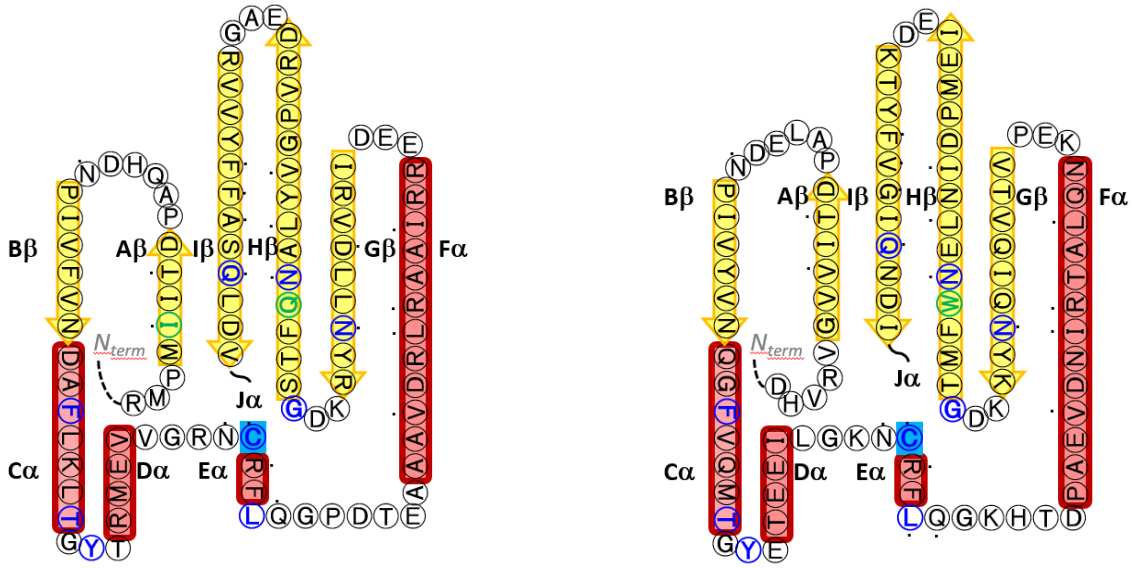

Figure 32: Left: topology of the LOV core of *Mr*4511 (from R33-137), with amino acids mapped onto the secondary structure elements, as derived from the structural model (SwissModel, template in PDB = 3ue6 = Aureochrome1 LOV domain, dark state). Yellow, β-strands; red, α-helices; marked in blue: the 10 superconserved residues in LOV domains, the reactive C71 is further highlighted in cyan; a dot marks aa within 4 Å from the FMN chromophore. Variants investigated include mutations at position I37 (marked in green, strand Aβ), C71 (loop Dα-Eα) and Q112 (marked in green, strand Hβ). Right: the LOV core of *Bs*YtvA (aa D21-I126, from thePDB entry 2pr5); here the reactive cysteine is C62 (highlighted in cyan). Note W103 (marked in green) corresponding to Q112 in *Mr*4511.

Absorbance and emission spectroscopy

Absorption and fluorescence spectra for *Mr*4511-WT and variants I37V and Q112W are reported in Figure 33, top: they show the typical features of other LOV domains, with a blue-region absorption maximum at 449 nm and a fluorescence maximum at 498 nm. The C71X (X = G or S) variants exhibit an absorption maximum at 447 nm (X = G) or 448 nm (X = S), and a fluorescence peak at 497 nm (X = G) and 496 nm (X = S) (Figure 33 bottom). Other photophysical properties are presented in Table 7. For the C71X variants, fluorescence parameters are fully in line with published values for FbFP (Flavin-binding Fluorescent Proteins) [17]. The quantum yields of triplet formation (Φ_T) for C71X variants were measured by laser flash photolysis technique, while for WT, I37V, Q112W the Φ_T values presented in Table 7 derives from time-resolved photoacoustic measurements (see next section for details). The

quantum yield of adduct formation (photoconversion quantum yield Φ_{390}) in Table 7 was optically determined, for a comparison with data from time-resolved photoacoustic signals see Table 9: this value is not inserted for C71X variants since the lack of the reactive C71 prevents the formation of the adduct.

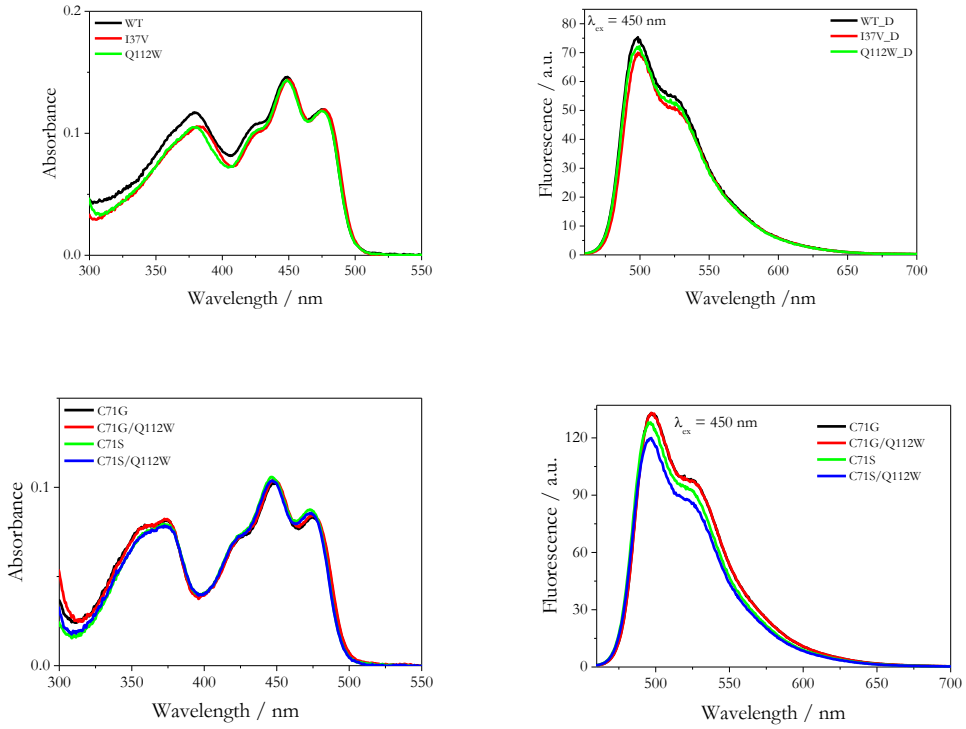

Figure 33: Absorption (left) and fluorescence (right) spectra (excitation at 450 nm, 20 °C) of *Mr*4511 WT, I37V, Q112W (top, dark adapted state) and *Mr*4511 C71X (X = S or G) variants (bottom).

Table 7: Photophysical properties of *Mr*4511 WT and variants. When not specified, errors are ± 10%.

***Mr*4511-**	ε_{448} / M^{-1} cm^{-1}	Φ_F	$\Phi_F x \varepsilon$ / M^{-1} cm^{-1}	τ_F /ns	Φ_T	Φ_{390} (optical)
WT	12700	0.14	1780	2.0 ± 0.3	0.78 ± 0.01	0.45 ± 0.09
I37V	13700	0.13	1780	2.0 ± 0.2	0.85 ± 0.01	0.3 ± 0.1
Q112W	12500	0.13	1620	2.0 ± 0.3	0.81 ± 0.01	0.4 ± 0.1
C71S	13800	0.35	4830	3.9 ± 0.1	0.46	-
C71S/Q112W	14500	0.32	4640	3.8 ± 0.1	0.50	-
C71G	13800	0.37	5100	4.5 ± 0.1	0.58	-
C71G/Q112W	13600	0.37	5030	4.3 ± 0.1	0.56	-

The *Mr*4511 protein in its WT form shows an extremely long photocycle, with τ_{rec} = 15160 s at 27 °C. In Figure 34 it is reported the thermal recovery to the dark-adapted state: after 20 min in the dark, the protein absorption spectrum is almost identical to that of the light state and only after 1 h the protein presents changes in the spectrum. Nevertheless, the photocycle can be accelerated introducing a change in Ile37: as a result, the variant I37V recovers to the dark state with a lifetime τ_{rec} = 3100 s at 27 °C, five-time shorter than the WT protein. Comparison between the thermal recovery kinetics for the WT protein and I37V can be appreciated in Figure 35. The residue at this position, on strand Aβ in close vicinity (< 0.4 nm) of the flavin 7a-methyl group in LOV domains crystal structures, is known to strongly affect the dynamics of the photocycle [18]: in many LOV domains it is a valine, and its mutation into isoleucine or leucine (e.g. V418I in *A. sativa* phot1-LOV2 or V28L in *B.subtilis* YtvA) largely increases τ_{rec} [19].

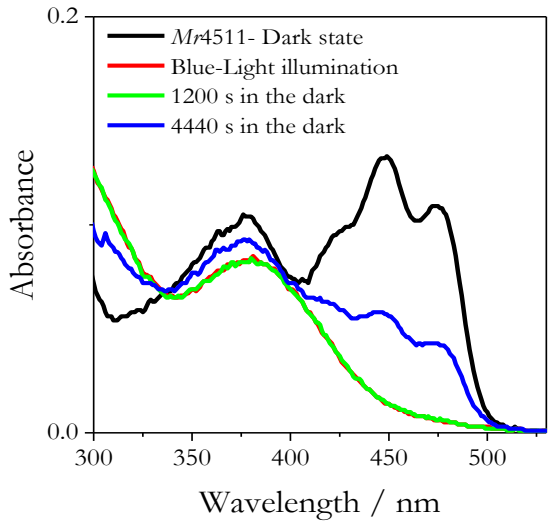

Figure 34: Different absorption spectra for *Mr*4511 thermal recovery to the dark-adapted state, at different time intervals.

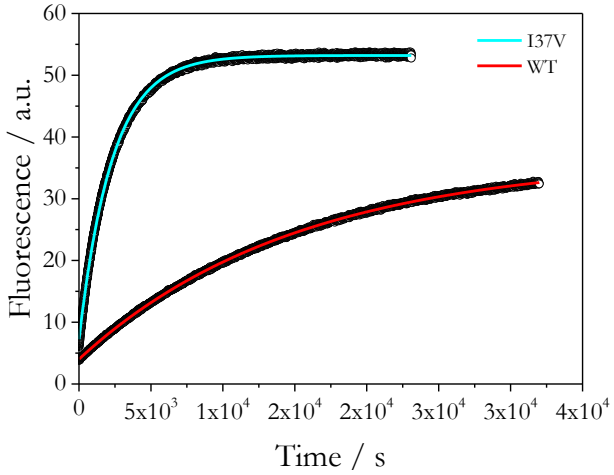

Figure 35: Recovery kinetics, measured at 27 °C as increase in fluorescence at 500 nm starting from the light state. Excitation was provided at 303 nm; the no influence of the the detection light on the measurement was checked by illuminating the protein dark state and observing no decrease in the fluorescence intesity. Fitting mono-exponential solid lines are superimposed.

The reason for mutation Q112W was to introduce a Trp residue, which is conserved in *ca.* 75% of LOV domains [20]. The importance of this Trp residue as one of the major quenchers of the FMN triplet state was highlighted in [21,22]: proteins with mutations in the position of that Trp (named SOPPs, enhanced miniSOG variants) showed an increase of up to 20-fold in the SO quantum yield [21] with respect to the miniSOG low value of Φ_Δ = 0.03. A prerequisite of a LOV-derived SO photosensitiser is the mutation of the reactive Cys, in order to prevent the formation of the photoadduct and so confer to the triplet state a lifetime long enough to produce SO via diffusion-limited energy transfer to molecular oxygen. For *Mr*4511, the reactive Cys is in position 71, and this was the reason why variants C71X were examinated. In the following, we will show that *Mr*4511 becomes a SO photosensitiser with a single mutation C71X (X = G or S). [23]

In Figure 36 aligned sequences of proteins belonging to the toolbox of LOV-derived photosensitisers are presented. "MiniSOG (Mini Singlet-Oxygen Generator) was derived from the LOV2 domain of *Arabidopsis thaliana* phototropin 2 (UniProt code: P93025) (*At*Phot2-LOV2) introducing six mutations (highlighted in grey in Figure 36),

[24] including the reactive cysteine (C426, that became G40 with miniSOG numbering). SOPP proteins were derived from miniSOG by rational design of further mutations. [25] Pp2FbFP has been engineered from the LOV protein Q88JB0 (UniProt) from *Pseudomonas putida* and used as a full length protein (151 aa) with two mutations; [26] *Ds*FbFP was derived from a LOV protein from *Dinoroseobacter shibae* (UniProt A8LP63, 133 aa) by mutation of the reactive cysteine (C72A), together with a further variant at position 49 (M49I, corresponding to L30 of Pp2FbFP); [27] note valine 113 in place of miniSOG tryptophan 81. *Mr*4511 (UniProt B1M516, 164 aa) has a single mutation C71X (X = G or S); note glutamine 112 in place of miniSOG tryptophan 81." [23]

```
AtPhot2-LOV2 386 IEKNFVISDP RLPDNPIIFA SDSFLELTEY SREEILGRNC RFLQGPETDQ
miniSOG        1 MEKSFVITDP RLPDNPIIFA SDGFLELTEY SREEILGRNG RFLQGPETDQ
SOPP           1 MEKSFVITDP RLPDNPIIFA SDGFLELTEY SREEILGRNG RFLQGPETDQ
SOPP2          1 MEKSFVITDP RLPDNPIIFA SDGFLELTEY SREEILGRNG RFLQGPETDQ
SOPP3          1 MEKSFVITDP RLPDNPIIFA SDGFLELTEY SREEILGRNG RFLQGPETDQ
Pp2FbFP-L30M  14 SNDGIVVAEQ EGNESIMIYV NPAFERLTGY CADDILYQDA RFLQGEDHDQ
DsFbFP        33 AEMSVVFSDP SQPDNPMIYV SDAFLVQTGY TLEEVLGRNA RFLQGPDTNP
DsFbFP_M49I   33 AEMSVVFSDP SQPDNPIIYV SDAFLVQTGY TLEEVLGRNA RFLQGPDTNP
Mr4511-C71X   32 TRMPMIITDP AQHDNPIVFV NDAFLKLTGY TRMEVVGRNX RFLQGPDTEA

AtPhot2-LOV2 436 ATVQKIRDAI RDQREITVQL INYTKSGKKF WNLFHLQPMR DQKGELQYFI GVQLDG
miniSOG       51 ATVQKIRDAI RDQREITVQL INYTKSGKKF WNLLHLQPMR DQKGELQYFI GVQLDG
SOPP          51 ATVQKIRDAI RDQREITVQL INYTKSGKKF WNLLHLQPMR DQKGELQYFI GVLLDG
SOPP2         51 ATVQKIRDAI RDQREITVQL INYTKSGKKF LNLLHLQPMR DQKGELQYFI GVVLDG
SOPP3         51 ATVQKIRDAI RDQREITVQL INYTKSGKKF LNLLNLQPIR DQKGELQAFI GVVLDG
Pp2FbFP-L30M  64 PGIAIIREAI REGRPCCQVL RNYRKDGSLF WNELSITPVH NEADQLTYYI GIQRDV
DsFbFP        83 HAVEAIRQGL KAETRFTIDI LNYRKDGSAF VNRLRURPIY DPEGNLMFFA GAQNPV
DsFbFP_M49I   83 HAVEAIRQGL KAETRFTIDI LNYRKDGSAF VNRLRIRPIY DPEGNLMFFA GAQNPV
Mr4511-C71X   82 AAVDRLRAAI RREEDIRVDL LNYRKDGSTF QNALYVGPVR DEAGRVVYFF ASQLDV
```

Figure 36: Aligned aminoacid sequences of the LOV core of *Mr*4511-C71X (X = G or S) and other photosensitising LOV domains. Adapted from [23].

The distance between W112 and FMN chromophore in the variants of *Mr*4511 protein is *ca.* 15 Å, according to crystal structures available for LOV domains. This latter information leads to another feature of the Q112W variants: FRET (Förster Resonance Energy Transfer) experiments indicate that there is energy transfer between W112 and the FMN. From Figure 37 it can be noticed that the increment of FMN fluorescence intensity in the presence of W112 was 55% for all the variants,

suggesting that FRET occurs from W112 (when present) to FMN. Unfortunately, the energy transfer efficiency could not be calculated, since it is not possible to obtain a precise value for fluorescence (lifetime or intensity) and absorbance of the donor (W112) in the absence of the acceptor (FMN). [23] This observation suggests that this Trp residue might serve as an energy donor to the FMN chromophore upon UVB radiation: however, his *in vivo* relevance in native LOV proteins still remains unclear.

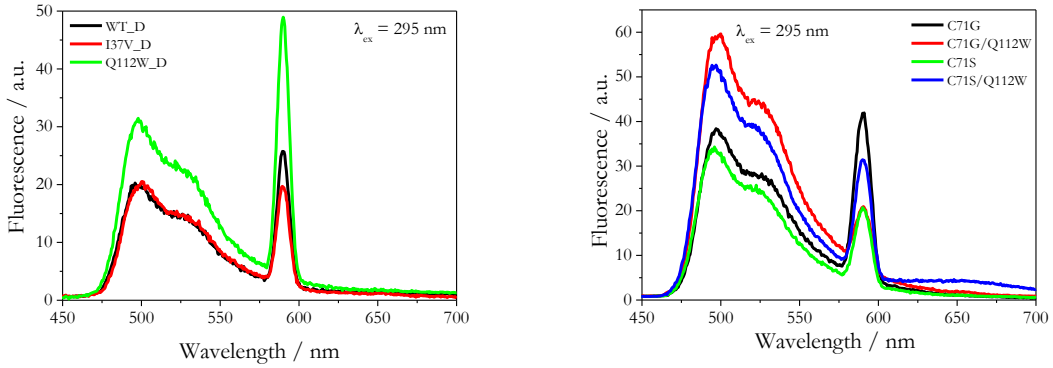

Figure 37: Fluorescence spectra of *Mr*4511 WT, I37V, Q112W in their dark state (left) and of *Mr*4511 C71X (X = S or G) variants (right) exciting the samples at 295 nm at 20°C. To compare the values, the absorbance for FMN at 448 nm was the same (0.1): this should ensure the same absorbance for FMN also at 295 nm.

Time-resolved spectroscopy

In order to calculate the triplet formation quantum yield (Φ_T) for the WT *Mr*4511 and I37V, Q112W variants, was used the time-resolved photoacoustic (PA) technique. The PA signals for photochemically active *Mr*4511 proteins (WT and the two variants I37V and Q112W) were best fitted by a two-exponential decay function as previously described [28]. The unresolved, "prompt" step ($\tau_1 < 20$ ns) can be safely assigned to the fast reactions resulting in the formation of the FMN triplet state (subscript T) . The microsecond process corresponds to the triplet decay with concomitant formation of the photoadduct (subscript 390). Energy balance considerations and the results of deconvolution directly provide the products $\Phi_T E_T$ and $\Phi_{390} E_{390}$ (Eq. 7 and Eq. 8), referring to the quantum yield of formation for the

triplet state and adduct, respectively, multiplied by the energy level of the two transients: [29]

Eq. 7

$$\Phi_T = \frac{E_T}{E_\lambda} = 1 - \alpha_1 - \Phi_F \frac{E_F}{E_\lambda}$$

Eq. 8

$$\alpha_2 = \Phi_T \frac{E_T}{E_\lambda} - \Phi_{390} \frac{E_{390}}{E_\lambda}$$

where E_F is the average energy for the fluorescence emission (232 kJ/mol for LOV proteins), and E_λ= 265.84 kJ/mol is the photonic excitation energy (λ_{ex} =450 nm).

Here was used a value for E_T = ca. 200 kj/mol, as previously measured for other LOV domains with diverse technique, [30–33] to obtain Φ_T. Furthermore was estimated a lower limit for Φ_{390} by taking E_T= 200 kJ/mol as the highest possible value for E_{390}.

The molecular volume changes experienced by *Mr*4511 proteins upon formation of the flavin triplet state (ΔV_T) and of the photoadduct (ΔV_{390}) - with respect to the unphotolysed state - can be calculated with Eq. 9 and Eq. 10, provided that quantum yields are known:

Eq. 9

$$\Delta V_T = \frac{\Delta V_1}{\Phi_T}$$

Eq. 10

$$\Delta V_{390} = \Delta V_T + \frac{\Delta V_2}{\Phi_{390}}$$

Formation of the triplet state for the *Mr*4511 WT and I37V, Q112W variants occurs with a small contraction, similar to other LOV domains and FMN itself [28,31–34] (Table 8 and Table 9); in sharp contrast to other LOV proteins, though the triplet state decays into the adduct concomitant with an expansion, which is smaller for I37V and equally large for WT and Q112W. There is still no explanation for this fact, but

possibly it could hint to a more rigid cavity of the chromophore cavity, also suggested by the robustness of *Mr*4511 to denaturation (*vide infra*).

Table 8: Photoacoustic data from deconvolution analysis for *Mr*4511 WT and I37V, Q112W variants.

***Mr*4511-**	α_1 (τ_1 < 20ns)	ΔV_1 mL/einstein	α_2	ΔV_2 mL/einstein	τ_2 **(10°C)**/μs
WT	0.29 ± 0.01	-0.72 ± 0.01	0.33 ± 0.03	+ 3.7 ± 0.2	1.64 ± 0.04
I37V	0.24 ± 0.01	-0.93 ± 0.01	0.38 ± 0.03	+ 1.4 ± 0.1	1.7 ± 0.2
Q112W	0.28 ± 0.01	-0.84 ± 0.02	0.38 ± 0.02	+ 3.5 ± 0.1	1.57 ± 0.02

Table 9: Photophysical and photochemical parameters from Eq. 7, Eq. 8, Eq. 9, Eq. 10.

***Mr*4511-**	Φ_T	Φ_{390}	ΔV_T mL/mol	ΔV_{390} mL/mol	Φ_{390} (optical)
WT	0.78 ± 0.01	≥ 0.34 ± 0.04	-0.93 ± 0.02	≤ +2.7 ± 0.2	0.45 ± 0.09
I37V	0.85 ± 0.01	≥ 0.35 ± 0.05	-1.09 ± 0.01	≤ +0.3 ± 0.1	0.3 ± 0.1
Q112W	0.81 ± 0.01	≥ 0.30 ± 0.03	-1.04 ± 0.01	≤ +2.4 ± 0.1	0.4 ± 0.1

The advantage of using PA to determine Φ_T and Φ_{390} over optical methods relies on the fact that absorption coefficients of transient species are not needed and spectral overlapping between parent and transient states are irrelevant; furthermore, an actinometer is not needed, given that the determination is absolute. Furthermore, given that the excitation volume is very small (4% of the total volume), this technique is particularly useful with photochemically competent LOV proteins, because it minimises photoconversion. Within the errors, the values of Φ_{390} are in line with those determined with optical methods (Table 9), *i.e.* the three variants show a very similar efficiency for adduct formation. The value of Φ_T is instead lager for I37V, showing that this mutation not only has a strong impact on τ_{rec} (one order of magnitude faster than for WT and Q112W), but also on the photophysics. The smaller expansion recorded for this variant upon adduct formation could be

correlated with the much faster τ_{rec}, *i.e.* the protein undergoes a smaller light-induced conformational change that WT and Q112W and must thus overcome a smaller conformational barrier to return to the parent state. This hypothesis could be verified by vibrational spectroscopy for the detection of light-induced protein conformational changes.

The WT *Mr*4511 protein and its I37V and Q112W variants exhibit a triplet lifetime (measured by single-shot laser flash photolysis) comparable with values of other LOV domains: in Figure 38 are reported fitted signals of the WT protein and of FMN for comparison, in Table 10 are presented the triplet-lifetime values.

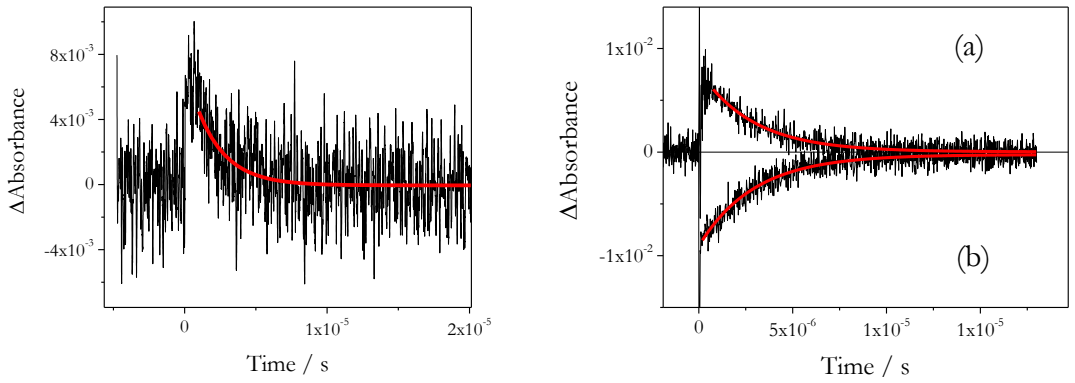

Figure 38: Left: triplet decay for the *Mr*4511 WT protein in H_2O Napi buffer obtained by a single-shot transient absorption experiment. The red curve derived from a mono-exponential fitting decay function of the flash photolysis signal (excitation at 475 nm) is overlaid with the black experimental trace. Right: (a) Triplet decay (detection at 660 nm) and (b) ground-state recovery (detection at 450 nm) for FMN in H_2O Napi buffer. The red curves derived from a monoexponential fitting decay function of the flash photolysis signals (excitation at 475 nm) are superimposed: the two processes are synchronous.

Transient absorption experiments on the C71X variants showed interesting features of this proteins: triplet lifetimes are in the order of hundreds of μs and the introduction of the second mutation Q112W dramatically shortens τ_T of one order of magnitude, as can be seen in Figure 39. Moreover, τ_T becomes longer after removing oxygen by purging with N_2 for 90 min (Figure 41). A resume of values and

a comparison with other LOV-derived photosensitisers from literature is given in Table 10.

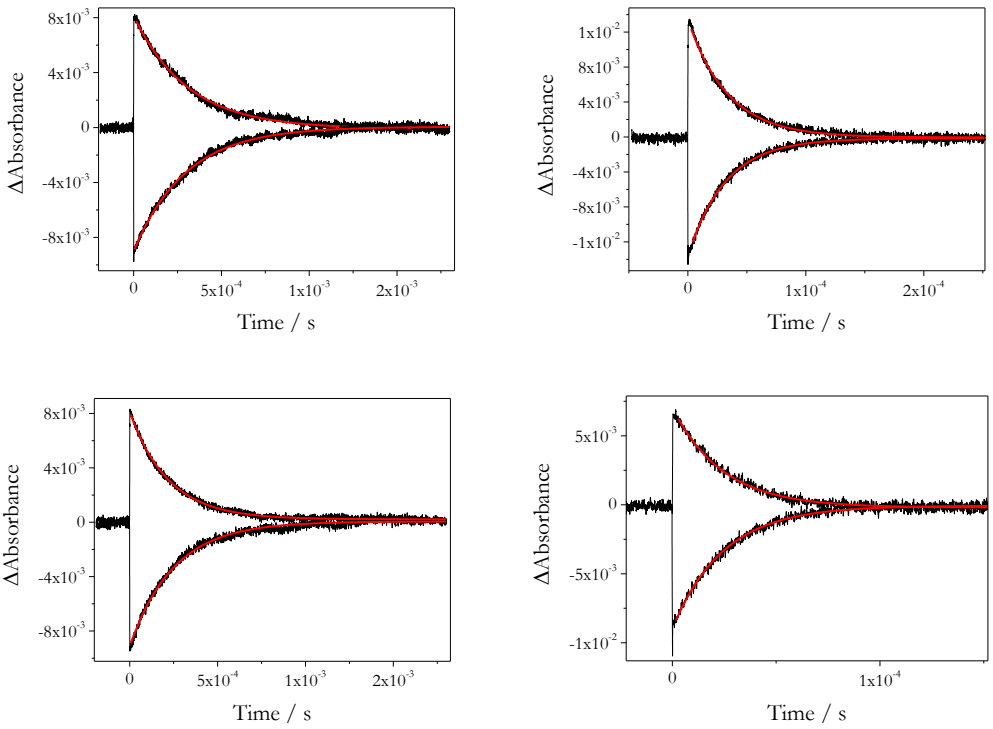

Figure 39: Triplet decay (detection at 660 nm) and bleaching of the parent state (detection at 450 nm) for the *Mr*4511 C71G (top left), C71G/Q112W (top right), C71S (bottom left), C71S/Q112W (bottom right) in H_2O Napi buffer, obtained by transient absorption laser flash photolysis. The red curve derived from mono-exponential fitting functions of the flash photolysis signal (excitation at 355 nm) is overlaid with the black experimental trace.

Table 10: Triplet lifetimes τ_T for *Mr*4511 variants, FMN and other proteins. Detection for C71X variants was 720 nm, to be on the maximum of the transient triplet spectrum shown in Figure 40. Errors are within 15%. Adapted from [23].

***Mr*4511-**	H_2O_{buffer}, τ_T / μs		D_2O_{buffer}, τ_T / μs	
	Air	**N_2**	**Air**	**N_2**
WT	2.0			
I37V	2.3			
Q112W	2.0			
C71S	240	362	446	549
C71S/Q112W	24.7	27.3	29.7	29.8
C71G	342	541	498	727
C71G/Q112W	31.2	32.5	38.0	41.5
Others, 23°C	**Air**	**N_2**	**Air**	**N_2**
FMN	2.9	--	3.07 [35]	--
miniSOG [35]	31.3	33.6	38.6	41.8
miniSOG-W81F [22]	-	-	265	1100
SOPP [35]	96.3	141	122	205
SOPP2 [21]			130	1000
SOPP3 [21]			135	3300

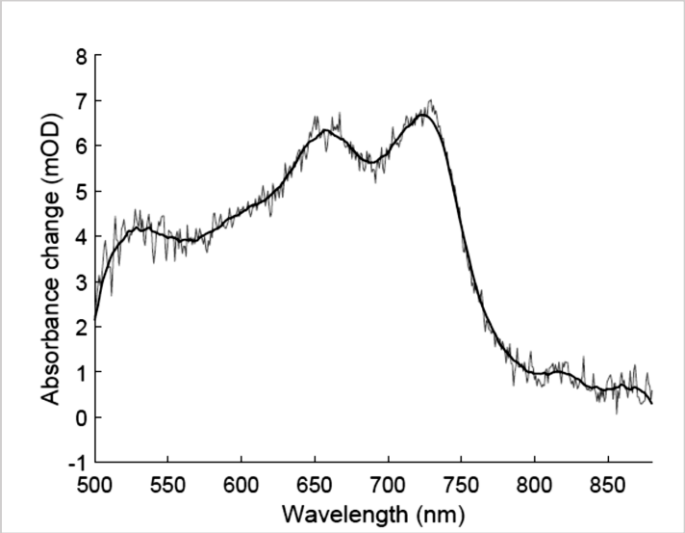

Figure 40: Transient absorption spectrum of *Mr*4511-C71G/Q112W in air-saturated H_2O Napi buffer. The solid line serves as a guide to the eye. Adapted from [23].

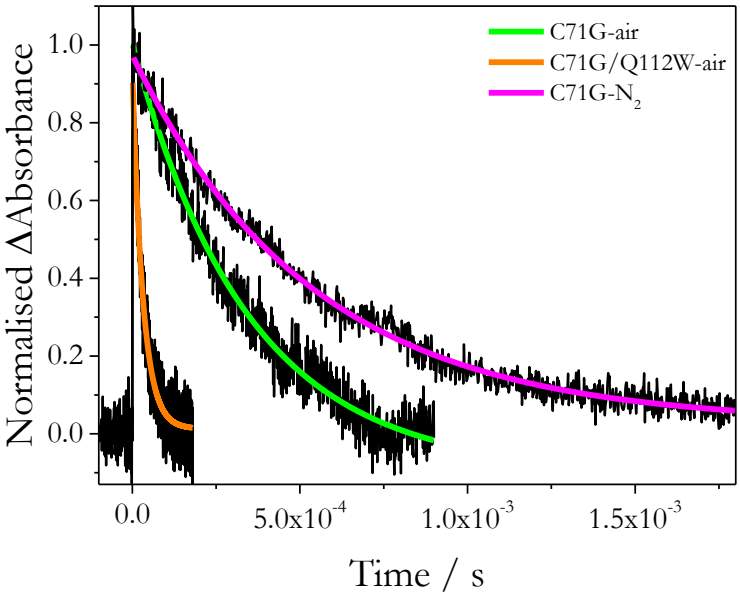

Figure 41: Influence of deoxygenation and tryptophan on FMN triplet-state decay (probe wavelength 720 nm, excitation 355 nm) for *Mr*4511-C71G, in single-shot transient absorption experiments (H_2O buffer). Fitting single-exponential functions are superimposed. Adapted from[23].

We noticed in the Introduction chapter that the triplet state can lead to ROS formation *via* type-I and type-II mechanisms: in order to identify and quantify the SO production, measurements based on direct and indirect methods for SO detection were performed to understand if this *Mr*4511 C71X variants could be efficient SO generators with only one mutation of the reactive Cys. Φ_Δ directly determined by time-resolved detection of phosphorescence at 1275 nm and indirecly measured by the fluorescent probe Singlet Oxygen Sensor Green® (SOSG) are presented in Table 11. Experiments were performed both in D_2O and H_2O buffer solutions, because the lifetime of SO is appreciably longer in D_2O (ca. 70 μs) than in H_2O (ca. 3.5 μs): in this way the 1275 nm signal amplitude is increased as well discrimination between the kinetics of SO formation and decay is facilitated. [36] SO phosphorescence traces are visible in Figure 42 for *Mr*4511 C71G in O_2-saturated D_2O Napi buffer, while the increasing in SOSG in the presence of the *Mr*4511 C71S photosensitiser is shown in Figure 43. Using SOSG, Φ_Δ for the proteins was derived by comparison with the slope for the FMN used as reference (see Materials and

Methods chapter). Control measurements showed that: a. in the absence of the photosensitiser, SOSG (dark) fluorescence at 530 nm increases negligibly; b. the protein alone shows a residual fluorescence at 530 nm that remains constant with LED462 illumination; c. in the presence of 40 mM azide (NaN_3), a quencher of SO, the increase of SOSG fluorescence is much lower.

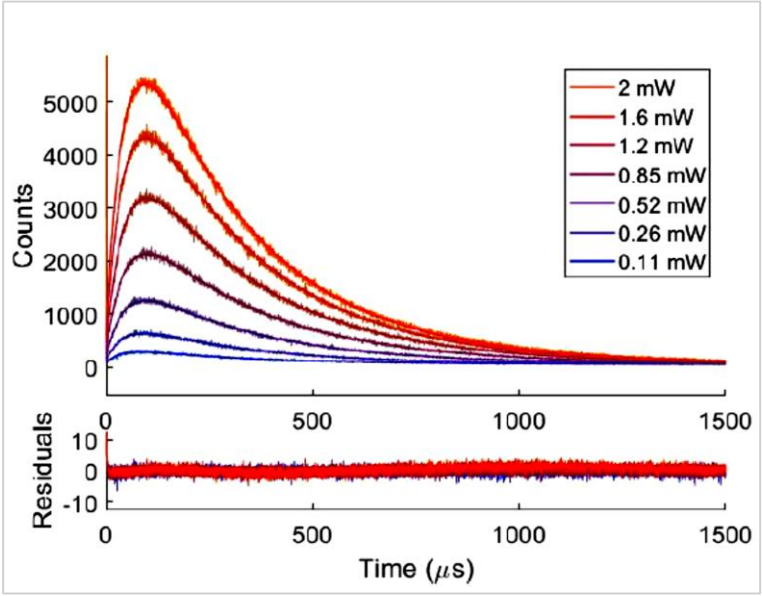

Figure 42: Singlet-oxygen phosphorescence traces from *Mr*4511-C71G in O_2-saturated D_2O Napi buffer for different incident-laser powers. [23] Three-exponential fitting lines [35] are superimposed on each kinetic trace. The intensity-normalised residuals are presented in the panel below.

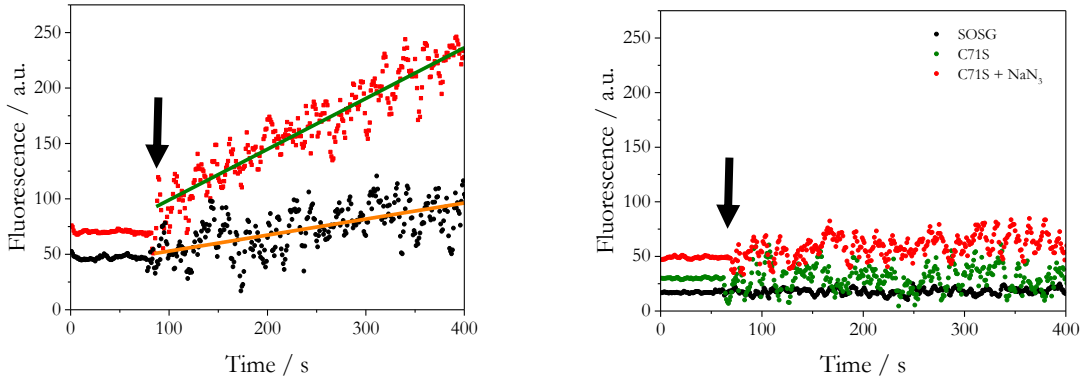

Figure 43: Left: linear increase in the fluorescence of Singlet Oxygen Sensor Green (SOSG) in the presence of the *Mr*4511 C71S photosensitiser, measured at 530 nm (λ_{ex} = 500 nm) upon illumination with LED 462 nm (black circles), compared to FMN (red circles). Starting illumination time is indicated by a dark arrow. Right: control measurements in the same experimental conditions using SOSG alone, protein alone, and SOSG with protein and the SO quencher NaN_3. Measurements were performed at 20 °C. Adapted from [23].

Table 11: Singlet oxygen quantum yields (Φ_Δ) for samples in H_2O and D_2O Napi buffer. Both values of Φ_Δ for air-saturated and oxygen-saturated conditions are presented. Errors are ± 15%. [23]

* Measured using SOSG, taking as reference FMN with Φ_Δ = 0.56 and 0.64 in H_2O and D_2O Napi buffer, respectively

***Mr*4511-**	Φ_Δ in H_2O_{buffer}		Φ_Δ in D_2O_{buffer}	
	Air	**+O_2**	**Air**	**+O_2**
C71S	0.17*	0.23	0.20/0.26*	0.45
C71S/Q112W	--	0.04	0.01	0.03
C71G	0.19*	0.31	0.20/0.19*	0.45
C71G/Q112W	--	0.04	0.01	0.04
Others	**Air**	**+O_2**	**Air**	**+O_2**
FMN[35]	0.56	0.58	0.64	0.68
miniSOG	0.03[37]		0.03[38]	0.14[38]
miniSOG-W81F			0.33[39]	
SOPP[40]	0.19		0.23	0.44
SOPP2[38]			0.51	0.55
SOPP3[38]			0.61	0.60
Pp2FbFP-L30M	0.09[22]		0.11[27]	
DsFbFP[27]			0.33	

From Table 11, it can been noticed that the absence of W112 ensures that *Mr*4511 C71X has Φ_Δ comparable to SOPP with only the mutation of the reactive Cys, while introduction of a tryptophan in this position results in values comparable to miniSOG. A similar enhancing effect has been recently reported for the W81F variant of miniSOG [22] and for *Ds*FbFP (designed from *Dinoroseobacter shibae*), which has a valine instead of a tryptophan and produces Φ_Δ = 0.33. [27] Another bacterial LOV protein studied as a SO photosensitiser was Pp2FbFP-L30M, presenting two mutations with respect to the native photoreceptor from *Pseudomonas putida*, [26] with Φ_Δ = *ca.* 0.11. [27] Although the Φ_Δ for both the C71X variants is not effected by this kind of mutation, it can be noticed that τ_F and τ_T are shorter for *Mr*4511 C71S than for *Mr*4511 C71G: this observation indicates that the internal conversion from the FMN singlet excited state and the intersystem crossing from the triplet state are faster in the C71S variant. [23]

Another interesting feature of *Mr*4511 C71X variants is that they are more photostable than free FMN, which instead is known to be converted to lumichrome

after prolonged illumination, with enhancement of SO production and oxidation of electron-rich aminoacids [22]. Data in Figure 44 show that the formation of lumichrome for BL-illuminated free FMN is evident from absorbance spectra taken after different time steps: during time there is a gradual production of a species with a blue-shifted absorption maximum around 350 nm [22]. [23] In contrast, under the same experimental conditions *Mr*4511 C71G shows only very limited evidence of degradation after prolonged illumination. [23] For comparison, it can be reminded that in literature [41,25] it has been demonstrated that, different to what here discovered for *Mr*4511 C71X variants, the miniSOG produces photodegradation products after prolonged BL illumination. However, this observation on the *Mr*4511 C71X-variants photostability has to be confirmed by future *in vivo* studies.

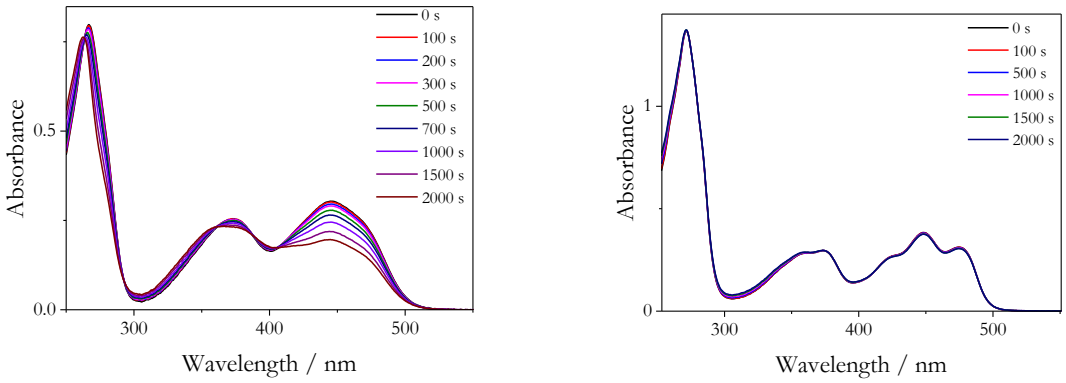

Figure 44: Absorption spectra of FMN (left) and *Mr*4511 C71G (right) under prolonged illumination with LED 462 nm. The spectra were recorded after the illumination time steps shown in legend. Illumination with BL was provided by LED 462 nm from the top of the cuvette ensuring homogeneous illumination of the sample; in order to ensure that the same number of photons were absorbed, the solutions were equally absorbing in the blue-light region. The measured LED462 power was P ≈ 3 mW. Adapted from [23].

The last astonishing feature emerged from the study of this BL-photoreceptor from *Methylobacterium radiotolerans* is its robustness against denaturation: after 24 h in Urea 8 M it is still partially photoactive. As a comparison, *Bs*YtvA from *Bacillus subtilis* after two hours in the same conditions is completely denatured, as shown in Figure 46.

Measuring fluorescence anisotropy of the FMN chromophore for *Mr*4511 C71 in Urea 7.8 M, after many days it partially retains anisotropy (Figure 45): qualitative analysis of circular dichroism spectra taken at different time steps confirms that the protein secondary structure goes very slowly to the random-coil conformation. In Guanidinium chloride 7.8 M the process is faster than in Urea, but it requires some hours and it was slow enough to measure absorption coefficients of Table 7. This property of roboustness exhibited by this photoreceptor could be extremely important for using *Mr*4511 as a fusion tag in *in vivo* applications.

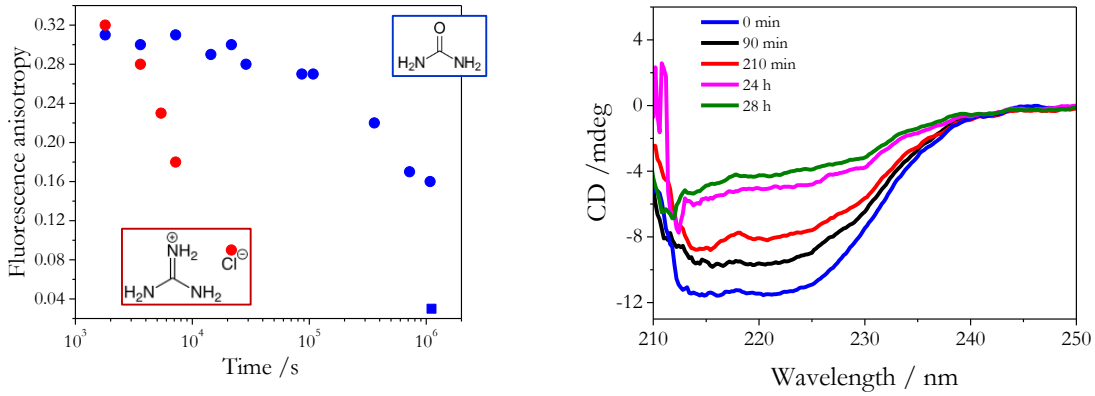

Figure 45: Left: fluorescence anisotropy of FMN bound to *Mr*4511-C71 in 7.8 M urea (blue circles) or GuHCl (red circles); blue square: free FMN in 7.8 M urea. Excitation at 450 nm. Adapted from [23]. Right: circular dichroism spectra of *Mr*4511 C71S in Urea 7.8 M, taken at different time steps.

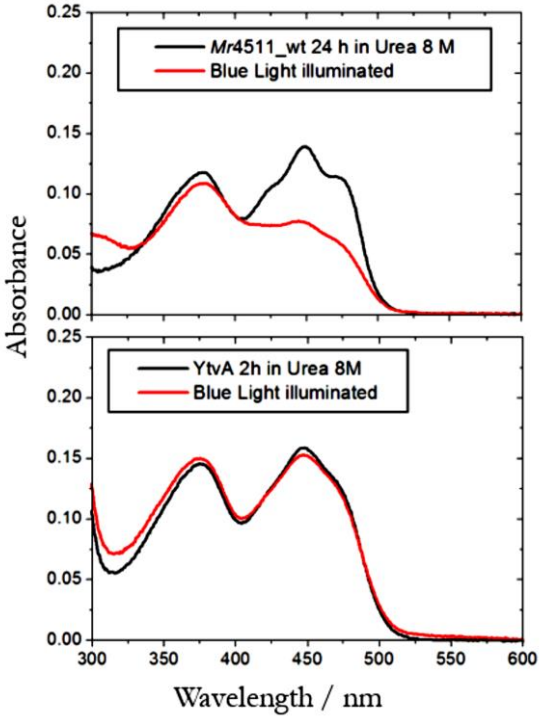

Figure 46: Comparison between absorption spectra of *Mr*4511 WT (top) and YtvA (bottom) in Urea 8 M.

Bibliography

1. Consiglieri, E. *et al.* Dynamics and efficiency of photoswitching in biliverdin-binding phytochromes. *Photochem. Photobiol. Sci.* **18**, 2484–2496 (2019).

2. Tasler, R., Moises, T. & Frankenberg-Dinkel, N. Biochemical and spectroscopic characterization of the bacterial phytochrome of Pseudomonas aeruginosa. *FEBS J.* **272**, 1927–1936 (2005).

3. Shah, R., Schwach, J., Frankenberg-Dinkel, N. & Gärtner, W. Complex formation between heme oxygenase and phytochrome during biosynthesis in Pseudomonas syringae pv. tomato. *Photochem. Photobiol. Sci.* **11**, 1026 (2012).

4. Brandt, S., von Stetten, D., Günther, M., Hildebrandt, P. & Frankenberg-Dinkel, N. The fungal phytochrome FphA from Aspergillus nidulans. *J. Biol. Chem.* **283**, 34605–14 (2008).

5. Otero, L. H. *et al.* Structure of the Full-Length Bacteriophytochrome from the Plant Pathogen Xanthomonas campestris Provides Clues to its Long-Range Signaling Mechanism. *J. Mol. Biol.* **428**, 3702–3720 (2016).

6. Gutt, A. Photochemische und strukturelle Untersuchungen neuartiger Bilin-bindender Photorezeptoren. (2016).

7. Zienicke, B. *et al.* Unusual spectral properties of bacteriophytochrome Agp2 result from a deprotonation of the chromophore in the red-absorbing form Pr. *J. Biol. Chem.* **288**, 31738–51 (2013).

8. Chizhov, I., Zorn, B., Manstein, D. J. & Gärtner, W. Kinetic and Thermodynamic Analysis of the Light-induced Processes in Plant and Cyanobacterial Phytochromes. *Biophys. J.* **105**, 2210–2220 (2013).

9. Lamparter, T. *et al.* Characterization of recombinant phytochrome from the cyanobacterium Synechocystis. *Proc. Natl. Acad. Sci. U. S. A.* **94**, 11792–7 (1997).

10. Pratt, L. H. Photochemistry of high molecular weight phytochrome in vitro. *Photochem. Photobiol.* **22**, 33–6

11. Pennacchietti, F. *et al.* Photochromic conversion in a red/green cyanobacteriochrome from Synechocystis PCC6803: Quantum yields in solution and photoswitching dynamics in living E. coli cells. *Photochem. Photobiol. Sci.* **14**, 229–237 (2015).

12. Buhrke, D., Kuhlmann, U., Michael, N. & Hildebrandt, P. The Photoconversion of Phytochrome Includes an Unproductive Shunt Reaction Pathway. *ChemPhysChem* **19**, 566–570 (2018).

13. Eilfeld, P. & Rüdiger, W. Absorption Spectra of Phytochrome Intermediates. *Zeitschrift für Naturforsch. C* **40**, 109–114 (1985).

14. Björling, A. *et al.* Structural photoactivation of a full-length bacterial phytochrome. *Sci. Adv.* **2**, e1600920 (2016).

15. Losi, A., Bonomi, H. R., Michael, N., Tang, K. & Zhao, K.-H. Time-Resolved Energetics of Photoprocesses in Prokaryotic Phytochrome-Related Photoreceptors. *Photochem. Photobiol.* **93**, 733–740 (2017).

16. Kottke, T., Xie, A., Larsen, D. S. & Hoff, W. D. Photoreceptors Take Charge: Emerging Principles for Light Sensing. *Annu. Rev. Biophys.* **47**, annurev-biophys-070317-033047 (2018).

17. Losi, A., Gardner, K. H. & Möglich, A. Blue-Light Receptors for Optogenetics. *Chem. Rev.* **118**, 10659–10709 (2018).

18. Losi, A. & Gärtner, W. Solving Blue Light Riddles: New Lessons from Flavin-binding LOV Photoreceptors. *Photochem. Photobiol.* **93**, 141–158 (2017).

19. Pudasaini, A., El-Arab, K. K. & Zoltowski, B. D. LOV-based optogenetic devices: light-driven modules to impart photoregulated control of cellular signaling. *Front. Mol. Biosci.* **2**, 18 (2015).

20. Losi, A., Mandalari, C. & Gärtner, W. The Evolution and Functional Role of Flavin-based Prokaryotic Photoreceptors. *Photochem. Photobiol.* **91**, 1021–1031 (2015).

21. Westberg, M., Bregnhøj, M., Etzerodt, M. & Ogilby, P. R. No Photon Wasted: An Efficient and Selective Singlet Oxygen Photosensitizing Protein. *J. Phys. Chem. B* **121**, 9366–9371 (2017).

22. Torra, J. *et al.* Tailing miniSOG: structural bases of the complex photophysics of a flavin-binding singlet oxygen photosensitizing protein. *Sci. Rep.* **9**, 2428 (2019).

23. Consiglieri, E. *et al.* Single mutation in a novel bacterial LOV protein yields a singlet oxygen generator. *Photochem. Photobiol. Sci.* **18**, 2657–2660 (2019).

24. Chow, B. Y., Han, X. & Boyden, E. S. Genetically encoded molecular tools for light-driven silencing of targeted neurons. *Prog. Brain Res.* **196**, 49 (2012).

25. Westberg, M., Holmegaard, L., Pimenta, F. M., Etzerodt, M. & Ogilby, P. R. Rational design of an efficient, genetically encodable, protein-encased singlet oxygen photosensitizer. *J. Am. Chem. Soc.* **137**, 1632–42 (2015).

26. Torra, J. *et al.* Singlet oxygen photosensitisation by the fluorescent protein Pp2FbFP L30M, a novel derivative of Pseudomonas putida flavin-binding Pp2FbFP. *Photochem. Photobiol. Sci.* **14**, 280–287 (2015).

27. Endres, S. *et al.* An optogenetic toolbox of LOV-based photosensitizers for light-driven killing of bacteria. *Sci. Rep.* **8**, 15021 (2018).

28. Raffelberg, S., Mansurova, M., Gärtner, W. & Losi, A. Modulation of the photocycle of a LOV domain photoreceptor by the hydrogen-bonding network. *J. Am. Chem. Soc.* **133**, 5346–5356 (2011).

29. Losi, A. & Braslavsky, S. E. The time-resolved thermodynamics of the chromophore–protein interactions in biological photosensors as derived from photothermal measurements. *Phys. Chem. Chem. Phys.* **5**, 2739–2750 (2003).

30. Gauden, M. *et al.* Low-temperature and time-resolved spectroscopic characterization of the LOV2 domain of Avena sativa phototropin 1. in (eds. Avrillier, S. & Tualle, J.-M.) **5463**, 97 (International Society for Optics and Photonics, 2004).

31. Losi, A., Polverini, E., Quest, B. & Gärtner, W. First evidence for phototropin-related blue-light receptors in prokaryotes. *Biophys J* **82**, 2627–2634 (2002).

32. Losi, A., Quest, B. & Gärtner, W. Listening to the blue: The time-resolved thermodynamics of the bacterial blue-light receptor YtvA and its isolated LOV domain. *Photochem. Photobiol. Sci.* **2**, 759–766 (2003).

33. Losi, A., Kottke, T. & Hegemann, P. Recording of blue light-induced energy and volume changes within the wild-type and mutated phot-LOV1 domain from Chlamydomonas reinhardtii. *Biophys. J.* **86**, 1051–60 (2004).

34. Raffelberg, S. *et al.* The amino acids surrounding the flavin 7a-methyl group determine the UVA spectral features of a LOV protein. *Biol. Chem.* **394**, 1517–28 (2013).

35. Westberg, M., Bregnhøj, M., Etzerodt, M. & Ogilby, P. R. Temperature Sensitive Singlet Oxygen Photosensitization by LOV-Derived Fluorescent Flavoproteins. *J. Phys. Chem. B* **121**, 2561–2574 (2017).

36. Ogilby, P. R. Singlet oxygen: there is indeed something new under the sun. *Chem. Soc. Rev.* **39**, 3181 (2010).

37. Ruiz-González, R. *et al.* Singlet Oxygen Generation by the Genetically Encoded Tag miniSOG. *J. Am. Chem. Soc.* **135**, 9564–9567 (2013).

38. Westberg, M., Bregnhøj, M., Etzerodt, M. & Ogilby, P. R. No Photon Wasted: An Efficient and Selective Singlet Oxygen Photosensitizing Protein. *J. Phys. Chem. B* **121**, 9366–9371 (2017).

39. Torra, J. *et al.* Tailing miniSOG: structural bases of the complex photophysics of a flavin-binding singlet oxygen photosensitizing protein. *Sci. Rep.* **9**, 2428 (2019).

40. Westberg, M., Holmegaard, L., Pimenta, F. M., Etzerodt, M. & Ogilby, P. R. Rational Design of an Efficient, Genetically Encodable, Protein-Encased Singlet Oxygen Photosensitizer. *J. Am. Chem. Soc.* **137**, 1632–1642 (2015).

41. Ruiz-González, R. *et al.* Singlet oxygen generation by the genetically encoded tag minisog. *J. Am. Chem. Soc.* **135**, 9564–9567 (2013).

Conclusions and perspectives

This research work on photoreceptors from plant-associated bacteria led to several novel results, opening up new questions and future perspectives.

The full spectral characterisation of the BV-binding phytochromes showed common features and peculiarities within this photoreceptor superfamily. Like other phys the photoconversion quantum yield Φ_P are modest, while fluorescence efficiency is extremely low for the Pr form and virtually zero for Pfr. [1] Nevertheless, the careful design of time-resolved experiments and global analysis of transient traces allowed to depict a full-scale scenario of light-induced reactions in the short-µs to long-ms time scale, for both routes of photoconversion. [1] A very peculiar reaction pathway emerged for the Pfr-to-Pr conversion of the fungal FphAN753: it is the first time that a phytochrome shows that the final product (Pr) is already formed on the short-µs time scale. [1] "Besides their intriguing and largely unknown role in nature, [2] BphPs are being actively studied as tools for imaging and optogenetics applications. [3] Their selected advantage is a photochromism covering the R-FR/NIR spectral interval, known to comprise the transparency window for mammalian tissues, and the fact that BV is ubiquitous as a degradation product of the heme pathway. Albeit very promising, these photofunctional proteins presents many drawbacks: they are poorly fluorescent in their native form, they tend to oligomerise, BV is often not efficiently incorporated *in vivo*, and they need extensive engineering for incorporation in chimeric proteins used as light driven actuators. [4] Detailed biophysical characterisation of BphPs is thus mandatory to gain better insight in these systems and envision novel tools." [1]

The most interesting results derived from the part of this research dealing with photoreceptors from *Methylobacterium radiotolerans*, a pink-pigmented facultative methylotrophic bacterium which belongs to the plant microbiota as a symbiont, able to metabolize carbon compounds [5,6]. As shown in Appendix A1, the genomic analysis found thirteen photoreceptors for visible light in this bacterium, albeit the *in vivo* role of these photoactive proteins is still to be understood and until now none of them was characterised at the molecular level. [7,8] In this project, two photoreceptors from this bacterium have been characterised for the first time: *Mr*BphP1, a BphP with R/NIR photochromism, and *Mr*4511, a BL-sensing photoreceptor. The molecular study of these proteins was performed with a set of spectroscopical techniques, both steady-state and time-resolved. *Mr*BphP1 presented special features, compared to the other BV-binding BphPs here studied:

i. a more NIR-shifted spectral absorbance range, with maxima of Pr at 707 nm and of Pfr at 764 nm. This feature could be important for biotechnological application, since that spectral range resides within the NIR tissue transparency window [3];
ii. a higher photoconversion quantum yield $\Phi_P = 0.2$ in both directions, possibly hinting to poorly efficient shunt pathways during the conversion or a larger conformational homogeneity with respect to other BphPs;
iii. a lack of transient species in long-μs time-window as suggested by global-fit analysis of laser flash photolysis experiments: the first measured lifetime for the Pr-to-Pfr route is 1.28 ms, while for the Pfr-to-Pr route it is 290 μs. The fact that the LUMI intermediate (formed on a time scale not detectable with our setup) is able to live so long is possibly related to the high photoconversion quantum yield (*vide supra*);

Regarding the LOV protein *Mr*4511, it was studied in its WT form and as the variants I37V, Q112W, C71X (where X = G or X = S), C71X/Q112W. For the I37V variant, the residue at this position, on strand Aβ in close vicinity (≤0.4 nm) to the flavin 7a-methyl group in published LOV-domains crystal structures, is known to strongly

affect the dynamics of the photocycle [9]: in many LOV domains it is a valine, and its mutation into isoleucine or leucine largely increases τ_{rec} [10]. In fact, *Mr*4511 I37V recovers to the dark state with a lifetime τ_{rec} = 3100 s at 27 °C, five-time shorter than the WT protein, which instead has a very long photocycle with τ_{rec} = 15160 s at 27 °C. Introduction of some other mutations will be necessary to obtain a shorter thermal τ_{rec} for the WT protein, e.g. for optogenetic applications. The reason for mutation Q112W was to introduce a Trp residue, which is conserved in *ca.* 75% of LOV domains [7] and was demonstrated to be one of the major quenchers of the FMN triplet state [11,12]. As a result, *Mr*4511 C71X variants were discovered in this work to be novel, efficient and robust genetically-encodable SO photosensitisers with only one mutation, increasing the toolbox of LOV-based photosensitisers: [13] both the C71X variants have a Φ_Δ of *ca.* 0.2 in air-saturated conditions and *ca.* 0.5 in deuterated buffer under oxygen-saturated conditions, while the introduction of W112 in the canonical position for LOV domains dramatically decreases Φ_Δ to values comparable to miniSOG, one of the early FMN-binding proteins touted as SO photosensitisers. [13] The FMN triplet- and singlet-state lifetimes of the two variants C71S and C71G were demonstrated to be affected by these changes in the protein around the chromophore, albeit they do not differ in their SO quantum yield: this aspect, noticed here for the first time in a LOV-based photosensitiser, may be important for their *in vivo* performance. [13] Furthermore, this protein was discovered to be more photostable than free FMN under prolonged BL illumination (although this feature has to be confirmed in *in vivo* studies) and it is very resistant to denaturation in Urea: [13] molecular-dynamics simulations are on going in the biophysical group of the University of Parma to better understand the reasons for this peculiar feature. With molecular dynamics it will be also possible to go deeper into the structure of the chromophore cavity, in order to clarify the accessibility pathways and channels for oxygen diffusion: this could indicate some significant point mutations able to improve oxygen diffusion in close proximity to FMN (since the energy transfer from FMN triplet state to oxygen is a diffusion-limited process) with the goal of obtaining a "no-photon-wasted" SO photosensitiser. Moreover, thinking about the unknown

functional role of these photoreceptors for RL and BL in *Methylobacteria,* it will be useful to create knock-out mutants (*i.e.* bacteria without the specific photoreceptor) for testing, through physical techniques and chemical assays, if and how the photoreceptors light-sensing can be involved in:

a. methanol utilisation [14], because methanol may play a major role as future alternative carbon source. [15] In recent years, metabolic engineering and targeted design of industrial strains have opened new possibilities for methanol-based biotechnological processes: besides their ecological relevance, *Methylobacteria* could play an important role as production platforms for bulk and fine chemicals. [16] However, any potential biotechnological application of these organisms requires detailed knowledge of the central carbon metabolism and its enzymatic activities. [16]
b. biofilm formation. For *Xcc* it was demonstrated that *Xcc*BphP downregulates biofilm formation in response to light: these results provided evidence for a novel Bph function affecting an infectious process. [17]
c. phytohormones secretion (like cytokinin, auxin), which induces plant growth through the molecular communication during plant-*Methylobacterium* species interaction [18];
d. nitrogen fixation, which favors plant-biomass increase and is an important factor for plant-growth promotion [19,20]. In fact, nitrogen is often the most-limiting nutrient for plants and, since nitrogen from the atmosphere is unavailable to plant metabolism, the process of nitrogen fixation can be done only by prokaryotes with the presence of the nitrogenase enzyme (es. *M. nodulans*): the biological reduction of nitrogen to ammonia performed by these bacteria involves the transformation of atmospheric nitrogen into ammonia, which is available for plant use;
e. pigmentation. [21] As an example, the *M. nodulans* is a non-pigmented bacterium and it has a number of photoreceptors lower than other *M.* species for which complete genome are available (Appendix A1): this could be an indication of a possible role of light in carotenoids production by these bacteria group.

In this context, *Methylobacteria* seem to be an important bacterial genus to be employed for improvement of crop quality and productivity: in particular, in sustainable agriculture application of growth-promoting bacteria may reduce the costs associated with the use of chemicals and the environmental impacts. [5] Since *Methylobacteria* are fully rich in not-yet characterised photoreceptors (see Appendix A1), future continuation in biophysical and biochemical analysis on these photoactive proteins is mandatory.

Bibliography

1. Consiglieri, E. *et al.* Dynamics and efficiency of photoswitching in biliverdin-binding phytochromes. *Photochem. Photobiol. Sci.* **18**, 2484–2496 (2019).

2. Beattie, G. A., Hatfield, B. M., Dong, H. & McGrane, R. S. Seeing the Light: The Roles of Red- and Blue-Light Sensing in Plant Microbes. *Annu. Rev. Phytopathol.* **56**, 41–66 (2018).

3. Chernov, K. G., Redchuk, T. A., Omelina, E. S. & Verkhusha, V. V. Near-Infrared Fluorescent Proteins, Biosensors, and Optogenetic Tools Engineered from Phytochromes. *Chem. Rev.* **117**, 6423–6446 (2017).

4. Gourinchas, G., Etzl, S. & Winkler, A. Bacteriophytochromes – from informative model systems of phytochrome function to powerful tools in cell biology. *Curr. Opin. Struct. Biol.* **57**, 72–83 (2019).

5. Bogas, A. C., C. I. Aguilar-Vildoso, A. A. Camargo-Neves, and W. L. A. Effects of growth-promoting endophytic Methylobacterium on development of Citrus rootstocks. *African J. Microbiol. Res.* **10**, 646–653 (2016).

6. Yadav, N. & Nath Yadav, A. Biodiversity and biotechnological applications of novel plant growth promoting methylotrophs. *J. Appl. Biotechnol. Bioeng.* **5**, (2018).

7. Losi, A., Mandalari, C. & Gärtner, W. The Evolution and Functional Role of Flavin-based Prokaryotic Photoreceptors. *Photochem. Photobiol.* **91**, 1021–1031 (2015).

8. Mandalari, C., Losi, A. & Gärtner, W. Distance-tree analysis, distribution and co-presence of bilin- and flavin-binding prokaryotic photoreceptors for visible light. *Photochem. Photobiol. Sci.* **12**, 1144–1157 (2013).

9. Losi, A. & Gärtner, W. Solving Blue Light Riddles: New Lessons from Flavin-binding LOV Photoreceptors. *Photochem. Photobiol.* **93**, 141–158 (2017).

10. Pudasaini, A., El-Arab, K. K. & Zoltowski, B. D. LOV-based optogenetic devices: light-driven modules to impart photoregulated control of cellular signaling. *Front. Mol. Biosci.* **2**, 18 (2015).

11. Westberg, M., Bregnhøj, M., Etzerodt, M. & Ogilby, P. R. No Photon Wasted: An Efficient and Selective Singlet Oxygen Photosensitizing Protein. *J. Phys. Chem. B* **121**, 9366–9371 (2017).

12. Torra, J. *et al.* Tailing miniSOG: structural bases of the complex photophysics of a flavin-binding singlet oxygen photosensitizing protein. *Sci. Rep.* **9**, 2428 (2019).

13. Consiglieri, E. *et al.* Single mutation in a novel bacterial LOV protein yields a singlet oxygen generator. *Photochem. Photobiol. Sci.* (2019). doi:10.1039/C9PP00328B

14. Wood, P. J. & Siddiqui, I. R. Determination of methanol and its application to measurement of pectin ester content and pectin methyl esterase activity. *Anal. Biochem.* **39**, 418–428 (1971).

15. Schrader, J. *et al.* Methanol-based industrial biotechnology: current status and future perspectives of methylotrophic bacteria. *Trends in Biotechnology* **27**, 107–115 (2009).

16. Šmejkalová, H., Erb, T. J. & Fuchs, G. Methanol assimilation in Methylobacterium extorquens AM1: Demonstration of all enzymes and their regulation. *PLoS One* **5**, (2010).

17. Bonomi, H. R. *et al.* Xanthomonas campestris attenuates virulence by sensing light through a bacteriophytochrome photoreceptor . *EMBO Rep.* **17**, 1565–1577 (2016).

18. Dourado, M. N., Camargo Neves, A. A., Santos, D. S. & Araújo, W. L. Biotechnological and agronomic potential of endophytic pink-pigmented methylotrophic methylobacterium spp. *BioMed Research International* **2015**, (2015).

19. Sy, A. *et al.* Methylotrophic Methylobacterium bacteria nodulate and fix nitrogen in symbiosis with legumes. *J. Bacteriol.* **183**, 214–220 (2001).

20. Lacava, P. T. *et al.* Detection of siderophores in endophytic bacteria Methylobacterium spp. associated with Xylella fastidiosa subsp. pauca. *Pesqui. Agropecu. Bras.* **43**, 521–528 (2008).

21. Lorquin, J., Molouba, F. & Dreyfus, B. L. Identification of the carotenoid pigment canthaxanthin from photosynthetic bradyrhizobium strains. *Appl. Environ. Microbiol.* **63**, 1151–4 (1997).

Summary

This thesis work is about BL and RL photoreceptors from plant-associated bacteria.

These photosensory proteins were studied by means of both steady-state and time-resolved biophysical techniques.

For the BV-binding phys it was possible to depict a full scale scenario of light-induce reactions in the short-µs to long-ms time-scale, for both directions of photoconversion: the most interesting result came from the fungal BphP-like FphAN753, for which the Pr final product is already formed on the µs time-scale.

*Mr*BphP1 and *Mr*4511 are two photoreceptors for RL and BL respectively, here characterised for the first time from the bacterium *Methylobacterium radiotolerans*, a pink-pigmented facultative methylotrophic bacterium that belongs to the plant microbiota as a symbiont. *Mr*BphP1 showed interesting features with respect to the other phys here studied, as an absorbance spectrum more NIR-shifted, while *Mr*4511 C71S-C71G variants were discovered to be novel, efficient and robust genetically-encodable SO photosensitisers with only one mutation, increasing the toolbox of LOV-based photosensitisers. Future studies on photoreceptors from bacteria of the group *Methylobacterium* are mandatory to explore not-yet defined functions of these photofunctional proteins in these bacteria and to design enhanced variants for applications.

Acknowledgments

First of all I want to thank my supervisor prof. Aba Losi for her scientific and human support during these three years: her experience and competence in the field of photoreceptors were for me always opportunities for improving my knowledge.

Thanks to prof. Wolfgang Gärtner from the University of Leipzig (Germany) for his continuous support, his suggestions and for having given me the possibility to go to Leipzig for training in protein expression.

Thanks to Qianzhao Xu from University of Leipzig for having prepared a lot of samples of very high quality.

Thanks to prof. Cristiano Viappiani and prof. Stefania Abbruzzetti of the University of Parma for having introduced me in the world of laser flash photolysis and photophysics, and for their help in the field of physics and not only.

Thanks to prof. Peter Ogilby from the University of Aarhus (Denmark) and his group for the very nice time I spent there to measure singlet oxygen, in particular thanks to Mikkel Bregnhøj for his mentoring during the lab activities.

Thanks to Roberta Bedotti for lab instructions and for her friendship.

Thanks to all the other people of the biophysical group at the University of Parma for the nice atmosphere of these years.

In the end I want to thank my family and my friends for their love.

Appendix A1

Genes for putative photoreceptors in bacteria belonging to the genera *Methylobacterium* and *Methylorubrum* (formerly both genera were grouped and known as *Methylobacteria*). [1] Only genomes completed by August 31st 2019 are taken into account, according to NCBI (National Center for Biotechnology Information) [2] database of prokaryotic genomes. Proteins were searched with the BLAST and PSI-BLAST [3] services at NCBI, using the following template sequences: **i.** for BphP (bacteriophytochromes) the PAS-GAF-PHY module of protein B1M2J7 (UniProt [4] code) from *Methylobacterium radiotolerans;* **ii.** for PYP (Photoactive Yellow Protein) the sequence of P16113 from *Halorhodospira halophila*, with further visual inspection for the presence of Cys69 [5]; **iii.** for LOV (LOV, Oxygen, Voltage) domains the previously published pattern [NS]-*x*(2)-[FPGHSA]-*x*(4)-[GEQR]-*x*(9,11)-C with PSI-BLAST, where *x* is any amino acid and the terminal C is the cysteine involved in the photocycle [6], with B1M516 from *M. radiotolerans* as a seed; **iv.** for BLUF domains (Blue Light sensing Using Flavins) using the pattern Y-*x*(21,27)-[NG]-x(8,9)-[LMVIFTK]-*x*(6,14)-[FALIYCV]-*x*(1)-Q, where the two residues at the terminal ends are the Tyr-Gln reactive pair [6]; **v.** rhodopsins were searched using A0A0C6F7V1 from *M. aquaticum* as a template [7]. The expect threshold of the BLAST or PSI-BLAST search was left at the default value of 10.

Table 12: Methylobacteria group: summary of photoreceptors types[a] and number of hits as X in fully sequenced species/strains[b]

Methylobacterium	**strain**	**BphP**	**PYP-BphP**	**LOV**	**BLUF**	**Rhodopsin**	**Bacteriochlorophyll**
M. aquaticum	MA-22A	X	X	XXXXXXXXXX	XXX	X	YES
M. nodulans	ORS 2060			XX	X		NO
M. oryzae	CBMB20	XX		XXXXXXX	XXXX		YES
M. phyllosphaerae	CBMB27	X	X	XXXXX	XXX		YES
M. radiotolerans	JCM 2831	XXX		XXXXXX	XXXX		YES
M. sp.	17SD2-17	XXXX		XXXXXXX	XXX		YES
M.sp.	17Sr1-1	XX	X	XXXXXXXXXX	XXXX		YES
M. sp.	17Sr1-28		X	XXXXXXXXX	XXXX		YES
M. sp.	17Sr1-43	XX		XXXXXXX	XXXX		YES
M. sp.	4-46	X	X	XX	XXXXX	X	YES
M. sp.	AMS5	XXX		XXXXX	XXX		YES
M.sp.	C1	XX		XXXXXX	XXX		YES
M. sp.	DM1	XXXX		XXXXXX	XXXX		YES
M. sp.	XJLW	XX		XXXXXXXXX	XXX		YES
Methylorubrum	**strain**	**BphP**	**PYP-BphP**	**LOV**	**BLUF**	**Rhodopsin**	**Bacteriochlorophyll**
M. extorquens	PSBB040	**X**		**XXXXXX**	**XXXXXX**		YES
M. extorquens	TK0001	**XX**		**XXXXX**	**XXX**		YES
M. extorquens	AM1	**X**		**XXXXXX**	**XX**		YES
M. extorquens	CM4	**X**		**XXXXXX**	**XXXXX**		YES
M. extorquens	DM4	**X**		**XXXXX**	**XX**		YES
M. extorquens	PA1	**X**		**XXXXX**	**XXX**		YES
M. populi	P-1M	**XXX**		**XXXXX**	**XX**		YES
M. populi	YC-XJ1	**XX**		**XXXXXX**	**XX**		YES
M. populi	BJ001	**XX**		**XXXXXXXX**	**XX**		YES
M. zatmanii	PSBB041	**XX**		**XXXXXX**	**XX**		YES

[a] BphP = Bacteriophytochrome; PYP-BphP = hybrid photoreceptors comrising photoactive yellow protein and a BphP; LOV = LOV, Light Oxygen and Voltage proteins; BLUF =Blue-Light sensing Using Flavins proteins; all listed bacteria but one possess genes for the synthesis of bacteriochlorophylls for photosystems; full sequenced genomes can be found at the NCBI database, https://www.ncbi.nlm.nih.gov/genome/browse#!/prokaryotes/ [2]

[b] Links to the genomes of listed *Methylobacteria*:

1. https://www.ncbi.nlm.nih.gov/nuccore/NZ_AP014704.1
2. https://www.ncbi.nlm.nih.gov/nuccore/NC_011894.1
3. https://www.ncbi.nlm.nih.gov/nuccore/CP003811.1
4. https://www.ncbi.nlm.nih.gov/nuccore/NZ_CP015367.1
5. https://www.ncbi.nlm.nih.gov/nuccore/NC_010505.1
6. https://www.ncbi.nlm.nih.gov/nuccore/NZ_CP029550.1
7. https://www.ncbi.nlm.nih.gov/nuccore/CP029552.1
8. https://www.ncbi.nlm.nih.gov/nuccore/NZ_CP029553.1
9. https://www.ncbi.nlm.nih.gov/nuccore/NZ_CP029551.1
10. https://www.ncbi.nlm.nih.gov/nuccore/NC_010511.1
11. https://www.ncbi.nlm.nih.gov/nuccore/984669198
12. https://www.ncbi.nlm.nih.gov/nuccore/1094003594
13. https://www.ncbi.nlm.nih.gov/nuccore/NZ_CP029173.1
14. https://www.ncbi.nlm.nih.gov/nuccore/NZ_CP016429.1

[c] Links to the genomes of listed *Methylobacterubra*:

1. https://www.ncbi.nlm.nih.gov/nuccore/NZ_CP019322.1
2. https://www.ncbi.nlm.nih.gov/nuccore/LT962688.1
3. https://www.ncbi.nlm.nih.gov/nuccore/NC_012808.1
4. https://www.ncbi.nlm.nih.gov/nuccore/NC_011757.1

5. https://www.ncbi.nlm.nih.gov/nuccore/NC_012988.1
6. https://www.ncbi.nlm.nih.gov/nuccore/NC_010172.1
7. https://www.ncbi.nlm.nih.gov/nuccore/NZ_AP014809.1
8. https://www.ncbi.nlm.nih.gov/nuccore/NZ_CP039546.1
9. https://www.ncbi.nlm.nih.gov/nuccore/NC_010725.1
10. https://www.ncbi.nlm.nih.gov/nuccore/NZ_CP021054.1

In the following Table 13, Table 14, Table 15, Table 16 are reported the protein accession codes (UniProt [4] and NCBI [8]), gene names and domain architectures (InterPro [9,10]) for each photoreceptor. Highlighted in yellow: the two *M. radiotolerans* photoreceptors investigated in this work (a BphP and a LOV protein, in text named respectively *Mr*Bphp1 and *Mr*4511). The acronym LOV is used in the literature: note that the databases name this domain as the more generic PAS.

Domain legend

BLUF = Blue-Light sensing Using Flavin

GAF = cGMP-specific phosphodiesterases, cyanobacterial adenylate cyclases, and formate hydrogen lyase transcription activator FhlA (embedding the chromophore in BphPs)

HWE= Signal transduction histidine kinase, HWE region: defined by the presence of conserved a H residue and a WXE motif

Kinase = His-Kinase of the two component signal transduction system

LOV = Light, Oxygen,Voltage

PAS = Per Arnt Sim domain

PHY = Phytochrome domain

RR = CheY-type Response regulator, receiver domain

Short-LOV or Short-BLUF = standalone LOV and BLUF domains, with flanking regions/no recognizable linked domain

Table 13: *Methylobacteria* and *Methylorubra* groups: BphP proteins, accession codes and domain architectures

	Methylobacterium	**strain**	**UniProt**	**NCBI**	**Gene name**	**aa**	**Domain architecture**
1	*M. aquaticum*	MA-22A	A0A0C6F3S7	WP_060848240.1	Maq22A_c21185	855	PYP+PAS+GAF+PHY+Kinase
			A0A0C6FKU5	BAQ49078.1	Maq22A_1p33980	755	PAS+GAF+PHY+Kinase
2	*M. nodulans*	ORS 2060	----	----	----	----	----
3	*M. oryzae*	CBMB20	A0A089QBR2	AIQ92004.1	MOC_4249	879	PAS_2+GAF+PHY+Kinase
			A0A089P3P6	AIQ92678.1	MOC_4923	751	PAS+GAF+PHY+Kinase
4	*M. phyllosphaerae*	CBMB27	----	APT33067.1	MCBMB27_03776	751	PAS+GAF+PHY+Kinase
			----	APT32498.1	MCBMB27_03207	871	PYP+PAS+GAF+PHY+Kinase
5	*M. radiotolerans*	JCM 2831	B1LWZ3	ACB25698.1	Mrad2831_3723	871	PAS_2+GAF+PHY+Kinase
			B1M2J7	ACB26237.1	Mrad2831_4270	751	PAS+GAF+PHY+Kinase
			B1M9J3	ACB28168.1	Mrad2831_6244	849	PAS+GAF+PHY+HWE+Kinase+RR
6	*M. sp.*	17SD2-17	A0A2U8W298	WP_109886955.1	DK389_01130	871	PAS_2+GAF+PHY+Kinase
			A0A2U8W9H7	WP_109891510.1	DK389_17640	774	PAS+GAF+PHY+Kinase
			A0A2U8W941	WP_109892731.1	DK389_21720	894	PAS+GAF+PHY+Kinase+RR
			A0A2U8WCF2	WP_109894975.1	DK389_28975	913	PAS+GAF+PHY+Kinase+RR
7	*M.sp.*	17Sr1-1	A0A2U8WYI2	WP_109970316.1	DK412_00385	847	PAS+GAF+PHY+Kinase+RR
			A0A2U8XA43	WP_109975043.1	DK412_03780	862	PYP+PAS+GAF+PHY+Kinase
			A0A2U8X9M0	WP_109974110.1	DK412_24610	751	PAS+GAF+PHY+Kinase
8	*M. sp.*	17Sr1-28	A0A2U8WWV6	WP_109962186.1	DK419_07875	862	PYP+PAS+GAF+PHY+Kinase
9	*M. sp.*	17Sr1-43	A0A2U8VST8	WP_109951552.1	DK427_12515	862	PAS_2+GAF+PHY+Kinase
			A0A2U8W074	WP_109953861.1	DK427_25725	751	PAS+GAF+PHY+Kinase
10	*M. sp.*	4-46	B0UDE6	WP_012332076.1	M446_2206	762	PAS+GAF+PHY+Kinase
			B0UNZ0	WP_012332998.1	M446_3192	864	PYP+PAS+GAF+PHY+Kinase
11	*M. sp.*	AMS5	A0A0X1SN35	WP_060771330.1	Y590_20345	875	PAS_2+GAF+PHY+Kinase
12	*M.sp.*	C1	----	WP_012321191.1	BKE41_RS19690	871	PAS_2+GAF+PHY+Kinase
			----	WP_012321191.1	BKE41_RS22315	751	PAS+GAF+PHY+Kinase

13	*M. sp.*	DM1	A0A2U8HM61	AWI86987.1	C0214_00570	764	PAS+GAF+PHY+Kinase
			A0A2U8HP59	AWI87707.1	C0214_04970	849	PAS+GAF+PHY+Kinase+RR
			A0A2U8HZE0	AWI90356.1	C0214_20165	849	PAS+GAF+PHY+Kinase+RR
			A0A2U8HXW5	AWI90731.1	C0214_22420	873	PAS_2+GAF+PHY+Kinase
14	*M. sp.*	XJLW	A0A2U9TZ38	AWV15807.1	A3862_10045	751	PAS+GAF+PHY+Kinase
			A0A2U9U7D0	AWV16289.1	A3862_12870	871	PAS_2+GAF+PHY+Kinase
	Methylorubrum	**strain**	**UniProt**	**NCBI**	**Gene name**	**aa**	**Domain architecture**
1	*M. extorquens*	PSBB040	A0A1P8QPG6	WP_076642174.1	BV511_12120	875	PAS_2+GAF+PHY+Kinase
2	*M. extorquens*	TK0001	A0A2N9AXF7	SOR31999.1	TK0001_5433	469	GAF+PHY+Kinase
			A0A2N9AKU2	SOR27981.1	TK0001_1379	875	PAS_2+GAF+PHY+Kinase
3	*M. extorquens*	AM1	C5AQ42	ACS42102.1	MexAM1_META1p4471	875	PAS_2+GAF+PHY+Kinase
4	*M. extorquens*	CM4	B7KNA8	ACK85225.1	MCHL_4449	875	PAS_2+GAF+PHY+Kinase
5	*M. extorquens*	DM4	C7CJI8	WP_017484084.1	METDI5076	875	PAS_2+GAF+PHY+Kinase
6	*M. extorquens*	PA1	A9W8V2	ABY32451.1	Mext_4081	895	PAS_2+GAF+PHY+Kinase
7	*M. populi*	P-1M	A0A169QFG4	BAU88817.1	MPPM_0212	760	PAS+GAF+PHY+Kinase
			A0A160PCB0	BAU88780.1	MPPM_0175	843	PAS+GAF+PHY+Kinase+RR
			A0A160PLA1	BAU93051.1	MPPM_4446	874	PAS_2+GAF+PHY+Kinase
8	*M.populi*	YC-XJ1	----	QDI79405.1	E8E01_02640	751	PAS+GAF+PHY+Kinase
			----	QDI82714.1	E8E01_20985	874	PAS_2+GAF+PHY+Kinase
9	*M.populi*	BJ001	B1ZK65	ACB78717.1	Mpop_0539	751	PAS+GAF+PHY+Kinase
			B1ZGY2	ACB82660.1	Mpop_4562	874	PAS_2+GAF+PHY+Kinase
10	*M. zatmanii*	PSBB041	A0A1W6RDZ4	WP_004447074.1	B2G69_02320	875	PAS_2+GAF+PHY+Kinase
			A0A1W6RI55	WP_085856811.1	B2G69_10960	751	PAS+GAF+PHY+Kinase

Table 14: *Methylobacteria* and *Methylorubra* groups: LOV proteins, accession codes and domain architectures

	Methylobacterium	**strain**	**UniProt**	**NCBI**	**Gene name**	**aa**	**Domain architecture**
1	*M. aquaticum*	MA-22A	A0A0C6F8L7	WP_060846160.1	Maq22A_c06770	813	LOV+PAS+Kinase+RR
			A0A0C6FFC2	WP_060846976.1	Maq22A_c12145	538	LOV+Kinase+RR
			A0A0C6FSQ1	WP_060847120.1	Maq22A_c13200	820	LOV+ PAS_2+Kinase+RR
			A0A0C6FBR7	WP_060847150.1	Maq22A_c13440	801	LOV+ PAS_2+Kinase+RR
			A0A0C6FEW7	WP_060848127.1	Maq22A_c20420	540	LOV+Kinase+RR
			A0A0C6FMC7	WP_060849616.1	Maq22A_c27090	553	LOV+Kinase+RR
			A0A0C6FMG4	WP_060849092.1	Maq22A_c27510	495	LOV+PAS+Kinase
			A0A1Y0ZBW9	WP_082742600.1	Maq22A_c28570	854	LOV+PAS+Kinase+RR
			A0A0C6FN59	WP_082742864.1	Maq22A_1p31385	375	LOV+Kinase
			A0A0C6G201	WP_060851125.1	Maq22A_2p41400	801	LOV+ PAS_2+Kinase+RR
2	*M. nodulans*	ORS 2060	B8IF91	WP_015927507.1	Mnod_0770	814	LOV+ PAS_2+Kinase+RR
			B8IAH5	WP_015932603.1	Mnod_6213	559	LOV+Kinase+RR
3	*M. oryzae*	CBMB20	A0A089NRS9	AIQ88543.1	MOC_0788	348	LOV+Kinase
			A0A089NVZ9	AIQ91572.1	MOC_3817	462	LOV+PAS+ Kinase
			A0A089QB82	AIQ91844.1	MOC_4089	499	LOV+Kinase+RR
			A0A089NYH1	AIQ92422.1	MOC_4667	813	LOV+ PAS_2+Kinase+RR
			A0A089NY43	AIQ92927.1	MOC_5101	186	Short-LOV
			A0A089NZW5	AIQ92927.1	MOC_5172	148	Short-LOV
			A0A089P3R8	AIQ93410.1	MOC_5655	461	LOV+PAS+Kinase
4	*M. phyllosphaerae*	CBMB27	----	WP_020093089.1	MCBMB27_02805	462	LOV+PAS+ Kinase
			----	WP_012320504.1	MCBMB27_03052	539	LOV+Kinase+RR
			----	WP_075381089.1	MCBMB27_04019	164	Short-LOV
			----	WP_075381240.1	MCBMB27_04400	495	LOV+PAS+ Kinase
			----	WP_075381708.1	MCBMB27_05465	807	LOV+ PAS_2+Kinase+RR
5	*M. radiotolerans*	JCM 2831	B1LWD2	ACB22634.1	Mrad2831_0623	334	LOV+Kinase
			B1M4V9	ACB25005.1	Mrad2831_3021	812	LOV+ PAS_2+Kinase+RR
			B1LSK7	ACB25309.1	Mrad2831_3331	503	LOV+PAS+Kinase
			B1LUV7	ACB25309.1	Mrad2831_3567	539	LOV+Kinase+RR

			B1M4A2	ACB26397.1	Mrad2831_4431	186	Short-LOV
			B1M516	ACB26477.1	Mrad2831_4511	164	Short-LOV
6	*M. sp.*	17SD2-17	A0A2U8W129	WP_012320504.1	DK389_03705	540	LOV+Kinase+RR
			A0A2U8W1K3	WP_109887680.1	DK389_04585	489	LOV+PAS+Kinase
			A0A2U8W3Y5	WP_109888201.1	DK389_06400	608	LOV+PAS_2+GAF
			A0A2U8W4X7	WP_109889038.1	DK389_09260	364	LOV+Kinase
			A0A2U8W806	WP_109891767.1	DK389_18695	364	LOV+Kinase
			A0A2U8WB98	WP_109893174.1	DK389_23370	541	LOV+Kinase+RR
			A0A2U8WD80	WP_109895442.1	DK389_30585	954	LOV+PAS_3+Kinase+RR
7	*M.sp.*	17Sr1-1	A0A2U8WWJ1	WP_109970416.1	DK412_01025	538	LOV+Kinase+RR
			A0A2U8WZH9	WP_109970637.1	DK412_02380	540	LOV+Kinase+RR
			A0A2U8WXL4	WP_109970985.1	DK412_04575	1108	LOV+PAS+GAF+PAS_2+Kinase+RR
			A0A2U8WY70	WP_109970993.1	DK412_04625	492	LOV+PAS+Kinase
			A0A2U8X1D7	WP_109971296.1	DK412_06590	559	LOV+Kinase+RR
			A0A2U8X1P7	WP_109971412.1	DK412_07310	810	LOV+PAS_2+Kinase+RR
			A0A2U8X098	WP_109971595.1	DK412_08485	493	LOV+PAS+Kinase
			A0A2U8XCR4	WP_109975163.1	DK412_09505	781	LOV+PAS_3+Kinase+RR
			A0A2U8XD68	WP_109975194.1	DK412_11010	504	LOV+Kinase+RR
			A0A2U8XCE2	WP_109974936.1	DK412_29695	382	LOV+Kinase
8	*M. sp.*	17Sr1-28	A0A2U8WWD0	WP_109962054.1	DK419_01520	778	LOV+PAS_2+Kinase+RR
			A0A2U8WIS2	WP_109957826.1	DK419_03285	538	LOV+Kinase+RR
			A0A2U8WKG6	WP_109958164.1	DK419_05290	549	LOV+Kinase+RR
			A0A2U8WNG3	WP_109959390.1	DK419_12660	820	LOV+PAS_2+Kinase+RR
			A0A2U8WNK1	WP_109960040.1	DK419_16520	375	LOV+Kinase
			A0A2U8WT64	WP_109960939.1	DK419_21720	496	LOV+PAS+Kinase
			A0A2U8WXU6	WP_109962446.1	DK419_22485	540	LOV+Kinase+RR
			A0A2U8WUH2	WP_109961378.1	DK419_24350	802	LOV+PAS_2+Kinase+RR
			A0A2U8WVC8	WP_109962528.1	DK419_26540	799	LOV+PAS_2+Kinase+RR
9	*M. sp.*	17Sr1-43	A0A2U8VZF9	WP_109953906.1	DK427_00790	164	Short-LOV
			A0A2U8VNL5	WP_109950266.1	DK427_04770	410	LOV+PAS_2
			A0A2U8VPS9	WP_109950513.1	DK427_06295	363	LOV+Kinase
			A0A2U8VPU1	WP_109950750.1	DK427_07665	540	LOV+Kinase+RR

			A0A2U8VUH2	WP_109952200.1	DK427_16430	804	LOV+PAS_2+Kinase+RR
			A0A2U8VZD2	WP_109954309.1	DK427_21670	361	LOV+Kinase
			A0A2U8VZN0	WP_109953855.1	DK427_25685	497	LOV+PAS+Kinase
10	*M. sp.*	4-46	B0UAI7	WP_012331917.1	M446_2045	812	LOV+PAS_2+Kinase+RR
			B0UDT0	WP_012334590.1	M446_4874	544	LOV+Kinase+RR
11	*M. sp.*	AMS5	A0A109QS47	WP_060768604.1	Y590_03300	488	LOV+PAS+Kinase
			A0A0X1SFS5	AMB44787.1	Y590_07770	541	LOV+Kinase+RR
			A0A0X1SJZ2	WP_060770523.1	Y590_15300	533	LOV+Kinase+RR
			A0A0X1SKE0	WP_060770644.1	Y590_16035	354	LOV+Kinase
			A0A0X1SMN7	WP_060771287.1	Y590_20105	366	LOV+Kinase
12	*M.sp.*	C1	----	WP_059407784.1	BKE41_RS02935	488	LOV+PAS+Kinase
			----	WP_041372668.1	BKE41_RS16035	810	LOV+PAS+Kinase+RR
			----	WP_024829373.1	BKE41_RS17735	495	LOV+PAS+Kinase
			----	WP_070999971.1	BKE41_RS18920	539	LOV+Kinase+RR
			----	WP_012321430.1	BKE41_RS23540	164	Short LOV
			----	WP_083374417.1	BKE41_RS25530	907	LOV+PAS_3+GAF+Kinase
13	*M. sp.*	DM1	A0A2U8HNC3	WP_108938844.1	C0214_03685	488	LOV+PAS+Kinase
			A0A2U8HU49	WP_108939664.1	C0214_09580	541	LOV+Kinase+RR
			A0A2U8HV39	WP_108940986.1	C0214_17430	531	LOV+Kinase+RR
			A0A2U8HWM0	WP_108941107.1	C0214_18110	354	LOV+Kinase
			A0A2U8HYZ4	WP_108941304.1	C0214_19325	190	Short LOV
			A0A2Y9CIT5	WP_108943061.1	C0214_22220	366	LOV+Kinase
14	*M. sp.*	XJLW	A0A2U9TQ90	WP_124262936.1	A3862_04950	860	LOV+PAS_3+GAF+Kinase
			A0A2U9TTV4	WP_111473376.1	A3862_04960	801	LOV+PAS_2+Kinase+RR
			A0A2U9TR90	WP_052083755.1	A3862_07115	495	LOV+PAS+Kinase
			A0A2U9TS28	WP_043351101.1	A3862_08855	164	Short-LOV
			A0A2U9TW39	WP_043387271.1	A3862_09190	186	Short LOV
			A0A2U9TZA3	WP_043381097.1	A3862_13620	539	LOV+Kinase+RR
			A0A2U9TUF6	WP_043356402.1	A3862_14865	496	LOV+PAS+Kinase
			A0A2U9TZM6	WP_111473771.1	A3862_15760	791	LOV+PAS+Kinase+RR
			A0A2U9U1C7	WP_051045086.1	A3862_27810	358	LOV+Kinase
	Methylorubrum	**strain**	**UniProt**	**NCBI**	**Gene name**	**aa**	**Domain architecture**

1	*M. extorquens*	PSBB040	A0A1P8QKE8	WP_076640931.1	BV511_03615	488	LOV+PAS+Kinase
			A0A1P8QPK0	WP_003599658.1	BV511_12335	366	LOV+Kinase
			A0A1P8QRK1	WP_076643086.1	BV511_16105	492	LOV+PAS+Kinase
			A0A1P8QS50	WP_076643255.1	BV511_17200	354	LOV+Kinase
			A0A1P8QSE4	WP_076643333.1	BV511_17905	533	LOV+Kinase+RR
			A0A1P8QW68	WP_076644147.1	BV511_25115	541	LOV+Kinase+RR
2	*M. extorquens*	TK0001	A0A1P8QPK0	SOR28036.1	TK0001_1434	366	LOV+Kinase
			A0A2N9ANY0	WP_015951675.1	TK0001_2444	354	LOV+Kinase
			A0A2N9APB6	WP_015951576.1	TK0001_2602	533	LOV+Kinase+RR
			A2N9AUC2	WP_085857055.1	TK0001_4342	541	LOV+Kinase+RR
			A0A2N9AX59	WP_003598918.1	TK0001_5339	488	LOV+PAS+Kinase
3	*M. extorquens*	AM1	C5B055	ACS39405.1	MexAM1_META1p1543	541	LOV+Kinase+RR
			C5AXM1	ACS41089.1	MexAM1_META1p3352	533	LOV+Kinase+RR
			C5B099	ACS39449.1	MexAM1_META1p1590	492	LOV+PAS+Kinase
			C5AYD0	ACS41229.1	MexAM1_META1p3492	354	LOV+Kinase
			C5AVA5	ACS38573.1	MexAM1_META1p0643	488	LOV+PAS+Kinase
			C5B328	ACS42058.1	MexAM1_META1p4427	351	LOV+Kinase
4	*M. extorquens*	CM4	B7L0N0	WP_003598918.1	Mchl_0835	488	LOV+PAS+Kinase
			B7KVX8	WP_012453493.1	Mchl_1931	541	LOV+Kinase+RR
			B7KUQ2	WP_015951576.1	Mchl_3461	533	LOV+Kinase+RR
			B7KW67	WP_015951675.1	Mchl_3604	354	LOV+Kinase
			B7KN66	WP_012255188.1	Mchl_4407	366	LOV+Kinase
			B7KX89	WP_015952969.1	Mchl_5380	890	LOV+PAS+GAF+Kinase+RR
5	*M. extorquens*	DM4	C7CDA8	WP_015821340.1	METDI1014	488	LOV+PAS+Kinase
			C7CG25	WP_003599902.1	METDI2317	541	LOV+Kinase+RR
			C7CC12	WP_015823367.1	METDI3923	533	LOV+Kinase+RR
			C7CCX6	WP_015823468.1	METDI4072	354	LOV+Kinase
			C7CJE3	WP_012255188.1	METDI5031	351	LOV+Kinase
6	*M. extorquens*	PA1	A9W124	WP_012252593.1	Mext_0875	488	LOV+Kinase
			A9W392	WP_003599902.1	Mext_1649	541	LOV+Kinase+RR
			A9VYT5	WP_012254440.1	Mext_3139	533	LOV+Kinase+RR
			A9W705	WP_012254549.1	Mext_3280	354	LOV+Kinase

			A9W8Q8	WP_012255188.1	Mext_4037	366	LOV+Kinase
7	*M. populi*	P-1M	A0A160PC43	WP_096484005.1	MPPM_0898	488	LOV+PAS+Kinase
			A0A169QVX5	WP_096484658.1	MPPM_1693	501	LOV+Kinase+RR
			A0A160PEM8	WP_096484928.1	MPPM_2008	907	LOV+PAS_3+GAF+Kinase
			A0A160PFS2	WP_096486089.1	MPPM_3464	531	LOV+Kinase+RR
			A0A160PJ51	WP_096486812.1	MPPM_4401	366	LOV+Kinase
8	*M.populi*	YC-XJ1	----	WP_141949819.1	E8E01_00790	807	LOV+PAS_2+Kinase+RR
			----	WP_141950417.1	E8E01_04015	488	LOV+PAS+Kinase
			----	WP_141950998.1	E8E01_08060	541	LOV+Kinase+RR
			----	WP_141952096.1	E8E01_15495	531	LOV+Kinase+RR
			----	WP_141952273.1	E8E01_16215	354	LOV+Kinase
			----	WP_141953429.1	E8E01_20770	366	LOV+Kinase
9	*M.populi*	BJ001	B1ZH86	ACB78490.1	Mpop_0309	190	Short-LOV
			B1ZI10	ACB78496.1	Mpop_0315	901	LOV+PAS_3+GAF+Kinase
			B1Z812	ACB78979.1	Mpop_0801	488	LOV+PAS+ Kinase
			B1ZG87	ACB79745.1	Mpop_1581	541	LOV+Kinase+RR
			B1ZJK1	ACB81487.1	Mpop_3336	531	LOV+Kinase+RR
			B1ZKQ8	ACB81628.1	Mpop_3478	354	LOV+Kinase
			B1ZCH2	ACB82221.1	Mpop_4105	888	LOV+PAS+GAF+Kinase+RR
			B1ZGT9	ACB82617.1	Mpop_4519	366	LOV+Kinase
10	*M. zatmanii*	PSBB041	A0A1W6RDY7	WP_003599658.1	B2G69_02090	366	LOV+Kinase
			A0A1W6RGV8	WP_085856634.1	B2G69_08090	1072	LOV+PAS_3+Kinase+RR
			A0A1W6RIL3	WP_056501423.1	B2G69_11355	488	LOV+PAS+Kinase
			A0A1W6RKL6	WP_085857055.1	B2G69_15905	541	LOV+Kinase+RR
			A0A1W6RPC0	WP_056499167.1	B2G69_23260	533	LOV+Kinase+RR
			A0A1W6RQ45	WP_056499415.1	B2G69_23955	354	LOV+Kinase

Table 15: *Methylobacteria* and *Methylorubra* groups: BLUF proteins, accession codes and domain architectures

	Methylobacterium	**strain**	**UniProt**	**NCBI**	**Gene name**	**aa**	**Domain architecture**
1	*M. aquaticum*	MA-22A	A0A0C6EYC5	WP_060846567.1	Maq22A_c09520	150	Short-BLUF
			A0A0C6FG98	BAQ46067.1	Maq22A_c14425	156	Short-BLUF
			A0A0C6FKV3	WP_060848619.1	Maq22A_c23995	165	Short-BLUF
2	*M. nodulans*	ORS 2060	B8IB70	WP_015928965.1	Mnod_2309	155	Short-BLUF
3	*M. oryzae*	CBMB20	A0A089NTJ6	AIQ90737.1	MOC_2982	134	Short-BLUF
			A0A089NY66	AIQ92332.1	MOC_4577	134	Short-BLUF
			A0A089P248	AIQ92835.1	MOC_5080	326	Short-BLUF
			A0A089QH30	AIQ93878.1	MOC_6124	155	Short-BLUF
4	*M. phyllosphaerae*	CBMB27	----	WP_075380907.1	MCBMB27_03493	134	Short-BLUF
			----	WP_075380932.1	MCBMB27_03588	158	Short-BLUF
			----	WP_075381057.1	MCBMB27_03931	326	Short-BLUF
5	*M. radiotolerans*	JCM 2831	B1LTA6	ACB22412.1	Mrad2831_0397	143	Short-BLUF
			B1M108	ACB24558.1	Mrad2831_2569	134	Short-BLUF
			B1M482	ACB26377.1	Mrad2831_4411	309	Short-BLUF
			B1M0G5	ACB27487.1	Mrad2831_5542	155	Short-BLUF
6	*M. sp.*	17SD2-17	A0A2U8W8D7	AWN41868.1	DK389_16890	155	Short-BLUF
			A0A2U8W8Y6	AWN41782.1	DK389_16325	158	Short-BLUF
			A0A2U8W305	AWN40447.1	DK389_07765	308	Short-BLUF
7	*M.sp.*	17Sr1-1	A0A2U8X091	AWN52044.1	DK412_10450	150	Short-BLUF
			A0A2U8X872	AWN54755.1	DK412_26675	194	Short-BLUF
			A0A2U8XCY0	AWN55656.1	DK412_15735	270	Short-BLUF
			A0A2U8X5G2	AWN53549.1	DK412_19670	156	Short-BLUF
8	*M. sp.*	17Sr1-28	A0A2U8WHD1	WP_109957997.1	DK419_04285	156	Short-BLUF
			A0A2U8WKG8	WP_109959083.1	DK419_10825	240	Short-BLUF
			A0A2U8WKV7	WP_109959101.1	DK419_10950	208	Short-BLUF
			A0A2U8WNB0	WP_109959285.1	DK419_12010	150	Short-BLUF
9	*M. sp.*	17Sr1-43	A0A2U8VXJ4	WP_109953153.1	DK427_21505	150	Short-BLUF
			A0A2U8VX32	WP_109953486.1	DK427_23415	155	Short-BLUF

			A0A2U8VRU8	WP_010687537.1	DK427_09910	310	Short-BLUF
10	*M. sp.*	4-46	B0U8I2	WP_012331722.1	M446_1828	296	Short-BLUF
			B0UJP3	WP_012332391.1	M446_2545	150	Short-BLUF
			B0UIK0	WP_012333772.1	M446_4017	373	Short-BLUF
			B0ULI8	WP_012333923.1	M446_4183	155	Short-BLUF
			B0UQT1	WP_012334306.1	M446_4576	162	Short-BLUF
11	*M. sp.*	AMS5	A0A109QSJ5	WP_056200705.1	Y590_03755	155	Short-BLUF
			A0A0X1SLI7	WP_060770931.1	Y590_17880	158	Short-BLUF
			A0A0X1SN06	WP_060771282.1	Y590_20075	148	Short-BLUF
			----	WP_083530896.1	Y590_RS25905	140	Short-BLUF
12	*M.sp.*	C1	----	WP_012317408.1	BKE41_RS02410	143	Short-BLUF
			----	WP_058607382.1	BKE41_RS23015	315	Short-BLUF
			----	WP_020092935.1	BKE41_RS29370	155	Short-BLUF
13	*M. sp.*	DM1	A0A2U8HS49	WP_108938908.1	C0214_04065	155	Short-BLUF
			A0A2U8HPZ9	WP_108939204.1	C0214_05920	311	Short-BLUF
			A0A2U8HZB6	WP_108941420.1	C0214_20025	150	Short-BLUF
			A0A2U8I2F9	WP_108943058.1	C0214_22190	157	Short-BLUF
14	*M. sp.*	XJLW	A0A2U9U2L3	WP_111473188.1	A3862_02970	155	Short-BLUF
			A0A2U9TWT9	WP_051045092.1	A3862_10910	158	Short-BLUF
			A0A2U9TXI1	WP_043759270.1	A3862_11365	134	Short-BLUF
	Methylorubrum	**strain**	**UniProt**	**NCBI**	**Gene name**	**aa**	**Domain architecture**
1	*M. extorquens*	PSBB040	A0A1S1P3U3	WP_003603713.1	BV511_02980	155	Short-BLUF
			A0A1P8QX67	WP_012251938.1	BV511_06935	150	Short-BLUF
			A0A1S1P5Q9	WP_012251938.1	BV511_10370	150	Short-BLUF
			A0A1P8QPL9	WP_012255183.1	BV511_12365	148	Short-BLUF
			A0A1P8QR36	WP_076642775.1	BV511_15100	307	Short-BLUF
			A0A1P8QR02	WP_076642777.1	BV511_15105	150	Short-BLUF
2	*M. extorquens*	TK0001	A0A1S1P0H0	WP_012255183.1	TK0001_1440	148	Short-BLUF
			A0A1S1P3U3	WP_003603713.1	TK0001_5244	155	Short-BLUF
			A0A2N9AYN7	WP_012251938.1	TK0001_5883	150	Short-BLUF
3	*M. extorquens*	AM1	C5AVI4	ACS38652.1	MexAM1_META1p0723	155	Short-BLUF
			C5B322	CAX26640.1	MexAM1_META1p4421	148	Short-BLUF

4	*M. extorquens*	CM4	B7L1R5	WP_012605615.1	Mchl_0527	150	Short-BLUF
			B7L240	WP_003603713.1	Mchl_0912	155	Short-BLUF
			B7KRN3	WP_015951503.1	Mchl_3364	150	Short-BLUF
			B7KN60	WP_015952252.1	Mchl_4401	148	Short-BLUF
			B7KRN3	WP_015951503.1	Mchl_4786	150	Short-BLUF
5	*M. extorquens*	DM4	C7CE09	WP_003603713.1	METDI1095	155	Short-BLUF
			C7CJD7	WP_015824174.1	METDI5025	148	Short-BLUF
6	*M. extorquens*	PA1	A9VWG7	WP_012251938.1	Mext_0114	150	Short-BLUF
			A9W198	WP_003603713.1	Mext_0949	155	Short-BLUF
			A9W8Q2	WP_012255183.1	Mext_4031	148	Short-BLUF
7	*M. populi*	P-1M	A0A160PBB3	WP_017487136.1	MPPM_0981	155	Short-BLUF
			A0A160PM13	WP_096486808.1	MPPM_4395	157	Short-BLUF
8	*M.populi*	YC-XJ1	----	WP_012452822.1	E8E01_04445	155	Short-BLUF
			----	WP_052300129.1	E8E01_20740	158	Short-BLUF
9	*M.populi*	BJ001	B1ZGT3	ACB82611.1	Mpop_4513	162	Short-BLUF
			B1Z908	ACB79066.1	Mpop_0888	155	Short-BLUF
10	*M. zatmanii*	PSBB041	A0A1W6RDU7	WP_052300129.1	B2G69_02060	148	Short-BLUF
			A0A1W6RIT6	WP_085856840.1	B2G69_11735	155	Short-BLUF

Table 16: *Methylobacteria* and *Methylorubra* groups: rhodopsins, accession codes

	Methylobacterium	**strain**	**UniProt**	**NCBI**	**Gene name**	**aa**	**Domain architecture**
1	*M. aquaticum*	MA-22A	A0A0C6F7V1	BAQ48891	Maq22A_1p32955	252	Rhodopsin
2	*M. nodulans*	ORS 2060	----	----	----	----	----
3	*M. oryzae*	CBMB20	----	----	----	----	----
4	*M. phyllosphaerae*	CBMB27	----	----	----	----	----
5	*M. radiotolerans*	JCM 2831	----	----	----	----	----
6	*M. sp.*	17SD2-17	----	----	----	----	----
7	*M.sp.*	17Sr1-1	----	----	----	----	----
8	*M. sp.*	17Sr1-28	----	----	----	----	----
9	*M. sp.*	17Sr1-43	----	----	----	----	----
10	*M. sp.*	4-46	B0UM74	WP_012330516.1	M446_0537	252	Rhodopsin
11	*M. sp.*	AMS5	A0A0C6F7V1	BAQ48891	Maq22A_1p32955	252	Rhodopsin
12	*M.sp.*	C1	----	----	----	----	----
13	*M. sp.*	DM1	----	----	----	----	----
14	*M. sp.*	XJLW	----	----	----	----	----
***Methylorubra* group: rhodopsins - none found**							

Bibliography

1. Green, P. N. & Ardley, J. K. Review of the genus Methylobacterium and closely related organisms: a proposal that some Methylobacterium species be reclassified into a new genus, Methylorubrum gen. nov. *Int. J. Syst. Evol. Microbiol.* **68**, 2727–2748 (2018).

2. Tatusova, T. *et al.* NCBI prokaryotic genome annotation pipeline. *Nucleic Acids Res.* **44**, 6614–6624 (2016).

3. Altschul, S. *et al.* Gapped BLAST and PSI-BLAST: a new generation of protein database search programs. *Nucleic Acids Res.* **25**, 3389–3402 (1997).

4. Consortium, T. U. UniProt: a hub for protein information. *Nucleic Acids Res.* **43**, D204–D212 (2015).

5. Meyer, T. E. *et al.* The growing family of photoactive yellow proteins and their presumed functional roles. *Photochem. Photobiol. Sci.* **11**, 1495 (2012).

6. Losi, A., Mandalari, C. & Gärtner, W. From plant infectivity to growth patterns: The role of blue-light sensing in the prokaryotic world. *Plants* **3**, 70–94 (2014).

7. Harris, A. *et al.* A new group of eubacterial light-driven retinal-binding proton pumps with an unusual cytoplasmic proton donor. *Biochim. Biophys. Acta - Bioenerg.* **1847**, 1518–1529 (2015).

8. Pruitt, K. D., Tatusova, T. & Maglott, D. R. NCBI reference sequences (RefSeq): a curated non-redundant sequence database of genomes, transcripts and proteins. *Nucleic Acids Res.* **35**, D61–D65 (2007).

9. R. Apweiler, T. K. Attwood, A. Bairoch, A. Bateman, E. Birney, M. Biswas, P. Bucher, L. Cerutti, F. Corpet, M. D. R. Croning, R. Durbin, L. Falquet, W. Fleischmann, J. Gouzy, H. Hermjakob, N. Hulo, I. Jonassen, D. Kahn, A. Kanapin, Y. Karavidopoulou, R. L, E. M. Z. The InterPro database, an integrated documentation resource for protein families, domains and functional sites. *Nucleic Acids Res.* **29**, 37–40 (2001).

10. Mitchell, A. L. *et al.* InterPro in 2019: improving coverage, classification and access to protein sequence annotations. *Nucleic Acids Res.* **47**, D351–D360 (2019).